DISTINCT LOCALIZATION OF NADPH OXIDASE FLAVOCYTOCHROME *B* IN RESTING AND INTERFERON GAMMA ACTIVATED MACROPHAGES

Amy Jo Casbon

Submitted to the faculty of the University Graduate School
in partial fulfillment of the requirements
for the degree
Doctor of Philosophy
in the Department of Microbiology and Immunology
Indiana University

May 2009

Accepted by the Faculty of Indiana University, in partial
fulfillment of the requirements for the degree of Doctor of Philosophy

_____
Mary C. Dinauer, MD Ph.D.
Committee Chair

_____
Mark H. Kaplan, Ph.D.

Doctoral Committee

April 3, 2009

_____
Margaret E. Bauer, Ph.D.

_____
Fredrick M. Pavalko, Ph.D.

ACKNOWLEDGMENTS

I would like to express my deepest gratitude to my advisor, Dr. Mary Dinauer for her guidance in directing my research and expanding my knowledge. Importantly, I thank her for giving me the opportunity to think freely and devise my own experiments, to visit other laboratories in order to master current technologies, and to meet many of the leaders in the field of phagocytosis and innate immunity.

I would like to thank the members of my committee, Dr. Mark Kaplan, Dr. Margaret Bauer, and Dr. Fred Pavalko for their continual support of my graduate work and for being there whenever I needed them. In addition to my official committee, I was fortunate to receive expert advice from Dr. Lee-Ann Allen, University of Iowa, on my experimental designs and analysis of my data. I also greatly appreciate the feedback provided by Dr. Kenneth Dunn, whose critical nature drove my interest in confocal microscopy and Rab11 trafficking.

I wish to express my appreciation to many colleagues in the Department of Microbiology and Immunology and in the Wells Center for Pediatric Research for their knowledge and friendship, especially the members of the Dinauer Lab: Christophe Marchal, Natalie Stuhl, Nancy Pech, Juan Matute, Andres Arias, Xingjun Liu, Yue Zeng and many members of the faculty of the Department of Microbiology and Immunology, in particular Dr. Janice Blum, Dr. Ann Roman, and Dr. Randy Brutkiewicz.

Finally, I am continually thankful for the love and support of my family and friends. Above all, my husband, Douglas Cleaveland, who emotionally and financially helped me throughout the years while I worked towards my Ph.D. degree.

ABSTRACT

Amy Jo Casbon

DISTINCT LOCALIZATION OF NADPH OXIDASE FLAVOCYTOCHROME *B* IN RESTING AND INTERFERON GAMMA ACTIVATED MACROPHAGES

Flavocytochrome *b*558, the catalytic core of the phagocytic NADPH oxidase, mediates the transfer of electrons from NADPH to molecular oxygen to generate superoxide for host defense. Flavocytochrome *b* is a membrane heterodimer consisting of a large subunit gp91^{phox} (NOX2) and a smaller subunit, p22^{phox}. Localization of flavocytochrome *b* to the phagosome is essential for microbial killing, yet the subcellular distribution of flavocytochrome *b* in macrophages and how it is incorporated into macrophage phagosomes is not well characterized. In neutrophils, flavocytochrome *b* localizes primarily to specific granules that are rapidly mobilized to the phagosome upon stimulation. In contrast to neutrophils, macrophages do not contain specific granules, and trafficking of membrane proteins to the phagosome is more dynamic, involving fission and fusion events with endosomal compartments. We hypothesized that in macrophages, flavocytochrome *b* localizes to both plasma membrane and endosomal compartments that deliver flavocytochrome *b* to the phagosome. We generated fluorescently tagged versions of both p22^{phox} and gp91^{phox}, and rigorously verified their functionality in Chinese Hamster Ovary cells. Localization of flavocytochrome *b* was then examined in both RAW 264.7 murine macrophages and primary murine bone marrow derived macrophages (BMDM) in the presence and absence of interferon gamma (IFNγ). We

found that in "resting" macrophages, flavocytochrome *b* localizes primarily to the Rab11-positive endosome recycling compartment that recycles to the plasma membrane. In addition, phagocytosis assays showed flavocytochrome *b* is incorporated into the phagocytic cup and colocalized with Rab11 at the base of the cup, suggesting Rab11-positive endosomes may be involved in trafficking of flavocytochrome *b* between intracellular membranes and forming or nascent phagosomes. However, in IFNγ activated macrophages, flavocytochrome *b* was localized predominantly in the plasma membrane, with little present in endosomal compartments. This shift in flavocytochrome *b* distribution occurred following sustained exposure to IFNγ and correlated with increased flavocytochrome *b* protein expression and increased extracellular production of superoxide. Taken together, our results suggest the IFNγ-induced redistribution of flavocytochrome *b* may be important for enhancing the production of superoxide at the cell surface and may be a potential new mechanism by which IFNγ enhances antimicrobial activity in macrophages.

Mary C. Dinauer, MD, Ph.D.
Committee Chair

.

TABLE OF CONTENTS

LIST OF TABLES

LIST OF FIGURES

ABBREVIATIONS

AA	arachidonic acid
Ab	antibody
AEBSF	4-(2-aminoethyl) benzenesulfonyl fluoride
BMDM	bone marrow derived macrophage
BSA	Bovine serum albumin
CFP	cyan fluorescent protein
CGD	chronic granulomatous disease
CHO	Chinese Hamster Ovary
DAPI	4',6-diamidino-2-phenylindole
Dex	Dextran
DMEM	Dulbecco's modified Eagle's low glucose medium
EDTA	ethylene diamine tetra-acetate
ECL	enhanced chemiluminescence
ER	endoplasmic reticulum
ERC	endocytic recycling compartment
FCS	fetal calf serum
GFP	green fluorescent protein
HI FCS	heat inactivated fetal calf serum
hr	hours
HRP	horseradish peroxidase
IFNγ	interferon gamma

LB	Luria-Bertani broth
LPS	lipopolysaccharide
M	molar
mAb	monoclonal antibody
MEM	Minimum Essential Medium
min	minutes
NADPH	nicotinamide adenine dinucleotide phosphate
NBT	nitroblue tetrazolium
NGS	normal goat serum
PBS	phosphate buffered saline
PBSG	PBS plus 0.5mM $MgCl_2$, 0.9mM $CaCl_2$, and 7.5 mM dextrose
PCR	polymerase chain reaction
PMA	phorbol 12-myristate 13-acetate
PMSF	phenylmethyl sulfonyl fluoride
RT	room temperature
SDS	sodium dodecyl sulfate
sec	seconds
SOD	superoxide dismutase
SOZ	serum opsonized zymosan
TBST	Tris buffered saline, 0.5% Tween-20
TNF	tumor necrosis factor
Tfn	transferrin
YFP	yellow fluorescent protein

CHAPTER ONE: INTRODUCTION

I. The immune system

We are constantly exposed to infectious agents and it is our immune system that enables us to resist infection (Nester, 2007). Our immune system combats invading microorganisms, such as bacteria, viruses, fungi, and parasites. All cells of the immune system originate from the bone marrow and include myeloid (neutrophils, basophils, eosinophils, macrophages, dendritic cells) and lymphoid (B and T lymphocytes, and Natural Killer cells) cells. Our immune system is divided into two parts: (i) innate and (ii) adaptive (Janeway and Travers, 1997). The innate immune system is the first line of defense and confers immediate protection against many different pathogens without requiring prior exposure. In contrast, the adaptive immune system responds more slowly upon first exposure, but "learns" to recognize a specific epitope, or antigen, of a pathogen during infection. Upon reinfection, B and/or T cells will become activated following recognition of this specific antigen. Activated B cells secrete antibodies that bind to additional antigens on the pathogen resulting in a rapid and more efficient removal of the pathogen. Activated T cells become effector cells that can kill cells infected with pathogens directly (cytotoxic T cells) or enhance killing of pathogens by activating macrophages or B cells (helper T cells). While the systems perform different functions, the systems are interlinked and together provide a remarkable defense system (Janeway and Travers, 1997).

II. Phagocytic leukocytes

Phagocytic leukocytes are cells of the innate immune system highly proficient in ingesting and killing microorganisms (Kantari *et al.*, 2008). Phagocytic leukocytes or "professional" phagocytes, primarily neutrophils and macrophages, express a multitude of cell surface receptors that recognize particles coated in opsonins, such as complement or immunoglobulin (IgG), or pathogen-associated-molecular-patterns (PAMPs). Receptors that initiate and/or enhance phagocytosis include, but are not limited to, Fcγ-receptors and different members of the integrin and complement family (Table I) (Underhill and Ozinsky, 2002). These receptors confer upon phagocytes the ability to recognize and respond to pathogen-associated motifs or opsonized particles in the absence of additional stimuli. Following recognition, macrophages and neutrophils kill invading microorganisms through the release of toxic products, such as reactive oxygen species (ROS), proteolytic enzymes, and antimicrobial peptides. In addition to removal of pathogens, phagocytes also survey their environment and alert the adaptive immune system when an inflammatory or immune response is required (Hoebe *et al.*, 2004). Thus, phagocytes are essential not only for innate immunity, but also for linking the innate to the adaptive immune system.

1. Neutrophils

Neutrophils are short-lived cells that are usually the first cells of the immune system recruited to a site of infection. Neutrophils make up the majority of circulating white blood cells (40 - 80%, (Lacy, 2005). Neutrophils are endowed with preformed granules carrying antimicrobial peptides, granzymes, perforins, and oxidants and are

Table I. Phagocytosis-promoting receptors[a]

Receptor	Target	Ligand
FcγR1 (CD64)	IgG-opsonized bacteria	Fc portion of IgG
FcγRIIa (CD32)	IgG-opsonized bacteria	Fc portion of IgG
FcγRIIIA (CD16)	IgG-opsonized bacteria	Fc portion of IgG
FcεRI	IgE-opsonized bacteria	Fc portion of IgE
FcαRI (CD89)	IgA-opsonized bacteria	Fc portion of IgA
FcεRII (CD23)	IgE-opsonized bacteria	Fc portion of IgE
CR1 (CD35)	Complement-opsonized bacteria	C3b, C4b
CR3	Complement-opsonized bacteria	C3b
(CD11b/CD18;$\alpha_M\beta_2$)	Gram-negative bacteria	Lipopolysaccharide
	Bordetella pertussis	Filamentous hemagglutinin
	Yeast	β-Glucan
CR4 (CD11c/CD18)	Complement-opsonized bacteria	C3b, C4b
Mannose receptor	*Pneumocystis carinii*	Mannosyl/fucosyl residues
	Candida albicans	
Scavenger receptor	Apoptotic lymphocytes	Bacteria, LPS,
	Gram-positive cocci	Lipoteichoic acid
β_1 integrins	*Yersinia*	Invasin
$\alpha_V\beta_3$ integrins	Vitronectin-coated apoptotic cells	Vitronectin

[a]Receptors and their ligands that initiate or enhance phagocytosis in phagocytic leukocytes are listed. This table was adapted from (Underhill and Ozinsky, 2002).

specialized for rapid antimicrobial killing. Granule formation develops via a "targeting and timing" mechanism (Borregaard and Cowland, 1997), which basically means there is a sequential order in the expression of granule proteins and the formation of the different granule populations. The three major granule populations were first named primary, secondary, and tertiary following their order of synthesis. They are distinguished by size and content (see Table II). The primary or azurophilic granules are the largest granules and contain numerous antimicrobial compounds, such as myleoperoxidase, defensins, and lysozyme that are important for killing in the phagosome. The secondary or specific granules are much smaller than the azurophilic granules, but are the major population of granules in neutrophils, based on number. Secondary and tertiary granules are comparable in size, but differ in their contents. In addition to granules, neutrophils also contain a novel secretory compartment, the 'secretory vesicle,' and store a multitude of cytokine and chemokine receptors (listed in Table II), which are absent or expressed at low levels on the surface of "quiescent" neutrophils (Borregaard *et al.*, 2007). Secretory vesicles quickly fuse with the plasma membrane following minor elevations in calcium and deliver these receptors to the cell surface (Borregaard *et al.*, 2007).

The importance of neutrophils to combat infection is clearly illustrated in the human disease severe congenital neutropenia (SCN). SCN is a genetically heterogeneous disease that is characterized by a reduction in circulating neutrophils to less than 0.5 $x10^9$/ L (Welte *et al.*, 2006). SCN patients present with recurrent infections, often life-threatening, during the first 6 months of life including pneumonia, skin, and deep organ abscesses, as well as septicemia (Welte *et al.*, 2006). In the majority of patients, the cause of SCN (reviewed in (Ward and Dale, 2009) is a mutation in the ELA2 gene

Table II. Neutrophil granule proteins[a,b,c]

	Primary/ Azurophil granules	Secondary/ Specific granules	Tertiary/Gelatinase granules	Secretory vesicles
Membrane proteins	TNFR, uPAR CD63, CD68, presenilin	CD11b/CD18, CD66 CD67 gp91^{phox}, p22^{phox} SNAP23, VAMP2, Stomatin,	CD11b/CD18, CD66, CD67 gp91^{phox}, p22^{phox} MMP25 TNFR SNAP23, VAMP2, Nrampl	CD11b/CD18, CD66, CD67 gp91^{phox}, p22^{phox} MMP25 CD35, CD16, C1q-R, MyD88, MD2, fMLPR, TREM1, Ig(G,A,E)FcR TNFR1 and R2 CXCR-1, -2, -4, CCR-1, -2, -3 IFN-αR1 and R2 IFN-γR1 and R2 IL(1,4,6,10,13,17,18)R TLR-1,-2,-4,-6, LIR1-4,6,7,9 SNAP23, VAMP2, Nrampl, alkaline phosphatase, DAF, CD10, CD13
Matrix proteins	Elastase, cathepsin G, proteinase 3, Defensins, BPI, Myeloperoxidase, lysozyme, Sialidase Azurocidin β-glucoronidase	Collagenase, Gelatinase, cystatin C & F, uPA, NGAL, vitamin B12 binding protein, Lysozyme, lactoferrin, haptoglobin, prodefensin, α1-anti-trypsin, orosomucoid, heparanase, β2- microglobuin, CRISP3	Gelatinase, arginase1, β2-microglobuin, CRISP3	Plasma proteins

[a]Localization of proteins in the matrix and membrane of neutrophil granules and secretory vesicles.

[b]Abbreviations; CRISP, cysteine-rich secretory protein; DAF; decay-accelerating factor; LIR, immunoglobulin-like receptor; uPA, urokinase plasminogen activator.

[c]Table was adapted from (Borregaard *et al.*, 2007)

(encoding neutrophil elastase), which has been shown to induce the unfolded protein response and lead to apoptosis of neutrophils (Kollner *et al.*, 2006).

2. Macrophages

Macrophages are a heterogeneous population of long-lived cells, distributed throughout virtually all host tissues that are essential not only for killing pathogens but also for maintaining tissue homeostasis (Gordon and Taylor, 2005; Mosser and Edwards, 2008). Macrophages express a plethora of receptors that enable them to respond to their environment and that program or "activate" them for specialized functions (Gordon and Taylor, 2005; Mosser and Edwards, 2008). In the absence of inflammation, macrophages differentiate from circulating peripheral blood mononuclear cells that migrate into tissues to replenish long-lived tissue-specific macrophages of the bone (osteoclasts), alveoli, central nervous system (microglial cells), connective tissue (histiocytes), gastrointestinal tract, liver (Kupffer cells), spleen, and peritoneum (Mosser and Edwards, 2008). Quiescent tissue-specific or resident macrophages act as "janitors" to remove cellular debris generated during tissue remodeling and apoptotic cells (Mosser and Edwards, 2008).

In marked contrast, during an infection, macrophages take on a different phenotype, functioning as an immune effector cells programmed to kill pathogens and alert the immune system through the release of chemokines, cytokines, and antigen presentation (Mosser and Edwards, 2008). In addition to the microbicidal activity of macrophages during the onset of an infection, macrophages also aid in tissue repair and turning off the immune response, mainly through the release of IL-10, at later stages

(Mosser and Edwards, 2008). In summary, macrophages survey their environment, remove dead cells and potential pathogens, and then alert the immune system through the release of cytokines and/or antigen presentation.

III. Phagocyte NADPH oxidase

1. Superoxide production is essential to innate immunity

Activation and appropriate localization of superoxide production by the phagocytic NADPH oxidase is essential to host defense. The NADPH oxidase is a multicomponent enzyme, comprised of a membrane-bound heterodimer, flavocytochrome b_{558}, which consists of a large subunit, gp91^{phox} (NOX2), and a small subunit, p22^{phox}, and cytosolic regulatory subunits, p67^{phox}, p47^{phox}, p40^{phox}, and Rac (Nauseef, 2004). The NADPH oxidase transfers electrons from NADPH to molecular oxygen to produce superoxide, which serves as a precursor for the formation of an arsenal of reactive oxygen species (ROS), such as hydrogen peroxide (H_20_2), hydroxyl radical ($OH^{\bullet}$), and hypochlorous acid ($HOCl^{-}$). Superoxide has a relatively weak antimicrobial activity, in contrast to the secondary products formed, and thus, confers its toxicity through the generation of these highly reactive products. The importance of superoxide production was first evident when the clinical syndrome, chronic granulomatous disease (CGD), was linked to the inability of neutrophils from CGD patients to produce a "respiratory burst" (Baehner and Nathan, 1967, 1968). CGD is a rare genetic disease with an incidence of approximately 1 in 250,000 live births (Winkelstein *et al.*, 2000), which results from a mutation in any 1 of the 4 subunits (gp91^{phox}, p22^{phox}, p47^{phox}, p67^{phox}) of the phagocytic NADPH oxidase. CGD is usually

diagnosed by the age of 1 year due to persistent and recurrent bacterial or fungal infections, such as *Aspergillus fumimatus, Salmonella typhimurium*, *Staphylococcus aureus*, *Serratia marcescens*, and *Burkholderia cepacia* and has been estimated to have an overall mortality rate of approximately 17.6% (Winkelstein *et al.*, 2000).

2. Biosynthesis and subcellular distribution of flavocytochrome *b*

The biosynthesis and subcellular distribution of flavocytochrome *b* has been well characterized in neutrophils (Figure 1). gp91^{phox} and p22^{phox} are synthesized as separate polypeptides in the endoplasmic reticulum (ER). Human gp91^{phox} is generated from a core protein of 58 kDa (Parkos *et al.*, 1987) that is subsequently glycosylated to gp65, a high mannose 65 kDa form in the ER which binds to heme, allowing for heterodimer formation with p22^{phox} (Porter *et al.*, 1994; Yu *et al.*, 1997; Yu *et al.*, 1999; DeLeo *et al.*, 2000). The heterodimer then traffics to the Golgi, and gp91^{phox} is further glycosylated to the mature, 91 kDa form (DeLeo *et al.*, 2000). Studies of neutrophils and promyelocytic cells, PLB-985, have shown that the individual subunits of flavocytochrome *b*, gp91^{phox} and p22^{phox}, are unstable and targeted to the proteasome in absence of their heterodimer partner (DeLeo *et al.*, 2000). In contrast, the individual subunits are stable when exogenously expressed in cell lines such as Chinese Hamster Ovary (CHO-K1) and monkey kidney (COS-7) (Yu *et al.*, 1997; Biberstine-Kinkade *et al.*, 2002; Price *et al.*, 2002), which have provided model systems for identifying regions within both p22^{phox} and gp91^{phox} that are important for heterodimer formation and assembly of the NADPH oxidase.

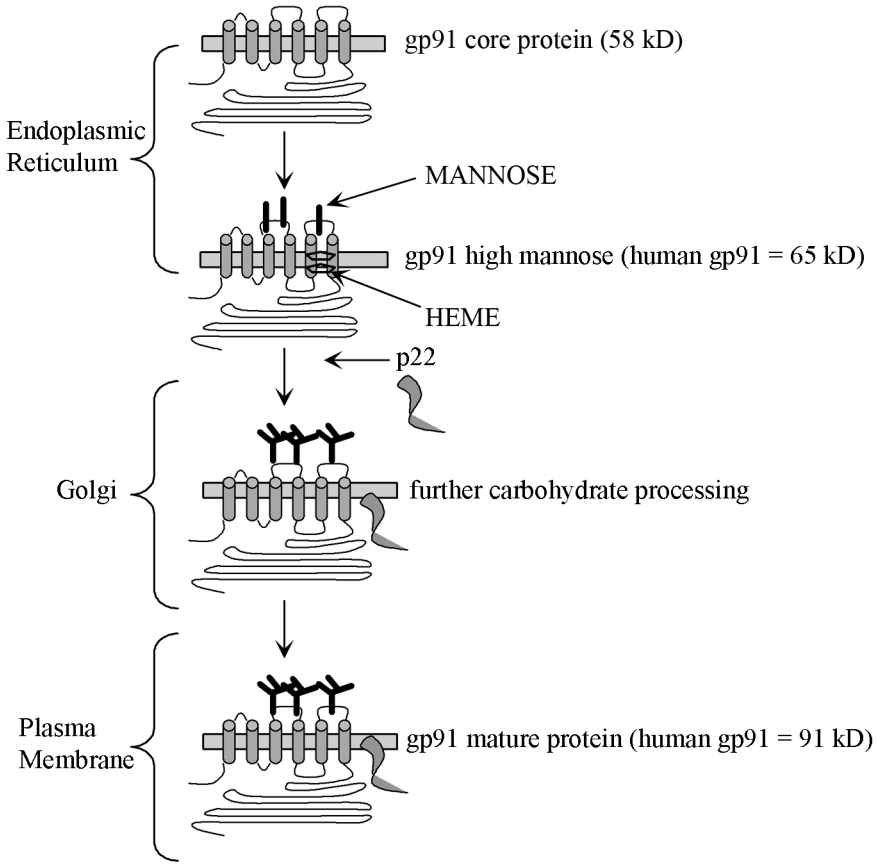

Figure 1. Biosynthesis of flavocytochrome *b* (in neutrophils). Flavocytochrome *b* is a heterodimer consisting of a large subunit, gp91^{phox}, and a smaller subunit, p22^{phox}. gp91^{phox} is first synthesized as a 58 kD core protein in the endoplasmic reticulum that is subsequently gylcosylated to a high mannose 65 kD form which binds heme. Heme binding enables binding of p22^{phox}, and the newly formed heterodimer traffics to the Golgi where gp91^{phox} is further glycosylated to a mature 91 kD form. In neutrophils, flavocytochrome *b* then traffics to specific granules, secretory vesicles, and the plasma membrane.

While the biosynthesis of flavocytochrome *b* is believed to be the same in both neutrophils and macrophages, the location of flavocytochrome *b* following biosynthesis is different in the two cell types. In neutrophils, the mature flavocytochrome is found primarily in the membrane of secondary granules, but also is present in secretory vesicles, a type of endosome, and in the plasma membrane (Borregaard *et al.*, 1983; Jesaitis *et al.*, 1990). Upon activation, these intracellular compartments fuse with the plasma membrane or phagosome where superoxide is produced. In contrast to neutrophils, macrophages do not contain specific granules, and the subcellular distribution of flavocytochrome *b* is not well characterized. Studies using immuno-electron microscopy showed that relatively little flavocytochrome *b* localized to the plasma membrane in resting human monocytes, and was mainly in small peroxidase-negative granules and vesicles, which, as in neutrophils, appears to be a pool that is rapidly mobilized to the plasma membrane upon cellular activation (Ginsel *et al.*, 1990; Calafat *et al.*, 1993; Borregaard and Cowland, 1997). Further characterization of these intracellular flavocytochrome *b* compartments in monocytes has not been reported. Studies in macrophages are even more limited. In human monocyte-derived macrophages, $p22^{phox}$ and $gp91^{phox}$ have been detected in the plasma membrane, as well as reticulo-vesicular intracellular structures that were not further characterized (Johansson *et al.*, 1995; Gallois *et al.*, 2001), and in the plasma membrane of murine peritoneal macrophages (Vazquez-Torres *et al.*, 2000).

In addition to differences in the distribution, neutrophils highly express $gp91^{phox}$ and $p22^{phox}$ subunits and produce a strong oxidative burst, while unactivated or "resting"

macrophages produce less superoxide and express much lower levels of these NADPH oxidase subunits (Yagisawa *et al.*, 1996).

3. Flavocytochrome *b* is the catalytic core of the NADPH oxidase

At rest, flavocytochrome *b* exists in an inactive conformation that requires binding of the cytosolic subunits to induce conformational changes required for superoxide production (Nisimoto *et al.*, 1999; Paclet *et al.*, 2000). Two main events are required for the assembly and activation of the cytosolic subunits ($p47^{phox}$, $p67^{phox}$, $p40^{phox}$, and Rac) onto the flavocytochrome, $p47^{phox}$ phosphorylation and Rac activation (reviewed in (Groemping and Rittinger, 2005). $p47^{phox}$ acts as a carrier protein for shuttling $p67^{phox}$ and $p40^{phox}$ to the membrane. Beginning at its N-terminus, $p47^{phox}$ contains a PX (*Phox* homology) domain, followed by two Src homology 3 (SH3) domains that target a proline-rich region (PRR) in $p22^{phox}$ of flavocytochrome *b*, an auto-inhibitory region (AIR) that masks the SH3 domains in the resting state, and a PRR that binds the C-terminus SH3a domain of $p67^{phox}$. $p67^{phox}$ contains an N-terminal tetratricopeptide repeat (TPR) domain, a PRR, and two SH3 domains (referred to as SH3a and SH3b) that are separated by a PB1 (*Phox* and Bem1) motif that binds to a similar C-terminal PB1 domain in $p40^{phox}$. In addition to the PB1 domain, $p40^{phox}$ has an N-terminal PX domain followed by an SH3 domain. Serine phosphorylation of $p47^{phox}$ at the AIR unmasks the SH3 domains within $p47^{phox}$, permitting binding to $p22^{phox}$ and driving translocation of the cytosolic subunits $p47^{phox}$, $p67^{phox}$, and $p40^{phox}$ to membrane-bound flavocytochrome *b*. Rac is a member of the Rho GTPase family and cycles from a GDP inactive state to an active GTP-bound state. Activation of Rac to the GTP-bound

state requires dissociation of Rho guanine-nucleotide-dissociation-inhibitor (Rho-GDI) that otherwise sequesters Rac in the cytosol, which unmasks the geranylgeranyl moiety of Rac important for membrane insertion, and binding by a guanine nucleotide exchange factor (GEF) to catalyze the exchange of GDP to GTP. Rac-GTP inserts into the membrane and binds to gp91^{phox} and p67^{phox}. Binding of Rac to p67^{phox} and to the flavocytochrome directly regulates electron transfer through the flavocytochrome. In summary (Figure 2), the membrane-bound flavocytochrome is the catalytic core of the oxidase, but requires the translocation and assembly of the cytosolic subunits to form an active complex (Groemping and Rittinger, 2005).

4. Regulation of superoxide production

A. Regulation of cytosolic subunits

Superoxide has the potential to harm the host, thus, multi-faceted levels of regulation control enzymatic activity, yet permit an immediate, localized response to invading pathogens. As described above, the spatial and temporal separation of the membrane-bound and cytosolic subunits of the NADPH oxidase is one method of regulation (Babior *et al.*, 2002) and was the first level to be recognized. In addition, the individual cytosolic subunits possess domains (or features) that are regulated via interactions with regulatory proteins. The NADPH oxidase is activated during phagocytosis and can be stimulated by various soluble and particulate stimuli, including chemoattractants, certain cytokines, different lectins, opsonized as well as various un-opsonized microorganisms, and pharmacological agents such as phorbol esters, calcium ionophores and arachidonic acid (AA). Many receptors can enhance and/or activate the

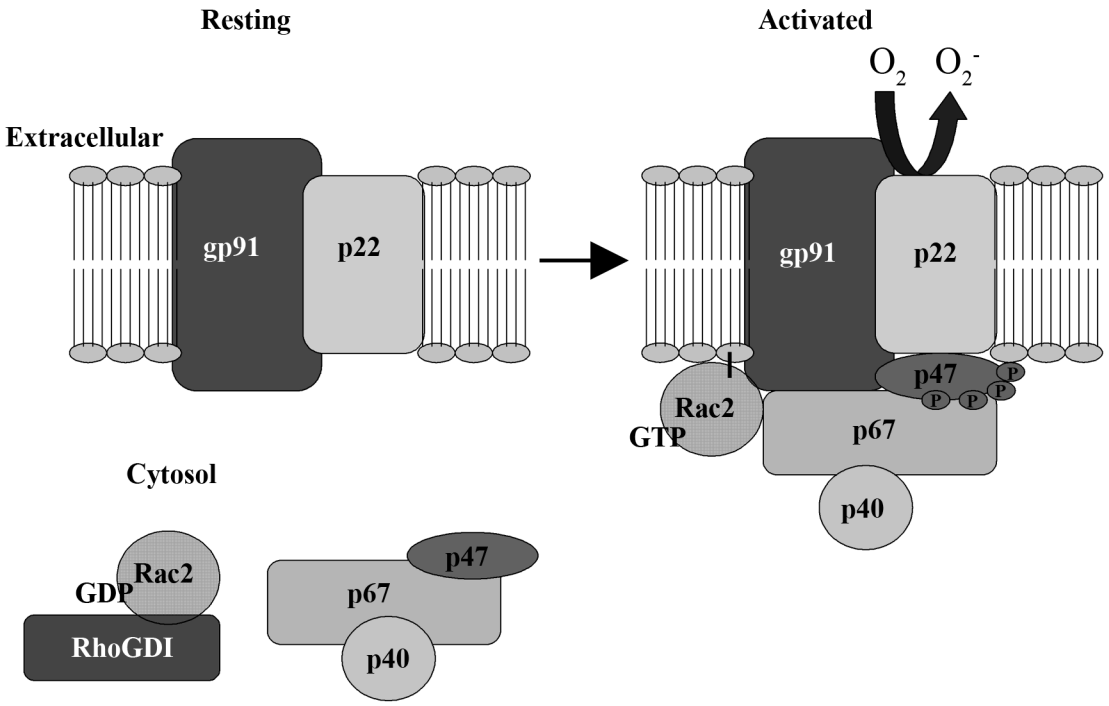

Figure 2. NADPH oxidase assembly and activation. In resting cells, the membrane-bound heterodimer flavocytochrome *b* is segregated spatially from the cytosolic subunits, Rac, $p47^{phox}$, $p67^{phox}$, and $p40^{phox}$. Upon stimulation, two events result in translocation of the cytosolic subunits to the membrane-bound heterodimer, leading to assembly and activation of the NADPH oxidase: phosphorylation of $p47^{phox}$ and activation of Rac. Cartoon was adapted from (Nauseef, 2007).

NADPH oxidase to produce superoxide (Underhill and Ozinsky, 2002). Following binding of its ligand, the different receptors then regulate NADPH oxidase activity through activation of kinases and guanine exchange factors (GEFs) that are important for $p47^{phox}$ phosphorylation and Rac activation. Several kinases are known to regulate phosphorylation of $p47^{phox}$, including protein kinase C, p21-activated kinase (PAK), protein kinase B/Akt, casein kinase 2, and p38-activated protein kinases (Groemping and Rittinger, 2005). Rac activation is regulated by at least two GEFs, Vav and P-Rex1 (Dinauer, 2003).

B. Localization of flavocytochrome *b*

In addition to the regulatory mechanisms governing activation of the NADPH oxidase, the assembly of the NADPH oxidase and the production of superoxide must be localized to either the plasma membrane or the phagosome for microbial killing. In neutrophils, flavocytochrome *b* is delivered to the phagosome and plasma membranes via granules and secretory vesicles (Nauseef, 2004). In macrophages, the mechanism by which flavocytochrome *b* is delivered to the phagosome is not known.

IV. Pathogen evasion of the oxidative burst

More recently, the importance of superoxide has been illustrated in studies showing that pathogenicity of some microorganisms is owed in part to their ability to evade oxidative killing by targeting the NADPH oxidase (Carlyon *et al.*, 2004). Examples include *Anaplasma phagocytophilum*, *Salmonella enterica serovar typhimurium* (*S. typhimurium*), and *Helicobacter pylori* (*H. pylori*). *Anaplasma*

phagocytophilum inhibits NADPH oxidase assembly and downregulates NADPH oxidase subunits by inhibiting interferon (IFN)γ-mediated expression of IRF-1 (Thomas *et al.*, 2005). *S. typhimurium* was the first pathogen to be described to evade oxidative killing not by targeting activation of the NADPH oxidase, but by preventing localization of flavocytochrome *b* to the phagosome. Studies by two groups (Vazquez-Torres *et al.*, 2000; Gallois *et al.*, 2001) found trafficking of flavocytochrome *b* to the Salmonella containing vacuole (SCV) to be impaired. *In vivo* studies found that a mutant of *S. typhimurium* carrying a mutation in the Salmonella pathogenicity island (SPI)-2 was virulent in the gp91^{phox} knockout mouse but not in wild-type mice, suggesting SPI-2 was important for targeting the NADPH oxidase flavocytochrome *b* (Vazquez-Torres *et al.*, 2000). Further *in vitro* studies found an increase in localization of flavocytochrome *b* to the SCV containing the SPI-2 mutant (Vazquez-Torres *et al.*, 2000; Gallois *et al.*, 2001). In addition, Vazquez-Torres and collaborators (Vazquez-Torres *et al.*, 2000) showed localized production of superoxide in vacuoles containing avirulent *E. coli* (approximately 50% positive), but vacuoles containing pathogenic *S. typhimurium* were devoid of superoxide. Notably, superoxide was produced following infection with *S. typhimurium* but was localized to vesicles and the plasma membrane (Figure 3). More recently, *H. pylori* was also found to prevent oxidase assembly at the phagosome (Allen and McCaffrey, 2007). Taken together, these data show that the ability of some pathogens to disrupt trafficking of flavocytochrome *b* to the phagosome is key to its virulence.

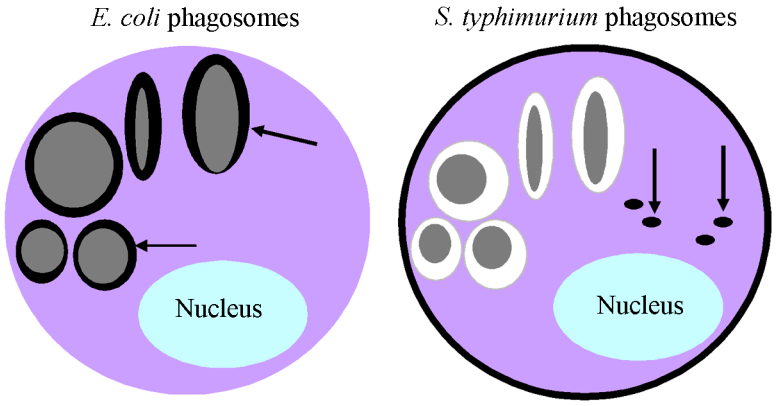

Figure 3. Location of superoxide production in murine macrophages. Superoxide production was detected by cerium perhydroxide precipitate in studies of macrophages (purple) infected with bacteria (grey). Superoxide production (black) colocalized with phagosomes cotaining *E. coli* (left, black arrows) but not wild-type *S. typhimurium*, where superoxide localized to vesicles discrete from phagosomes (right, black arrows) and to the plasma membrane. Cartoon was adapted from (Vazquez-Torres *et al.*, 2000).

V. Phagocytosis

Phagocytosis is the cellular engulfment of large particles. While first discovered as a mechanism of innate immune defense by Elie Methcnikoff in 1893 (Stossel, 1999), phagocytosis is not unique to cells of the immune system. In primitive organisms, phagocytosis primarily serves as a means of nutrient uptake (Aderem, 2003), while in higher organisms, phagocytosis is the main mechanism by which specialized cells of the immune system kill invading microorganisms or remove apoptotic cells from the extracellular milieu (Groves *et al.*, 2008). Phagocytosis is an integrated process that requires the activation of cell surface receptors. Activation of these receptors initiates signaling cascades that regulate internalization and subsequent phagosome maturation. As mentioned earlier, there are many receptors that regulate phagocytosis (Table II). In addition to these phagocytosis-inducing receptors, many other receptors are engaged during phagocytosis that can regulate a variety of processes such as cell proliferation, removal of dead cells, motility, apoptosis, and antigen presentation (Underhill and Ozinsky, 2002). Due to the complexity of the many signals generated during phagocytosis, the functional roles of individual receptors have been dissected in simpler experimental systems. For example, the signaling pathways of the Fcγ-receptor (Downey *et al.*, 1999) and the dectin-1 receptor (Underhill *et al.*, 2005) have been elucidated in cell lines expressing the receptor from a transgene.

1. Internalization

The initial engulfment or "uptake" process of phagocytosis seems to universally require actin remodeling (May and Machesky, 2001), but different signaling cascades

seem to regulate the process of engulfment, which appears to be receptor and cell-type specific. One of the best studied phagocytic receptor is the Fcγ-receptor (FcγR). IgG-opsonized particles/pathogens crosslink FcγRs upon engagement, leading to phosphorylation of intrinsic tyrosine activation motifs (ITAMS) by Src kinase family members, which provide docking sites that lead to activation of Syk family kinases (Greenberg and Grinstein, 2002). In addition to Syk, activation of phosphoinositide 3-kinase (PI3K), protein kinase C (PKC), phospholipase C (PLC), and Rho GTPases are also important regulators of early stages of phagocytosis (Underhill and Ozinsky, 2002). Activation of Src kinases are essential for local actin polymerization and phagocytosis. Recent studies suggest Src kinases may also play a role in receptor clustering and subsequently particle binding (Groves *et al.*, 2008). Src, Syk, and Rho GTPases, such as Rac and Cdc42, are all involved in regulating actin dynamics at phagocytic cups and are essential for uptake. PI3K is involved in membrane remodeling and is necessary for phagosome closure (Swanson and Hoppe, 2004). PLC activates PKC, which is important for phagosome formation (Larsen *et al.*, 2000), and PLC regulates membrane fusion which is suggested to be an additional mechanism by which PLC regulates phagocytosis (Swanson and Hoppe, 2004).

2. Phagosome maturation

After internalization, a particle and/or pathogen is sealed off from the extracellular milieu in a vacuole called the phagosome. The phagosome undergoes maturation, a process by which phagosomes change their functional capacity as they as age (Griffiths, 2004). Phagosome maturation involves the combination of membrane

remodeling, fusion events, and cell signaling, which ultimately lead to pathogen destruction (Scott *et al.*, 2003) or removal of dead cells (Kinchen *et al.*, 2008). Hence, phagosome maturation can also be viewed as the degradative stage of phagocytosis. Until recently, a more simplistic view of phagosome maturation was theorized in which a pathogen was engulfed into one vacuole, which fused with early endosomes, then late endosomes, and ended with fusion with the acidic lysosomes to form a phago-lysosome (Mayorga *et al.*, 1991). Due to emerging novel techniques, such as the use of fluorescently tagged proteins for live imaging and the identification of molecules important in endosome fusion, such as members of the Rab family and SNARE proteins, this model is now disputed with clear evidence revealing phagosome maturation is more complex and dynamic.

The new model of phagosome maturation, named "Kiss and Run" (Desjardins, 1995), involves fusion and fission, where vacuoles or endosomal compartments come into contact with the phagosome forming a pore between the compartments (the Kiss) to acquire selected sets of proteins and lipids through fusion, and then disengage (the Run) from the developing phagosome (Vieira *et al.*, 2002).

VI. Similar mechanisms regulate endocytosis and phagocytosis

Receptor-mediated endocytosis and phagocytosis are similar in their requirement of a specific ligand to initiate internalization and in their machinery that regulates the internalization and/or degradation of the ligand (Scott *et al.*, 2003; Kinchen *et al.*, 2008). A plethora of receptors are regulated by endocytosis and include, but are not limited to, the following receptors: β2-adrenergic, dopamine, muscarinic acetylcholine, epidermal

growth factor, V2 vasopressin, δ-opioid, nutrient (low density lipoprotein and transferrin), integrins, and glucose transporter GLUT4, which all have their own unique ligand (Sorkin and Von Zastrow, 2002; Gaborik and Hunyady, 2004). In the case of phagocytosis, the ligand is bacteria, yeast, or apoptotic cells. In both processes, the binding of the ligand to specific receptors regulates not only the fate of the ligand but also regulates a cellular reaction. In phagocytosis of bacteria, the ligand is degraded (or killed) and the main reaction is an inflammatory response.

1. Internalization and degradation

Endocytosis and phagosome maturation are processes that require vesicular fission and fusion events that are regulated by the Rab family of GTPases (Scott *et al.*, 2003; Kinchen *et al.*, 2008). Rab GTPases serve as molecular switches, which cycle between an inactive GDP bound state to an active GTP bound state (recently reviewed in (Brumell and Scidmore, 2007). Different Rab proteins have been shown to regulate distinct intracellular membrane trafficking pathways and hence define key steps during endocytosis and phagocytosis (Figure 4). During receptor-mediated endocytosis, the binding of a ligand to its receptor initiates internalization of the ligand:receptor complex into early endosomes, which is regulated by Rab5. From the Rab5-positive compartment, the ligand and receptor are then destined to one of two pathways: degradation or recycling back to the cell surface (Figure 4).

Many receptors are downregulated following binding to their ligands and are targeted for degradation. One of the best characterized receptors that is downregulated following ligand binding is the epidermal growth factor (EGF) receptor (recently

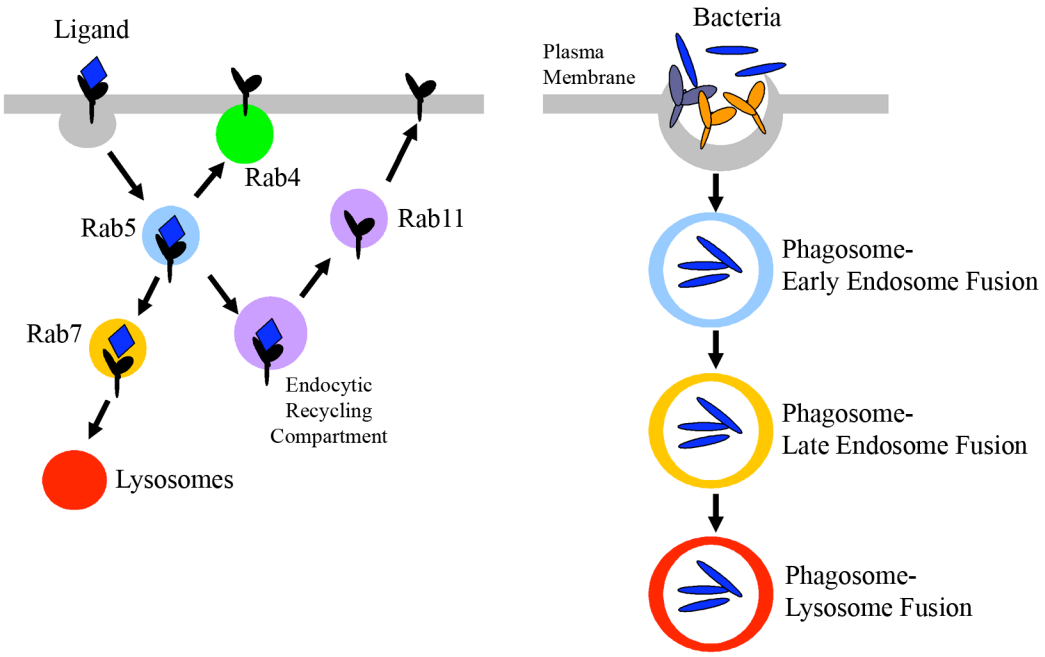

Figure 4. Receptor-mediated endocytosis and phagosome maturation**.** Receptor-mediated endocytosis is shown on the left panel and phagosome maturation is shown on the right panel. Both processes are regulated by members of the Rab family of GTPases. **Left panel:** Upon binding of a ligand to a receptor, the ligand:receptor complex is internalized into vesicles which quickly fuse with Rab5-positive early endosomes (shown in blue). From early endosomes or sorting endosomes, receptors are targeted to one of two pathways. If targeted to the degradative pathway, receptors will traffic to Rab7-positive late endosomes (yellow), and then traffic to lysosomes, where they will be degraded. In contrast, receptors not targeted for degradation will traffic along the recycling pathway and localize to Rab4-(green) or Rab11-(purple) positive endosomes. Rab4- and Rab11-positive endosomes are considered the "fast" track and "slow" track, respectively. Receptors that traffic back to the cell surface via Rab11-positive endosomes accumulate in a perinuclear compartment called the endocytic recycling compartment. **Right panel:** Similar to receptors destined for degradation, phagosomes also sequentially fuse with Rab5-, Rab7-positive endosomes, and finally will fuse with lysosomes to form phagolysosomes.

reviewed (Sorkin and Goh, 2008). Receptors and/or ligands destined for degradation are trafficked from the early (or sorting) Rab5-positive endosome to late endosomes, which are regulated by Rab7. Rab7-positive endosomes then fuse with acidic lysosomes and degradation occurs. Targeting of receptors to lysosomes functions to terminate signaling and make the cells unresponsive to further signal input (Katzmann *et al.*, 2002).

Similar to the pathway of receptor downregulation, a maturing phagosome will first interact with early Rab5-positive endosomes, then Rab7-, and finally with lysosomes to form the phagolysosome (Figure 4)(Scott *et al.*, 2003). Described as a unique hybrid organelle, phagolysosomes contain hydrolytic enzymes, defensins, bactericidal peptides, proteases, and a very low pH (Vieira *et al.*, 2002), and thus, are programmed to destroy microorganisms. The drop in pH during maturation of the phagosome is not only important for harming the phagocytosed pathogen, but is also required to activate many of the enzymes within the phagolysosome, such as the cathepsin family of proteases, and thus, is often considered a marker for a "functional" phagosome (Kinchen *et al.*, 2008). The ability of many intracellular pathogens to prevent phagosome-lysosome fusion and survive within macrophages clearly illustrates that formation of the phagolysosome is essential for killing. Examples include *Mycobacterium tuberculosis* and *Legionella pneumophila* (reviewed in (Brumell and Scidmore, 2007).

2. Recycling of membrane proteins

Instead of degradation, receptors can also be recycled back to the cell surface and re-used up to several hundred times (Maxfield and McGraw, 2004). Interestingly, recycling of membrane proteins is not limited to receptors and is essential for maintaining

the composition of various organelles and returning important molecules back to specific compartments (Maxfield and McGraw, 2004). Receptors can recycle either directly from the early Rab5-positive endosomes or indirectly through the endocytic recycling compartment (ERC). Rab4 regulates direct trafficking back to the plasma membrane, while Rab11 regulates trafficking from an endocytic recycling compartment (ERC) back to the cell surface (Figure 4). Recycling of receptors via the Rab4 and Rab11 pathways have been shown to be important for many receptor tyrosine kinases and G-protein-coupled receptors (Sorkin and Von Zastrow, 2002). The biological role of the ERC has been best illustrated in studies of GLUT4, which regulates the intake of glucose. In the presence of stimulus (insulin), GLUT4 traffics through the ERC to the plasma membrane to increase cell surface expression of GLUT4. In the absence of insulin, GLUT4 is transported from the ERC to an insulin-regulated compartment (IRC) to maintain a predominant intracellular distribution of GLUT4. Thus, the ERC is involved in sorting of GLUT4 and serves as a reservoir for insulin-recruited GLUT4 (Maxfield and McGraw, 2004).

3. Recycling endosomes and phagocytosis

Less is known about the role of recycling endosomes in regulating internalization and phagosome maturation, yet interestingly some of the first studies of recycling of membrane proteins utilized phagocytosis in macrophages as their model system (Steinman, Cohn, 1983). After only 30 min of phagocytosis, its estimated that macrophages can engulf the equivalent of 48 - 145% of their surface area (Cox *et al.*, 2000), yet the surface area of the plasma membrane does not decrease, but rather

increases during phagocytosis (Hackam *et al.*, 1998). While many intracellular compartments, such as the Golgi, lysosomes, or ER, could provide additional membrane to the newly forming phagosome, endosomes are suggested to be more likely involved since disruption of the Golgi does not inhibit phagocytosis, lysosomes are not required for phagocytosis, and endosomes accumulate at the base of newly forming phagosomes (Cox *et al.*, 2000). Specifically, recycling endosomes are believed to be one resource of membrane to the phagosome. Inhibition of recycling using a GTP-binding deficient Rab11 mutant, Rab11 25N, reduced both the rate and extent of phagocytosis, while a GTPase-deficient Rab11, Rab11 70L enhanced phagocytosis, suggesting recycling endosomes are important in the initial stages of phagocytosis (Cox *et al.*, 2000). Recycling of Texas-Red labeled antibodies from phagosomal compartments to the plasma membrane has been shown and the recycling of these antibodies to be reduced in the presence of a dominant negative mutant of the Rab coupling protein (RCP), an effector of Rab11 (Damiani *et al.*, 2004). In addition, a proteomic analysis of phagosomes in macrophages localized Rab4 and Rab11 to early phagosomal membranes (Garin *et al.*, 2001). These data, along with more recent studies showing recycling of membrane proteins from the *Salmonella* containing phagosome (Smith *et al.*, 2005), suggest recycling endosomes may be involved in phagosome maturation.

In addition to removal of proteins from the nascent phagosome, recycling endosomes provide a direct route for localizing key proteins to the phagocytic cup. For example, tumor necrosis factor-α (TNFα) localizes to the ERC and, following stimulation with interferon gamma (IFNγ) and lipopolysaccharide (LPS) in macrophages, is targeted to the phagocytic cup via vesicle-associated membrane protein 3 (VAMP3)-

positive recycling endosomes (Murray *et al.*, 2005). Transgenic expression of GFP-tagged VAMP3 was shown to increase TNFα secretion (Murray *et al.*, 2005), illustrating the role of recycling endosomes in localizing the release of a proinflammatory cytokine during phagocytosis.

While the mechanisms that regulate phagosome maturation are quite similar to those regulating receptor-mediated endocytosis, the two processes are distinct. Key differences are that phagocytosis involves engulfment of particles greater than 0.5 μm and requires actin cytoskeleton rearrangements (May and Machesky, 2001).

VII. Enhanced antimicrobial activity in IFNγ and LPS stimulated macrophages

1. Classical activation of macrophages

While macrophages have the ability to phagocytose and kill microorganisms without requiring exogenous stimuli, these functions are greatly enhanced following stimulation with certain cytokines. The major "classical" activators of macrophages are two cytokines, IFNγ and TNFα, and bacterial LPS (Mosser and Edwards, 2008). Classically activated macrophages have increased antimicrobial activity and enhanced antigen presentation. Thus, classically activated macrophages are not only important for killing but are also essential for eliciting an inflammatory response. In contrast, other states of activation of macrophages such as alternatively and/or M2 activated do not result in release of inflammatory cytokines (Benoit *et al.*, 2008; Mosser and Edwards, 2008).

2. Interferon gamma (IFNγ)

IFNγ was first identified as the macrophage activating factor released by lymphocytes that enhanced the secretion of superoxide and the ability to kill intracellular microbial pathogens, referred to as the "cardinal criterion" of macrophage activation by C. Nathan (Nathan *et al.*, 1983). Currently, IFNγ is still believed to be the most important stimulus to activate antimicrobial mechanisms in macrophages, which include (i) superoxide produced by the NADPH oxidase, (ii) nitric oxide (NO) generated from inducible NO synthetase (iNOS), and (iii) up-regulation of immunomodulating genes that recruit or activate T and/or NK cells, or monocyte/macrophages (Schroder *et al.*, 2004). Additionally, IFNγ up-regulates antigen processing and presentation pathways in macrophages which correlate with increased transcription of MHCII (Schroder *et al.*, 2004).

The importance of IFNγ is illustrated in human disease and mouse models with defects in IFNγ signaling. In humans, defects in IFNγ signaling cause selective deficiencies in innate and adaptive immunity that typically manifest as recurrent and relapsing nontuberculous mycobacterial infections among infected individuals (Haverkamp *et al.*, 2006). In mouse models in which IFNγ signaling is disrupted by monoclonal antibodies to IFNγ or by germline mutations of the IFNγ-receptor (Huang *et al.*, 1993), mice are more susceptible to infections by certain pathogens, such as *Leishmania major* (Belosevic *et al.*, 1989; Muller *et al.*, 1989), and in the case of infection with avirulent Bacillus Calmette-Guerin (BCG), the vaccine strain of *Mycobacterium bovis*, are unable to combat infection and die (Kamijo *et al.*, 1993).

Many different cells of the immune system can produce IFNγ, including CD4+ T helper cell type 1 (Th1) lymphocytes, CD8+ cytotoxic lymphocytes, NK and NKT cells, monocytes, macrophages, and dendritic cells (Schroder *et al.*, 2004). IFNγ activates macrophages mainly through gene regulation and signals through the Janus kinase – signal transduction and activator of transcription (Jak-Stat) pathway, but it is not the only pathway identified (Gough *et al.*, 2008). Jak-Stat signaling is used by over 50 cytokines, growth factors, and hormones (Subramaniam *et al.*, 2001). Upon binding to the IFNγ-receptor (IFNGR), consisting of two signal transducing IFNGR1 and IFNGR2 chains, IFNγ induces Jak2 autophosphorylation and consequent transphorylation of Jak1. Phosphorylated Jak2 phosphorylates tyrosine residues on the IFNGR1 chains, which provide adjacent docking sites for the SH2 domains of Stat1 and subsequent Stat1 homodimer formation. Stat1 homodimers quickly dissociate from the receptor and travel to the nucleus to initiate/suppress gene transcription at IFNγ-activation site (GAS) elements. It is important to note that some of the genes activated via GAS elements encode transcription factors (such as IFNγ regulatory factor-1, IRF-1) that further drive transcription alone or in combination with Stat1, leading to "waves" of transcription (Schroder *et al.*, 2004).

3. IFNγ increases CYBB gene expression.

IFNγ induces CYBB expression, the gene encoding gp91^{phox}, in neutrophils and macrophages (Newburger *et al.*, 1988), which is Jak/Stat regulated (Kakar *et al.*, 2005). Transcription factors PU.1, IRF1, and ICSBP were found to act cooperatively to induce CYBB expression following IFNγ stimulation in a promyelocytic cell line, U937 (Eklund

et al., 1998). In addition to CYBB, the genes encoding $p47^{phox}$ and $p67^{phox}$, NCF1 (Cassatella *et al.*, 1990; Levy *et al.*, 1990; Amezaga *et al.*, 1992) and NCF2 (Levy *et al.*, 1990; Gupta *et al.*, 1992), have also been found to be regulated by IFNγ. Currently, it is believed that the primary mechanism by which IFNγ stimulation amplifies superoxide production is through increased transcription of CYBB and NCF2 genes, leading to increased protein expression of $gp91^{phox}$ and $p67^{phox}$ subunits (Schroder *et al.*, 2004).

4. Lipopolysaccharide (LPS)

LPS, the major structural component of the outer membrane of Gram-negative bacteria, has also been shown to activate macrophages to release a plethora of cytokines and chemokines important for pathogen clearance (Guha and Mackman, 2001). Through activation of the Toll-like-receptor 4 (TLR4), LPS has been shown to activate two major transcription factors, AP-1 and NFκB, through MyD88-dependent signaling and to activate STAT1 through a MyD88-independent mechanism. These transcription factors increase expression of TNFα, IL-1β, IL-6, and iNOS (Kopydlowski *et al.*, 1999). In neutrophils, it has been shown that LPS can increase protein expression of $gp91^{phox}$ (Cassatella *et al.*, 1990), but little or no data exists on the regulation of CYBB by LPS in macrophages.

In addition, activation of macrophages with IFNγ and LPS decreases the rates of fluid phase pinocytosis, phagocytosis, and delays the progression of phagosomes to late endosomes and lysosomes, which was suggested to enhance killing and antigen processing (Tsang *et al.*, 2000).

VIII. SCOPE OF THIS WORK

In macrophages, many intracellular pathogens avoid oxidative killing by targeting the NADPH oxidase. Studies of *Salmonella typhimurium* suggest localization of the membrane-bound heterodimer, flavocytochrome *b*, to the phagosome is essential for microbial killing, yet the subcellular distribution of flavocytochrome *b* in macrophages is not well characterized. The goal of our studies was to more fully characterize the distribution and trafficking of flavocytochrome *b* in resting and IFNγ and LPS stimulated macrophages. We generated fluorescently tagged $p22^{phox}$ and $gp91^{phox}$ probes and rigorously tested their functionality in Chinese Hamster Ovary cells (CHO). Initial studies in CHO cells also investigated the role of the individual subunits in directing trafficking of the heterodimer. Localization of flavocytochrome *b* was then examined in both RAW 264.7 murine macrophages and primary murine bone marrow derived macrophages (BMDMs) in the presence and absence of IFNγ and/or LPS stimulation. Our results show that endogenous and transfected flavocytochrome *b* localizes to similar intracellular compartments in these three cell types in the absence of stimuli and demonstrate for the first time that macrophage flavocytochrome *b* is present in intracellular compartments that recycle to the plasma membrane. In the presence of IFNγ, but not LPS, we found a time-dependent increase in the cell surface expression of flavocytochrome *b*, which correlated with increased flavocytochrome *b* protein expression and NADPH oxidase activity. The enhanced release of superoxide in IFNγ activated cells was found to be inhibited by superoxide dismutase (SOD), which suggests an extracellular release of superoxide. Our results suggest the change in distribution of flavocytochrome *b* may be important for the production of extracellular superoxide in

macrophages and that the change in trafficking of flavocytochrome *b* may be a potential new mechanism by which IFNγ enhances antimicrobial activity in macrophages.

CHAPTER TWO: MATERIALS AND METHODS

I. Antibodies and Reagents

Anti-gp91^{phox} monoclonal antibodies (mAbs) 54.1 and CL5 (Burritt *et al.*, 1995; Baniulis *et al.*, 2005), and anti-p22^{phox} mAbs NS2 and 44.1 (Taylor *et al.*, 2004) were kindly provided by A.J. Jesaitis (Montana State University). 7D5 mAb (anti-gp91^{phox}), collected from hybridoma cells kindly provided by M. Nakamura (Nagasaki University) (Yamauchi *et al.*, 2001), and a rabbit polyclonal anti-p22^{phox} (Dinauer *et al.*, 1991) were described previously. The following antibodies were purchased: anti-calnexin (StressGene, Victoria British Columbia, Canada), anti-Rab11 (Zymed Laboratories, San Francisco, CA,), anti-β-actin (Sigma-Aldrich St. Louis, MO), anti-GFP (Santa Cruz Biotechnology, Santa Cruz, CA, Cat#sc-8334), secondary HRP-conjugated antibodies (Promega, Madison, WI) and R-Phycoerythrin (PE)-conjugated Rat anti-mouse IgG_1, Rat anti-mouse CD16/C32, and Rat anti-mouse MHCII-I-A/I-E (BD Pharmingen, San Jose, CA). Alexa Fluor labeled secondary antibodies, and Alexa Fluor 647-labeled Dextran (10,000 MW) and labeled human transferrin were from Molecular Probes (Invitrogen, Carlsbad, CA). Mouse transferrin (Sigma-Aldrich) was iron loaded and tagged to Alexa Fluor 647 (Molecular Probes) to generate mTfn-AF647 as previously described (Yamashiro *et al.*, 1984). Phosphate buffered saline (PBS, pH 7.2), penicillin/streptomycin, neomycin, trypsin/ethylene diamine tetra-acetate (EDTA), Dulbecco's modified Eagle's medium (DMEM) with low glucose, α-Minimum Essential Medium (αMEM), Ham's F12K medium, cell dissociation Buffer, and Lipofectamine^{TM} 2000 were purchased from Invitrogen Life Technologies. Fetal calf serum (FCS) and

bovine growth serum (BGS) were purchased from HyClone Laboratories (Logan, UT). Murine macrophage colony stimulating factor (M-CSF) and recombinant IFNγ (>1x10^7 units/mg) were purchased from Peptrotech (Rocky Hill, NJ). LPS of *S. typhimurium*, was obtained from Calbiochem. All other reagents were from Sigma-Aldrich.

II. Labeling of cells with fluorescently tagged ligands

Cells plated on coverslips were washed once in their corresponding media (37°C, no serum) and then incubated with Alexa Fluor 647-labeled transferrin (Tfn-AF647) or Alexa Fluor 647-labeled Dextran (Dex-AF647) diluted in the same media for the times indicated. For live cell imaging, cells plated on Mat-tek® coverslip dishes were washed once in PBS (37°C) and then incubated with fluorescently tagged ligands diluted in 0.01M HEPES buffer in PBSG (PBS plus 0.5 mM $MgCl_2$, 0.9 mM $CaCl_2$ and 7.5 mM dextrose). 20 μg/ml Tfn-AF647 was used for labeling recycling endosomes in CHO cells and 5 μg/ml for labeling recycling endosomes in macrophages. 10 μg/ml Dex-AF647 was used for labeling lysosomes in CHO cells. In some experiments, cells were chased with media (37°C) as described.

III. Mouse strains

Homozygous nmf333 mice (A.B6-Tyr+/J genetic background), which harbor a T to C point mutation in the *Cyba* gene encoding $p22^{phox}$ and lack expression of $p22^{phox}$, were kindly provided by Botond Banfi (University of Iowa, Iowa City, IA) (Nakano *et al.*, 2008). The C57BL/6Ai $p47^{phox-/-}$ mouse, purchased from Taconic (Hudson, New York), was originally generated by Jackson and colleagues (Jackson *et al.*, 1995) by

insertion of a neomycin (neo) resistant cassette into exon 7 of the mouse p47^{phox} gene (NCF1) in embryonic stem (ES) cells. gp91$^{phox-/-}$ (referred to as CGD) mice were also generated by gene targeting and a neo cassette was placed into exon 3 of the gp91^{phox} gene (CYBB) (Pollock *et al.*, 1995). C57BL/6J and A.B6-Tyr+/J mice were obtained from the Jackson Laboratory (Bar Harbor, ME).

IV. Differentiation of bone marrow derived macrophages

1. BMDM Protocol One

Three days following intraperitoneal injection of 150 mg/kg 5-fluorouracil (5-FU), BM cells were harvested from femurs and tibias by flushing with αMEM. The day of BM harvest was considered Day 0. BM cells were pelleted and re-suspended in prestimulation media, αMEM with 20% heat inactivated fetal calf serum, 100 ng/ml stem cell factor (SCF), 100 U/ml Interleukin-6 (IL-6), 10 U/ml penicillin, and 100 μg/ml streptomycin) for 96 hr. On day 4, the combined suspended and adherent cells were collected using cell dissociation buffer and differentiated into BMDMs as described previously (Racoosin and Swanson, 1989) with some minor changes. 5 x 10^5 BM cells were suspended in 3 ml of αMEM media containing 20% heat inactivated FCS, 25 ng/ml murine M-CSF (Peprotech), 10 U/ml penicillin, and 100 μg/ml streptomycin (referred to as differentiation media). In addition, we initially plated BM cells in one well of a 6-well tissue culture dish for 3 days in differentiation media and then aspirated the non-adherent cells (Day 3 of differentiation) and transferred them to a 150 mm Petri dish, whereas adherent cells were discarded. Following 3 more days of differentiation (Day 6 of differentiation), adherent cells were then collected, or new differentiation media was

added for an additional 3 more days. To collect adherent BMDMs, the media was aspirated and discarded, and cold PBS (10 ml) was added to the dish. The dish was placed on ice, or at 4°C, for 10 - 15 min. Cells were then collected by aspirating the PBS and adding it back to the dish, repeating this multiple times until the cells were lifted, which was monitored using a light microscope. Day 6- to Day 9-differentiated BMDMs were plated according to the experiment, as described in the methods.

2. BMDM Protocol Two

Bone marrow derived macrophages were obtained using conditions adapted from Racoosin and Swanson (Racoosin and Swanson, 1989). Total bone marrow cells flushed from mouse femurs were washed twice in αMEM media (4°C). Total bone marrow cells from each mouse were suspended in 20 ml αMEM with 20% HI FCS, 25 ng/ml M-CSF, 10 units/ml penicillin, and 100 μg/ml streptomycin and plated onto a single 150 mm Petri dish (non-tissue culture plastic) (Day 0). Following 2 hr at 37°C, non-adherent cells were aspirated and transferred to a new 150 mm Petri dish, whereas adherent cells were discarded. After 3 days of differentiation, non-adherent cells were collected, centrifuged, re-suspended in fresh differentiation media, and added back to the 150 mm Petri dish. On Day 6 of differentiation, adherent cells were either collected using cold PBS, as described above, or new media was added. Day 6- to Day- 9 differentiated BMDMs were plated according to the experiment, as described in the following methods.

V. Expression vectors

1. Generation of fluorescently tagged $p22^{phox}$ and $gp91^{phox}$ constructs

For generation of $p22^{phox}$ full length (wild-type) and $p22^{phox}$ C-terminal deletion fragments, primers specific to $p22^{phox}$ (listed in Table III) were developed to amplify the desired region of $p22^{phox}$ and to add HindIII and EcoRI restriction sites at the 5' and 3' regions of the amplified human $p22^{phox}$ cDNA. Amplified fragments were cloned into the HindIII and EcoRI sites of the mammalian expression vector eYFP-N1 (Clontech, Palo Alto, CA) to generate $p22^{phox}$ (1-195)/eYFP-N1 (referred to as 22YFP), $p22^{phox}$ (1-171)/eYFP-N1 (referred to as 172YFP), $p22^{phox}$ (1-148)/eYFP-N1 (referred to as 149YFP), and $p22^{phox}$ (1-130)/eYFP-N1 (referred to as 131YFP) constructs. Full length $p22^{phox}$ (1-195), $p22^{phox}$ (1-148), and $p22^{phox}$ (1-130) cDNA were also subcloned from 22YFP into the mDsRED-N1 (Clontech), the mCFP-N1, or the mCIT-N1 (both were kindly provided by J. Swanson, University of Michigan) vectors using the HindIII and EcoRI restriction sites to generate 22RED, 22CFP, 22CIT, 22C149CIT, and 22C131CIT. Fluorescently tagged probes utilized in our studies are listed in Table IV.

The human $gp91^{phox}$ cDNA was excised from $gp91^{phox}$/KS+Bluescript (Zhen *et al.*, 1993) using BamHI, and ligated into the BamHI site in pcDNA3.1+ (Invitrogen) to generate gp91/pcDNA3.1+. The cDNA $gp91^{phox}$ was then subcloned into the HindIII and SalI sites of peCFP-C1 by digesting gp91/pCDNA3.1+ with HindIII and XhoI to generate peCFP-C1/gp91 (referred to as CFP91, sequence available upon request). This construct expressed $gp91^{phox}$ tagged at its N-terminus with CFP, with an intervening 31 amino acids, where 22 were derived from polylinker sequence carried over from the insert in $gp91^{phox}$/KS+Bluescript and 9 were from the multiple cloning site within pECFP-C1.

Table III. Primers designed for 22YFP constructions[a]

cDNA fragment generated	Primer sequence
HindIII-p22^{phox}(1-585)_EcoRI 22YFP	Fwd: 5'_TATAC**AAGCTT**CAATGGGGCAGATCGAG_3' Rev: 5'_TGAATTCTCACGACCTCGTCGGTCA_3'
HindIII-p22^{phox}(1-513)_EcoRI 172YFP	Fwd: 5'_TATAC**AAGCTT**CAATGGGGCAGATCGAG_3' Rev: 5'-TGAATTCTCTCCTCCTCGCTG-3'
HindIII-p22^{phox}(1-444)_EcoRI 149YFP	Fwd: 5'_TATAC**AAGCTT**CAATGGGGCAGATCGAG_3' Rev: 5'-TGAATTCTGATGGTGCCTCCGATC-3'
HindIII-p22^{phox}(1-390)_EcoRI 131YFP	Fwd: 5'_TATAC**AAGCTT**CAATGGGGCAGATCGAG_3' Rev: 5'-TGATTCTCTGCTCGCCACGCAC-3'

[a]Primers designed for generation of fluorescently tagged human p22^{phox} full length and C-terminal truncated proteins are listed above (right column) along with the cDNA fragments generated (left column). Coding sequences within the primers for p22^{phox} are underlined, while restriction enzymes are in bold.

Table IV. Fluorescently tagged proteins used in this study[a]

Fluorescently tagged proteins	Abbreviation
p22^{phox} (1-195)/eYFP	22YFP
p22^{phox} (1-171)/eYFP	172YFP
p22^{phox} (1-148)/eYFP	149YFP
p22^{phox} (1-130)/eYFP	131YFP
p22^{phox}/eCFP	22CFP
p22^{phox}/mDsRED	22RED
p22^{phox}/mCIT	22CIT
p22^{phox} (1-148)/mCIT	149CIT
p22^{phox} (1-130)/mCIT	131CIT
eCFP/gp91^{phox}	eCFP91
mCFP/gp91^{phox}	mCFP91
mCIT/gp91^{phox}	YFP91
Rab5/eGFP	Rab5GFP
Rab7/eGFP	Rab7GFP
Rab11/eCFP *	CFPRab11
eGFP/Rab11a*	GFPRab11
PH(PLCγ)/eGFP	PHGFP
FcγR11a/eGFP	FcγRGFP
(1-72)GAD65-eGFP	mGAD65GFP

[a]The fluorescently tagged proteins used in this study (left column) are shown along with the abbreviated nomenclature (right column). All transgenes were of human origin except those marked by *, which are of rabbit origin. For constructs expressing YFP-tagged p22^{phox} and C-terminal deleted derivatives, the amino acids present in full length (amino acids 1-195) and truncated forms are indicated.

gp91^{phox} was further subcloned from pECFP-C1/gp91^{phox} into mCFP-C1 (provided by J. Swanson, University of Michigan) and mCIT-C1 to generate pmCFP-C1/gp91^{phox} and pmCIT-C1/gp91^{phox} using the HindIII and XhoI multiple cloning sites to maintain the same linker between the fluorescent tag and gp91^{phox}. mCIT-N1 is a derivative of YFP with a single amino acid change that reduces potential changes in fluorescence due to low pH, but otherwise functions essentially the same as YFP (Griesbeck *et al.*, 2001) for simplicity pmCIT-C1/gp91^{phox} will be referred to as YFP91 (see Table IV).

pEF- and pRK5-based vectors for expression of p47^{phox} and p67^{phox} were described previously (Price *et al.*, 2002). Rab11eCFP (Babbey *et al.*, 2006) and Rab11eGFP (Wang *et al.*, 2001) were described previously. The following expression vectors were generous gifts: Rab5eGFP (G. Li, Washington University), Rab7eGFP (A. Wandinger-Ness, University of New Mexico), 1-72GAD65(C30,45A)-GFP (referred to as mGAD65GFP, S. Baekkeskov, University of California San Francisco), and FcγRIIa-GFP and PH-(PLCγ)-GFP (S. Grinstein, Hospital for Sick Children, Toronto).

2. Retroviral vectors

A YFP-expressing retroviral vector MSCV-eYFPN1 was generated by subcloning the eYFP cDNA and the multiple cloning sites up to and including BglII at the 5' end of eYFP from peYFP-N1 (Clontech) into the MSCV-pac vector backbone (Clontech) after removing the puromycin expression cassette. Human p22^{phox} was then subcloned from p22eYFP-N1 (described above) using the HindIII and EcoRI sites and inserted into pMSCV-eYFP-N1 to generate pMSCV-p22eYFP-N1 (referred to as MSCV-22YFP).

Retroviruses were packaged using the Pantropic Retroviral Expression System (Clontech) and stored at -80°C until use, according to the manufacturer's instructions.

3. Transgene expression in CHO-K1 cell lines

CHO-K1 (CHO) cell lines utilized in these studies are listed in Table V. Parental CHO cells or derivatives expressing NADPH oxidase transgenes were transfected using Lipofectamine™ 2000 according to manufacturer's instructions. CHO-22 and CHO-91-67-47 [which will be referred to as CHO-22 and CHO-91 (Biberstine-Kinkade *et al.*, 2002), respectively] were previously generated for stable expression of untagged $p22^{phox}$ and $gp91^{phox}$. Similarly, CHO cells were transfected with YFP91 or co-transfected with $p47^{phox}$ and $p67^{phox}$ to generate CHO-YFP91 and CHO-47-67 cell lines. 22YFP was transfected in the CHO-91 cell line to generate CHO-91-22YFP cells. CHO-91-22YFP cells express $p47^{phox}$ and $p67^{phox}$, but for the purposes of these experiments, the absence or presence of $p47^{phox}$ and $p67^{phox}$ has no significant effect on the localization of $p22^{phox}$, which is illustrated by the similar distributions of 22CFP, expressed in CHO-YFP91 cells that lack $p47^{phox}$ and $p67^{phox}$, and 22YFP, expressed in CHO-91-22YFP cells that express $p47^{phox}$ and $p67^{phox}$ (Figures 11C and 14C). For stable expression of YFP-tagged proteins in CHO-YFP91 and CHO-91-22YFP cell lines, cells were selected in 1.6 mg/ml neomycin for at least two weeks, followed by flow cytometric cell sorting (FacsAria, Becton Dickinson Biosciences) to collect strongly fluorescent cells and to discard cells with little to no fluorescence. Cell sorting increased the percent positive 22YFP cells from 18% to 75% in the CHO-91-22YFP cell line and 22% to 70% in CHO-YFP91 cell line. After sorting, CHO-YFP91 cells were maintained in 0.8 mg/ml neomycin, and

Table V. CHO-K1 and RAW 264.7 cell lines used in this study[a]

Cell line	Parental cells	Transgene (s)
CHO-WT	CHO-K1	--
CHO-22*	CHO-K1	$p22^{phox}$/PGKneo
CHO-YFP91	CHO-K1	mCIT/$gp91^{phox}$
CHOf-22-YFP91	CHO-K1	MFG-FcγRIIa+$p22^{phox}$/PGKneo+ mCIT/$gp91^{phox}$
CHO-91	CHO-K1	MFG-S/$gp91^{phox}$+$p47^{phox}$/PGKhygro+$p67^{phox}$/PGKpuro
CHO-91-22YFP	CHO-91	$p22^{phox}$ (1-195)/eYFP
CHO-91,67,47,22	CHO-K1	MFG-S/$gp91^{phox}$+$p47^{phox}$/PGKhygro+$p67^{phox}$/PGKpuro+$p22^{phox}$/PGKneo
CHO-47-67*	CHO-K1	$p47^{phox}$/PGKhygro+$p67^{phox}$/PGKpuro
RAW-WT	RAW 264.7	--
RAW-22YFP*	RAW 264.7	$p22^{phox}$ (1-195)/eYFP
RAW-YFP91	RAW 264.7	mCIT-C1/$gp91^{phox}$
RAW-91,22*	RAW 264.7	$gp91^{phox}$/pEFpacpuro+$p47^{phox}$/PGKhygro+ $p22^{phox}$/PGKneo
RAW-22CIT	RAW 264.7	$p22^{phox}$(1-195)/mCIT
RAW-22C149CIT	RAW 264.7	$p22^{phox}$ (1-148)/mCIT
RAW-22C131CIT	RAW 264.7	$p22^{phox}$ (1-130)/mCIT

[a]The nomenclature for CHO-K1 and RAW 264.7 cell lines used in this study (left column) are shown, along with the parental cell line and transgenes (right columns). *denotes a clonal cell line.

CHO-91-22YFP cells were maintained in 0.8 mg/ml neomycin, 1 μg/ml puromycin, and 0.2 mg/ml hygromycin. CHO cells were co-transfected with expression vectors for $p47^{phox}$ and $p67^{phox}$, and clones were obtained by limiting dilution in medium containing puromycin and hygromycin as described previously (Price *et al.*, 2002). CHO parental and derivative cell lines were maintained in Ham's F12 medium, 10% BGS, 0.15% sodium bicarbonate, 10 units/ml penicillin, and 100 μg/ml streptomycin as previously described (Zhu *et al.*, 2006).

4. Transgene expression in RAW 264.7 cell lines

RAW264.7 cell lines utilized in these studies are listed in Table V. RAW 264.7 macrophages were transfected using AMAXA (Cell Line Nucleofactor Solution Kit V, Gaithersburg, MD), according to the manufacturer's instructions. RAW 264.7 cells were transfected with the 22YFP vector to generate a RAW-22YFP stable cell line. After at least two weeks in selection in 1.6 mg/ml neomycin, RAW-22YFP clones were selected by limiting dilution in 96 well plates followed by screening using flow cytometry for YFP. RAW 264.7 cells were also transfected with YFP91, FcγRIIa-GFP, PH-(PLCγ)-GFP, 22CIT, 22C149CIT, or 22C131CIT and selected in 0.8 mg/ml neomycin to generate RAW-mCIT-C1/$gp91^{phox}$ (referred to as RAW-YFP91), RAW-FcγRIIa-GFP (referred to as RAW-FcγR-GFP), RAW-PH-(PLCγ)-GFP (referred to as RAW-PH-GFP), RAW-22CIT, RAW-22C149CIT, and RAW-22C131CIT cell lines. RAW 264.7 cells were also transfected with $gp91^{phox}$/pEFpacpuro, $p47^{phox}$/PGKhygro, $p22^{phox}$/PGKneo using Fugene-6 transfection reagent (Roche Diagnostics) to generate RAW-91,22,47 cells, which will be referred to as RAW-91,22 for simplicity in these studies. RAW-91,22,47 cells were

made sequentially by first generating RAW-47, then RAW-91,47, and then RAW-91,22,47 cells, clones were selected from each cell line by limiting dilution. RAW 264.7 cells were maintained with or without selection antibiotics in low glucose DMEM, 10% heat inactivated FCS, 10 units/ml penicillin, and 100 μg/ml streptomycin.

For passaging of cells in culture or collecting cells for analysis, CHO and RAW 264.7 cells were harvested using trypsin (0.05% in EDTA) as described previously for CHO cells (Zhu *et al.*, 2006).

5. Retroviral transduction of primary murine bone marrow cells

Retroviral transduction of murine bone marrow (BM) cells with MSCV-22YFP was performed as previously described (Yamauchi *et al.*, 2005). Briefly, three days following intraperitoneal injection of 150 mg/kg 5-fluorouracil (5-FU), BM cells were harvested from femurs and tibias by flushing with αMEM. The day of BM harvest was considered Day 0. BM cells were pelleted and re-suspended in prestimulation media αMEM with 20% heat inactivated fetal calf serum, 100 ng/ml stem cell factor (SCF), 100 U/ml Interleukin-6 (IL-6), 10 U/ml penicillin, and 100 μg/ml streptomycin) for 48 hr. On days 2 - 4, cells were transduced every 24 hr with retrovirus supernatant for 4 hr. After the 4 hr transduction, the retroviral supernatant was removed and "fresh" media and cytokines (IL-6 and SCF) were added. On day 4, after the last 4 hr of transduction, the combined suspended and adherent cells were collected using cell dissociation buffer and differentiated into BMDMs as described for BMDM Protocol One.

VI. Cytokine stimulation

After 6 - 9 days of differentiation, as indicated in M-CSF, following Protocol One (page 33), BMDMs were counted, centrifuged, re-suspended in the presence or absence of differentiation media or stimuli as described, and re-plated onto 100 mm Petri dishes at $1x10^6$ cells/dish.

RAW 264.7 cells proliferate in culture, but proliferation of many cells is inhibited by IFNγ treatment (Maher *et al.*, 2007). Thus, to obtain approximately 60 - 90% confluency for RAW 264.7 cells cultured in the presence or absence of IFNγ and to prevent cells cultured in the absence of IFNγ from overgrowing, the following cell numbers were plated in 100 mm culture treated dishes for the indicated times: $1.2x10^6$ (no IFNγ and IFNγ 24 hr), $6x10^5$ (no IFNγ and IFNγ 48 hr), $3x10^5$ cells (no IFNγ 72 hr) and $6x10^5$ (IFNγ 72 hr). Following treatment, RAW 264.7 macrophages were collected by trypsinization from tissue culture treated plates, while primary transduced BMDMs (Protocol One) were collected from Petri dishes with cold PBS.

Stimulants were used at the following working concentrations: murine IFNγ (0.1 - 500 ng/ml), murine TNFα (20 - 200 ng/ml), or LPS of *S. typhimurium* (0.02 - 1.0 μg/ml) in DMEM (for RAW) and αMEM (for BMDMs) with 10% heat inactivated FCS and P/S for 24 - 72 hr. For IFNγ studies with multiple concentrations of IFNγ, serial dilutions of IFNγ were prepared. IFNγ (0.1 - 0.5 mg/ml) was stored in aliquots at -20°C for up to 6 months, and LPS (2.5 mg/ml) was stored at 4°C for up to 1 year. A blocking antibody for TNFα was used at 0.2 - 10 μg/ml and stored at 4°C for up to 1 year.

VII. Analysis of protein expression

1. SDS/PAGE and Western blotting

Ten to thirty micrograms of total protein from Triton X-100 cell extracts was added to each well of a 9% or 12% SDS-polyacrylamide gel, electrophoresed, transferred to nitrocellulose membranes and probed for protein expression by immunoblotting as described (Price *et al.*, 2002; Zhu *et al.*, 2006). Primary antibodies were used at the following dilutions in Tris buffered saline with 0.1% Tween 20 (TBST): Rabbit anti-GFP, which also recognizes YFP, (1:1,000), mouse anti-gp91^{phox} (1:1-5,000 for either 54.1 or CL5), rabbit anti-p22^{phox} (1:5-10,000), mouse anti-p22^{phox} (1:500-1,000), mouse β-actin (1:10,000), rabbit anti-p67^{phox} (1:5,000), rabbit anti-p47^{phox} (1:15,000), rabbit anti-p40^{phox} (1:3,000), mouse anti-iNOS TypeII (1:2,000), and secondary HRP-conjugated antibodies (1:10,000).

2. Flow Cytometry

gp91^{phox} cell surface expression and the transfection efficiency of fluorescently tagged proteins were evaluated by flow cytometry. CHO and RAW 264.7 cells were suspended at 0.5 - 1.0 x10^6 cells/ ml in FACS buffer (0.1% BSA in PBS) with 10% normal goat serum for 30 min and kept at 4°C throughout the staining procedure. 7D5 supernatant (1:20 dilution) and PE-conjugated primary (1:100) or secondary antibodies (1:200) were diluted in FACS buffer and incubated with cells for 30 min. Fluorescence was measured by FAC-Scan (Becton Dickinson, San Jose, CA). In some experiments, stained cells were fixed with 1% paraformaldehyde at 4°C overnight, and subsequently

analyzed 24 - 48 hr later, with results the same as those obtained with freshly stained, unfixed cells.

3. Isolation of biotinylated proteins

Immunoprecipitation of biotinylated cell surface proteins was performed using the EZ Link Sulfo-NHS-SS-Biotin kit from Pierce (Catalog #89881) per manufacturer's instructions with minor changes. The manufacturer's instructions suggested biotinylation assays be performed in 75 mm flasks with a maximum of $1x10^7$cells /flask per condition. RAW 264.7 cells were plated in quadruplicate flasks for each condition for 72 hr. One set of duplicate flasks was combined following biotinylation of surface proteins. The other set of duplicate flasks was combined without biotinylating the cell surface and was used as a control to biotinylate total proteins in the cell lysate as described previously (Turvy and Blum, 2001). To compensate for differences in proliferation, as described above, $9x10^5$ cells were plated in the presence of IFNγ and $3x10^5$ cells in the absence of IFNγ for 72 hr.

Following biotinylation of the cell surface or cell lysate, biotinylated proteins were immunoprecipitated using the Neuravidin columns and eluted in a total volume of 200 μl. Due to the substantial increase in gp91^{phox} isolated from IFNγ stimulated samples, the amount of each sample was optimized to result in approximately the same density following Western blotting for gp91^{phox} protein expression. Densitometric analysis was performed and any differences in the amount of sample added to the well was included in the calculation and is described in the figure legend.

VIII. NADPH Oxidase Activity

1. Isoluminol

NADPH oxidase activity in CHO cells was measured by isoluminol-enhanced chemiluminescence following stimulation with arachidonic acid (AA) as described previously (Zhu *et al.*, 2006). Briefly, $1x10^5$ cells/well of a 96-well plate were pre-incubated at 37°C in PBSG, horseradish peroxidase (HRP, 20 U/ml), and isoluminol (50 μM) for 10 min. For each experiment, one well containing all solutions but no cells was used to calculate background luminescence. Relative light units (RLU) were recorded every 100 sec for 30 min by the Fast Kinetic module in an Lmax microplate luminometer from Molecular Devices (Sunnyvale, CA) following stimulation with AA. Integrated RLU values (area under the curve) were calculated by SOFTmax software (Molecular Devices) and background chemiluminescence was subtracted to report superoxide production. The number of cells per assay was increased from $1x10^5$ cells/well to $2x10^5$ cells/well for CHO-22 cells transfected with $p47^{phox}$, $p67^{phox}$, CFP91, or CFP (Figure 9, middle panel) due to lower transfection efficiency when introducing three plasmids.

2. Luminol

NADPH oxidase activity was assessed using luminol-enhanced chemiluminescence in RAW 264.7 cells and BMDMs (Protocol One). $1x10^5$ cells, unless stated differently in the figure description, were suspended in PBSG with horseradish HRP and luminol (final concentrations of 20 U/ml and 50 μM) and plated into each well of a 96 well plate in the presence or absence of superoxide dismutase (SOD, 75 μg/ml). Cells were pre-heated at 37°C for 10 min before addition of phorbol 12-myristate 13-

acetate (PMA, 300 ng/ml) or serum opsonized zymosan (SOZ, 0.4 mg/ml). To synchronize SOZ stimulated superoxide production, chemiluminescence was measured immediately following centrifugation at 700 rpm for 30 sec. RLUs were monitored at 60- to 90-sec intervals for 30 or 50 min by the Long Kinetic module in an Lmax microplate luminometer from Molecular Devices (Sunnyvale, CA). Integrated RLU values were calculated by SOFTmax software (Molecular Devices) and background chemiluminescence was subtracted (described above).

3. Nitroblue tetrazolium

BMDMs (Protocol Two) were plated in 8-well glass chamber slides for 24 to 72 hr to detect superoxide production using Nitroblue tetrazolium (NBT) as described previously (Ochs and Igo, 1973). $1x10^4$ BMDMs were plated to each well for 24 to 72 hr. Following 24 or 72 hr, NBT diluted in sterile αMEM with no FCS, was added to cells and incubated for 30 min at 37°C. Cells were then placed on ice, washed twice with cold PBS, fixed with cold methanol for 1 min, and dried overnight at room temperature. Finally, cells were counterstained with 0.2% safrinin. NBT is reduced in the presence of superoxide and forms an insoluble purple formazan deposit, which can be evaluated by light microscopy.

IX. Phagocytosis Assays

1. Serum opsonization of zymosan

Human serum was collected from 6 donors as described previously (Quinn *et al.*, 2007) using a protocol approved by the Institutional Review Board of Indiana University,

and all donors provided informed consent. Zymosan A (from *Saccharomyces cerevisiae*, Sigma) was suspended at 20 mg/ml in PBS, sonicated at max speed on ice for 10 sec intervals (repeated 5 times), washed in PBS, and resuspended to 20 mg/ml. Sonicated zymosan was opsonized with human serum as described previously (Quinn *et al.*, 2007).

2. Synchronized phagocytosis

RAW 264.7 cells and BMDMs (Protocol One) were plated on coverslips at approximately 50-70% confluency 24 hrs before phagocytosis assay. SOZ was diluted 1:100-1:500 in DMEM (for RAW) or αMEM (for BMDM) and added at approximately 3 - 5 zymosan particles per cell. Immediately after adding SOZ, cells were centrifuged at RT for 2 min at 800 g and then fixed immediately or incubated for an additional 13 min at 37°C for a total of 2 or 15 min to allow for internalization. Cells were then washed twice with PBS (RT) and then fixed, permeabilized, and stained as described below.

3. Frustrated phagocytosis

BSA (3 mg/ ml), followed by anti-BSA (Rabbit polyclonal, Sigma, 0.3 mg/ml) were coated onto acid-washed coverslips. Frustrated phagocytosis assays were performed as described previously (Takemura *et al.*, 1986). Briefly, RAW 264.7 cells were plated on coverslips coated with BSA-Rabbit IgG complexes, incubated for 60 min at 4°C for adherence, and then warmed to 37°C in cell incubator for 15 or 60 min. Cells were then fixed, permeabilized, and immunolabeled for confocal analysis as described below. BSA in the absence of rabbit IgG was used as our negative control.

X. Indirect immunofluorescence and confocal microscopy

1. Indirect immunofluorescence

CHO cells were plated on glass coverslips coated with 0.01% gelatin. RAW 264.7 cells were initially plated on glass coverslips coated with 0.01% gelatin for studies in the absence of IFNγ, but changed to uncoated, acid-washed coverslips for later experiments comparing the distribution of flavocytochrome *b* in the absence and presence of IFNγ. No difference in the distribution of flavocytochrome *b* on the different coverslips was observed (see Figures 23 and 39). BMDMs (Protocol One) were plated on uncoated, acid-washed coverslips for all experiments. Following 24 - 48 hr incubation, when cells were 50 - 80% confluent, monolayers were washed once in PBS, fixed in 4% paraformaldehyde for 10 min at room temperature, permeabilized in methanol:acetone (50:50) for 5 min at 4°C as described (Allen, 2008), washed in PAB (2% BSA, 0.05 g/L NaN_3 in PBS), and then blocked in 10% goat serum in PAB for 30 min at room temperature or overnight at 4°C. Primary antibodies were diluted in 5% goat serum in PAB at the following concentrations: anti-calnexin (1:400), anti-Rab11 (1:400), 54.1 mAb anti-gp91^{phox} (1:1,000), 44.1 mAb anti-p22^{phox} (1:2), and anti-CD16/CD32-PE (1:50). After 1 hr incubation, coverslips were washed and incubated with Alexa Fluor secondary Abs (1:600) in 10% goat serum in PAB for 45 - 60 min at room temperature. Coverslips were washed and mounted with Dako fluorescent mounting media (DakoCytomation). The specificity and optimal concentration of mAbs NS5 (anti-human p22^{phox}), 44.1 (anti-human p22^{phox}), and 54.1 (anti-gp91^{phox}) for immunofluorescence microscopy was evaluated in CHO parental, CHO-22, or CHO-91,67,47,22 cells (Figures 5A and 5B). In addition, the specificity of 54.1 for

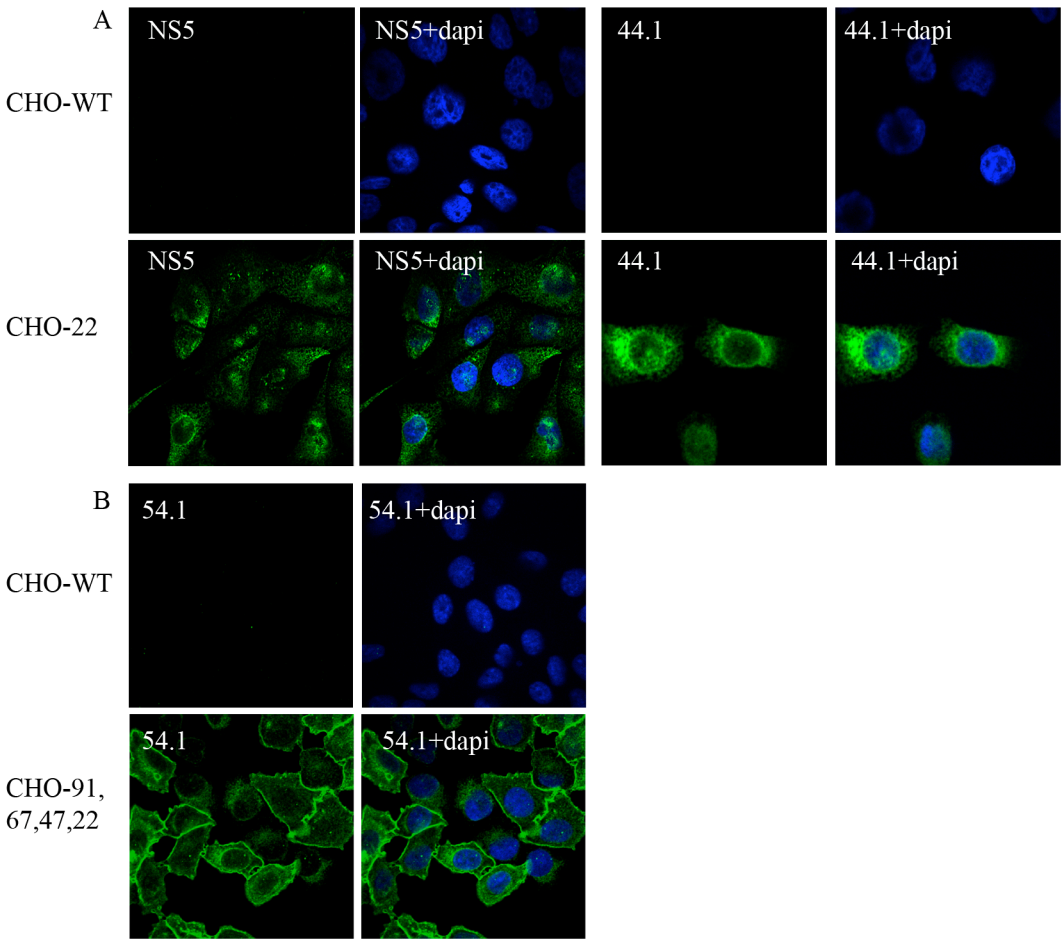

Figure 5. Validation of the specificity of $p22^{phox}$ and $gp91^{phox}$ antibodies in CHO cells. (A) CHO-WT and CHO-22 cells were fixed in 4% paraformaldehyde (10 min RT), permeabilized with 0.02% saponin (30 min RT), immunolabeled for $p22^{phox}$ using monoclonal antibodies NS5 (left panels) or 44.1 (right panels), and stained with the nuclear dye DAPI (10 μg/ml, 10 min RT). (B) CHO-WT and CHO-91,67,47,22 cells were fixed in 4% paraformaldehyde (10 min RT), permeabilized with methanol:acetone (5 min at 4°C), immunolabeled for $gp91^{phox}$ using monoclonal antibody 54.1, and stained with the nuclear dye DAPI (10 μg/ml, 10 min RT).

immunofluorescent staining of gp91^{phox} in macrophages was analyzed by comparing wild-type BMDMs to BMDMs obtained from gp91^{phox}-null CGD mice (Pollock *et al.*, 1995)(not shown). Preliminary experiments were also conducted in both CHO and RAW 264.7 cells to determine the optimal permeabilization method for immunofluorescent staining of flavocytochrome *b* subunits. In CHO cells, methanol:acetone appeared to be the best method based on the clear reticular distribution of p22^{phox} and surface expression of gp91^{phox} in CHO-91,67,47,22 cells (Figure 6A), which will be described in detail in the results section. In addition, a preliminary experiment in RAW 264.7 cells compared three methods of permeabilization (Triton, Saponin, and Methanol/Acetone) and found the combination of methanol and acetone to result in the highest fluorescent intensity (Figure 6B) and was used for all experiments in both RAW 264.7 cells and BMDMs (Protocol One).

2. Live cell imaging

Cells were plated onto Mat-tek® coverslip dishes 24 - 72 hr before imaging to result in approximately 50 - 70% confluency at the time of analysis. Cells were washed with PBSG (Price *et al.*, 2002) and then imaged in 0.01M HEPES buffer (Sigma) in PBSG at 37°C.

3. Confocal microscopy

Images from cells grown on coverslips or Mat-tek® coverslip dishes were acquired on one of two confocal systems: a Zeiss LSM510 (Carl Zeiss, Inc., Thornwood, NY) or a Perkin-Elmer Cetus Ultraview (Norwalk, CT) mounted on a Nikon TE 2000U

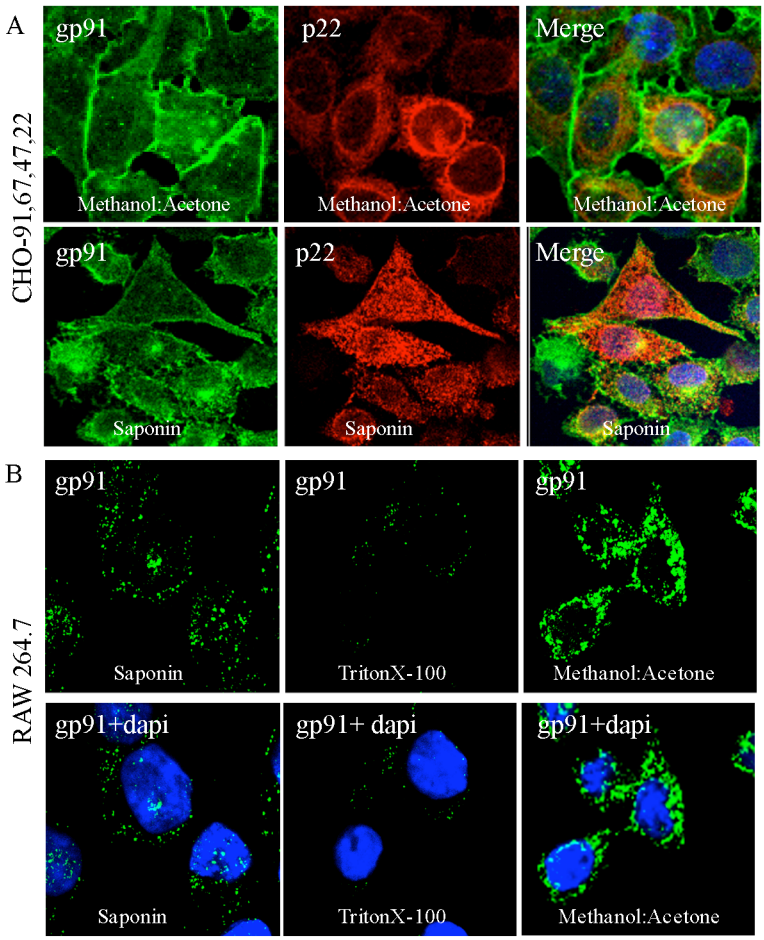

Figure 6. Optimal immunofluorescent staining of flavocytochrome *b* subunits in CHO and RAW 264.7 cells following methanol:acetone permeabilization. Cells were fixed in 4% paraformaldehyde for 10 min at room temperature (RT), permeabilized, immunostained for gp91^{phox} (mAb 54.1) or p22^{phox} (mAb 44.1) and then stained with the nuclear dye Dapi (10 μg/ml, 10 min RT). (A) Immunofluorescent staining of p22^{phox} and gp91^{phox} in CHO-91,67,47,22 cells. Cells were permeabilized with methanol:acetone (top panel) or 0.02% saponin (bottom panel). (B) Immunofluorescent staining of gp91^{phox} in RAW 264.7 cells. **From left to right:** cells were permeabilized with 0.02% Saponin, 0.1% TritonX-100, or methanol:acetone. Images were collected using the same settings to compare fluorescent intensity of p22^{phox} and gp91^{phox} staining using the methods described.

inverted microscope equipped with an Andor CCD camera. On both systems, a vertical series of images was collected using a Nikon 100X, NA 1.4x oil immersion planapochromatic objective (Melville, NY). For most images, the optimal single plane for each subcellular compartment is shown as follows: for the ER or the plasma membrane, the substrate-adherent surface is shown, and for the endocytic recycling compartment, the middle of the cell is shown.

4. Image analysis using ImageJ

Images acquired from confocal systems were opened in ImageJ and single plane images (0.16 – 0.5 μm Z sections) were saved as individual TIFF files after only cropping or adjusting the brightness and/or contrast; no other modifications were performed. For some images acquired from BMDMs, a vertical stack was merged using the Z stack projection tool of ImageJ (Rasband, 1997-2004). A total of at least 50 cells from at least three independent experiments were analyzed unless otherwise stated in the figure legend.

CHAPTER THREE: RESULTS

I. Generation of a model system in CHO cells for evaluating localization of flavocytochrome *b*

1. Construction of functional fluorescently tagged $p22^{phox}$ and $gp91^{phox}$ chimeras

In neutrophils, the stability of the individual flavocytochrome *b* subunits ($gp91^{phox}$ and $p22^{phox}$) is dependent on heterodimer formation, and free monomers are rapidly degraded by the proteasome. However, in CHO cells, which lack detectable endogenous $gp91^{phox}$ or $p22^{phox}$, the individual subunits are stable, and can be highly expressed (Biberstine-Kinkade *et al.*, 2002; Zhu *et al.*, 2006). In the absence of $p22^{phox}$, $gp91^{phox}$ is expressed in CHO cells predominantly as gp65, with little detected on the cell surface. Co-expressed $gp91^{phox}$ and $p22^{phox}$ form heterodimers and co-immunoprecipitate in CHO cells, which correlates with carbohydrate maturation of $gp91^{phox}$ resulting in an increase in size to 91 kDa and a marked increase in $gp91^{phox}$ cell surface expression (Zhu *et al.*, 2006). These results suggest that either $p22^{phox}$ or the heterodimer harbor localization signals that direct trafficking of flavocytochrome *b* to the cell surface, although the intracellular compartments where each subunit was localized in the absence or presence of its binding partner was not well defined in these studies.

To examine the subcellular distribution of individual subunits and the flavocytochrome *b* heterodimer, we developed constructs to express fluorescently tagged derivatives of $p22^{phox}$ and $gp91^{phox}$ to visualize their location by confocal microscopy. YFP-, CFP-, and RED-tagged constructs were generated (Figure 7A) to allow analysis of

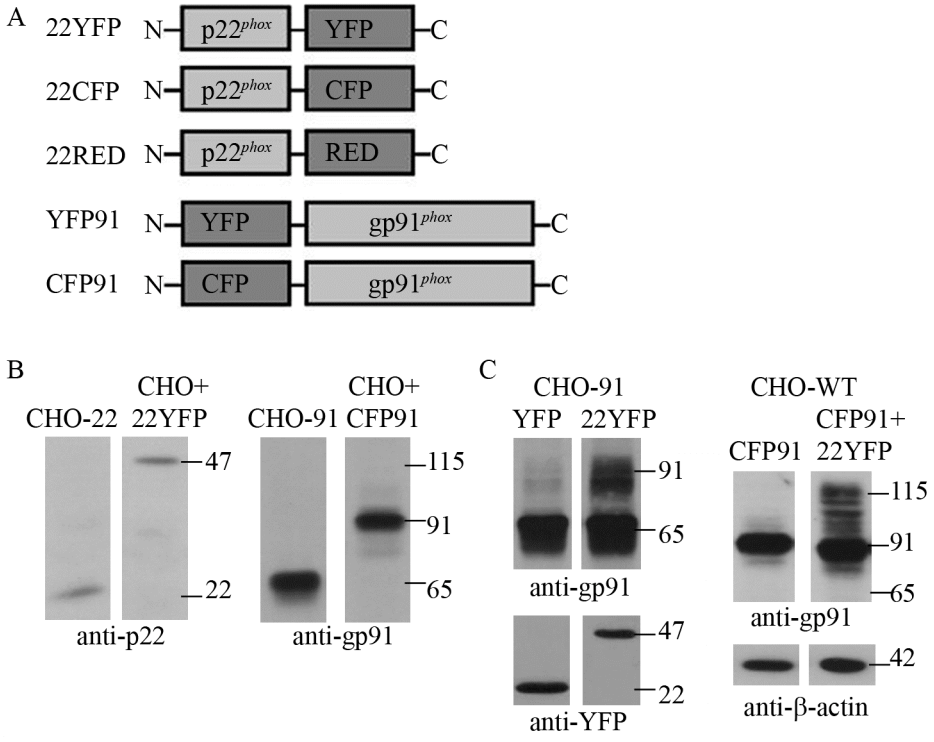

Figure 7. Fluorescently tagged p22^{phox} and gp91^{phox} are expressed at the correct molecular weights. (A) Schematic of constructs encoding fluorescently tagged p22^{phox} and gp91^{phox}. (B) 22YFP or CFP91 were transiently expressed in CHO-WT cell lines. Cell lysates prepared 48 hr post-transfection were analyzed by Western blotting using polyclonal anti-p22^{phox} and monoclonal anti-gp91^{phox} (CL5) antibodies. Cell lysates from CHO-22 and CHO-91 cells were used as controls. (C) Cell lysates from CHO-91 cells transiently expressing YFP or 22YFP, and CHO-WT cells expressing CFP91 or co-expressing CFP91 and 22YFP were analyzed by Western blotting at 48 hr post transfection for maturation of untagged and CFP-tagged gp91^{phox} (mAb CL5). YFP and 22YFP protein expression were validated with an antibody to YFP. Data shown are representative of at least 3 independent experiments.

subcellular targeting and the extent of subunit colocalization. Tags were placed on the C-terminus of $p22^{phox}$ and the N-terminus of $gp91^{phox}$, as depicted in Figure 7A. We hypothesized tags at these positions would less likely impair protein function based on previous studies that found the N-terminus of $p22^{phox}$ and the C-terminus of $gp91^{phox}$ were sensitive to mutagenesis and/or placement of an epitope tag (Zhen *et al.*, 1998; Zhu *et al.*, 2006). Fluorescently tagged subunits were each expressed in parental CHO cells following transient transfection, and Western blotting of cell lysates confirmed that the chimeras were expressed at the predicted molecular weights (Figure 7B and not shown). For example, with the addition of the YFP or CFP tag (~25 kDa), 22YFP was expressed at 47 kDa (Figure 7B) and CFP91 was expressed predominantly as a 91 kDa protein, corresponding to gp65 detected in CHO-91 cells (Figure 7B).

It was essential that the tagged subunits were capable of heterodimer formation. As mentioned earlier, this correlates with increased molecular weight of $gp91^{phox}$ as a result of carbohydrate maturation, and increased $gp91^{phox}$ cell surface expression. In CHO-91 cells, transient expression of 22YFP but not YFP induces formation of the 91 kDa form of $gp91^{phox}$, consistent with heterodimer formation between 22YFP and $gp91^{phox}$ (Figure 7C, left panel). Conversely, transient expression of CFP91 and 22YFP resulted in increased maturation of CFP91 to the 115 kDa form of CFP91 showing CFP91 is capable of heterodimer formation with fluorescently tagged $p22^{phox}$ (Figure 7C, right panel). In addition, untagged and fluorescently tagged $gp91^{phox}$ cell surface expression increased when co-expressed with tagged or untagged $p22^{phox}$ (Figure 8). Thus, fluorescent tags on $p22^{phox}$ or $gp91^{phox}$ do not interfere with heterodimer formation.

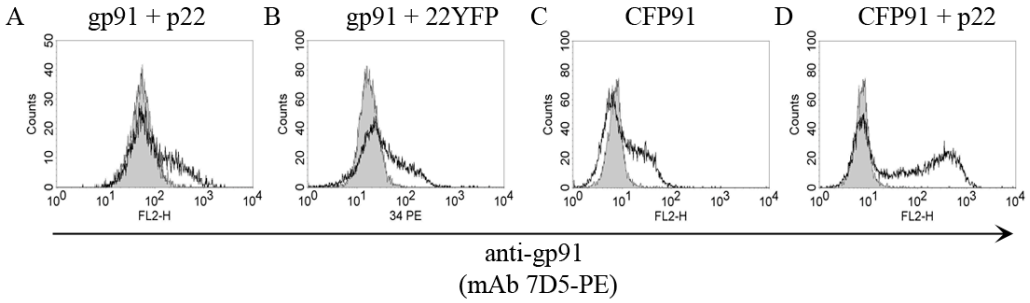

Figure 8. gp91^{phox} and CFP91 surface localization in CHO cells. Cells were stained for cell surface expression of gp91^{phox} or CFP91 (mAb 7D5) followed by a PE-labeled secondary antibody and analyzed by flow cytometry. CHO-91 cells (grey fill) transiently expressing (A) untagged p22^{phox} (black line) or (B) 22YFP (black line). (C) CHO-WT cells (grey fill) transiently expressing CFP91 (black line). (D) CHO-22 cells (grey fill) transiently expressing CFP91 (black line).

Next, we analyzed whether flavocytochrome *b* containing the fluorescent-tagged subunits was functional. Exogenous expression of p22^{phox}, gp91^{phox}, p47^{phox}, and p67^{phox} in CHO cells reconstitutes NADPH oxidase activity (Biberstine-Kinkade *et al.*, 2002; Zhu *et al.*, 2006). Transient expression of 22YFP but not YFP in CHO cells stably expressing gp91^{phox}, p47^{phox}, and p67^{phox} supported superoxide production similar to transient expression of untagged p22^{phox} (Figure 9A, left panel). CFP-tagged gp91^{phox} but not CFP alone was also functional when transiently co-expressed with p47^{phox} and p67^{phox} in CHO-22 cells (Figure 9A, middle panel). Transient co-expression of CFP91 and 22YFP in CHO cells with stable expression of p47^{phox} and p67^{phox} also supported NADPH oxidase activity (Figure 9A, right panel). Western blot analysis confirmed expression of p47^{phox} and p67^{phox} in CHO-47,67 cells (Figure 9B). These results establish that fluorescently tagged gp91^{phox} and p22^{phox} form functional heterodimers with each other and with the untagged partners.

2. Unassembled flavocytochrome *b* subunits localize to the ER in CHO cells

The intracellular compartments in CHO cells where p22^{phox} and gp91^{phox} reside in the absence or presence of each other were not well characterized in previous studies (Biberstine-Kinkade *et al.*, 2002; Zhu *et al.*, 2006). In promyelocytic PLB-985 cells, which are an undifferentiated neutrophil precursor cell line, unassembled gp91^{phox} and p22^{phox} reside in the ER membrane prior to heterodimer formation (DeLeo *et al.*, 2000). To determine if the distribution of unassembled subunits in CHO cells is similar to neutrophil precursors and to examine whether placement of the fluorescent tag altered this distribution, the subcellular location of untagged and fluorescently tagged p22^{phox} and

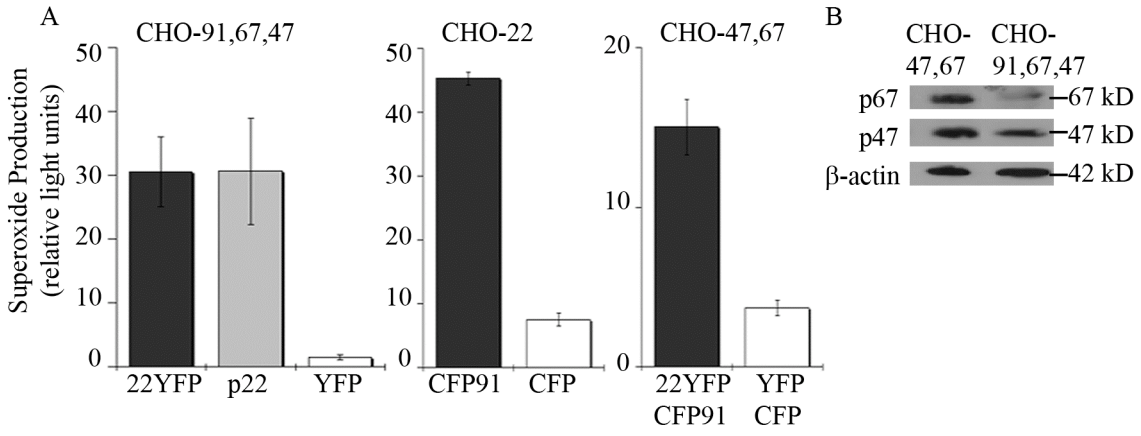

Figure 9. Fluorescently tagged p22^{phox} and gp91^{phox} form functional heterodimers in CHO cells. NADPH oxidase activity was measured using isoluminol chemiluminescence in arachidonic acid stimulated CHO cells transiently and/or stably expressing p47^{phox} and p67^{phox} with untagged or fluorescently tagged flavocytochrome subunits as indicated. Integrated RLU (relative light units) are shown. (A) **From left to right:** CHO-91-67-47 cells transfected with 22YFP (n=5), untagged p22^{phox} (n=3), or YFP (n=2). CHO-22 cells transfected with p47^{phox}, p67^{phox}, CFP91 (n=2), or CFP (n=1). CHO-47-67 cells transfected with 22YFP and CFP91 (n=5) or YFP and CFP (n=2). Mean +/- standard deviation of data for the number of experiments listed above. (B) Cell lysates from CHO-91,67,47 and CHO-47,67 stable cell lines were analyzed by Western blotting using polyclonal anti-p47^{phox} and monoclonal anti-p67^{phox} antibodies.

gp91^{phox} was evaluated by confocal microscopy. Both untagged p22^{phox} and gp91^{phox} in CHO-22 and CHO-91 cell lines, respectively, had an intracellular reticular distribution as visualized by immunofluorescence microscopy (Figure 10A). A similar distribution for 22YFP and for YFP91 when each was transiently expressed in CHO-WT cells was detected in living cells (Figure 10B) and in cells fixed and permeabilized (Figure 10C, left panel). These results show that neither subunit localized predominantly to the plasma membrane and that neither the fluorescent tag nor cell fixation and permeabilization altered the apparent location of p22^{phox} or gp91^{phox}.

The intracellular reticular distribution of p22^{phox} and gp91^{phox} shown in Figures 10A and 10B is characteristic of the endoplasmic reticulum (ER). Moreover, 22YFP and the ER marker calnexin strongly colocalized as shown in Figure 10C (merged image, top panel). Similar data were obtained for YFP91 and calnexin (Figure 10C, bottom panels). Thus, these data indicate that p22^{phox} and gp91^{phox} localize primarily to the ER when each is expressed individually in CHO-WT cells, consistent with studies performed using immature myeloid cells (DeLeo *et al.*, 2000).

3. Heterodimers of p22^{phox} and gp91^{phox} traffic to the plasma membrane

Formation of heterodimers upon co-expression of p22^{phox} and gp91^{phox} in CHO cells correlates with a marked increase in gp91^{phox} cell surface expression as detected by flow cytometry (Zhu *et al.*, 2006). Based on these studies and our current results localizing the individual subunits to the ER, we hypothesized that heterodimer formation may direct trafficking of flavocytochrome *b* to the plasma membrane. To test this, we transiently expressed increasing amounts of a plasmid for 22CFP into CHO cells with

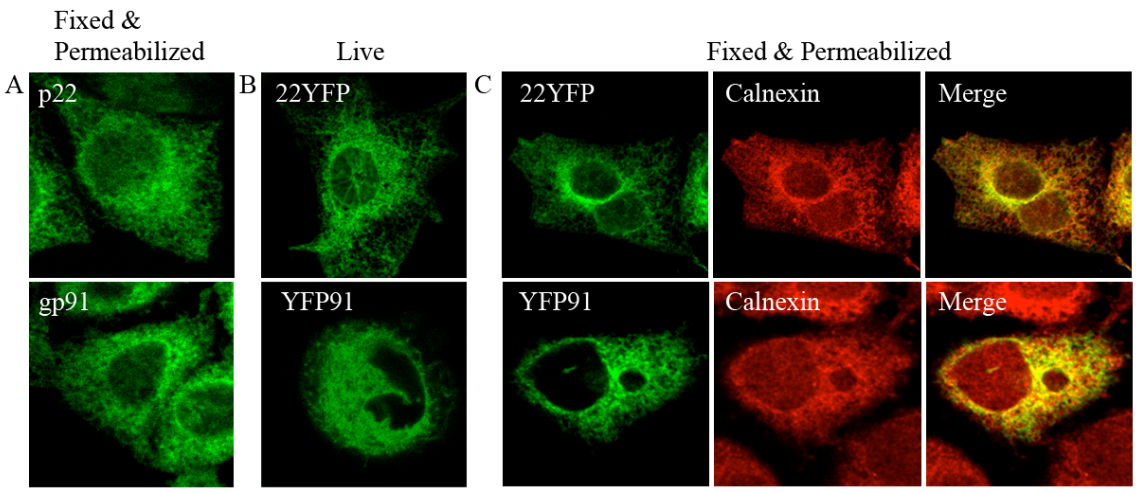

Figure 10. The subunits of flavocytochrome *b*, gp91^{phox} and p22^{phox}, localize to the endoplasmic reticulum when expressed individually in CHO cells. (A) CHO cells stably expressing untagged p22^{phox} (top panel) or gp91^{phox} (bottom panel) were fixed, permeabilized, and stained for p22^{phox} (mAb 44.1) or gp91^{phox} (mAb 54.1). 22YFP or YFP91 transiently expressed in CHO-WT cells were imaged 48 hr post transfection in (B) living cells and (C) cells fixed, permeabilized and co-stained for calnexin. Merged images show 22YFP and calnexin (top panel) and YFP91 and calnexin (bottom panel), and are single plane z stack slices acquired from the bottom of the cell.

stable expression of YFP91 (CHO-YFP91 cells). Western blot analysis showed that increasing expression of 22CFP resulted in increasing amounts of the mature ~115 kDa form of YFP91 (Figure 11B), consistent with increasing formation of the flavocytochrome *b* heterodimer.

We next evaluated the subcellular distribution of YFP91 and 22CFP following transient expression of increasing amounts of 22CFP in CHO-YFP91 cells. As previously shown for transiently expressed YFP91, stably expressed YFP91 was present in a reticular pattern in the absence of 22CFP (Figure 11A), consistent with localization to the ER (Figures 10C). The reticular distribution of YFP91 disappeared in parallel with increasing expression of 22CFP and was replaced by enrichment of YFP91 in the plasma membrane (Figure 11C, *arrowheads and arrows*). The change in YFP91 distribution was dependent on the amount of 22CFP. In transfections with only 1.0 μg of 22CFP plasmid DNA, cells showed localization of YFP91 to either the ER (*asterisks*), to the ER and plasma membrane (*arrowheads*), or to the plasma membrane (*arrows*) (Figure 11C). In contrast, cells transfected with 4.0 μg of 22CFP plasmid DNA, YFP91 is almost always detected in the plasma membrane.

Parallel effects were seen for the distribution of $p22^{phox}$. Unlike the ER localization of $p22^{phox}$ when expressed in the absence of $gp91^{phox}$ (Figures 10C), 22CFP expressed in the presence of YFP91 localized to the plasma membrane (Figure 11C, top panel). In some cells overexpressing 22CFP, 22CFP was present both in the plasma membrane and a reticular distribution (Figure 11C, *wide arrows*), but only the plasma membrane protein colocalized with YFP91, suggesting the reticular pattern corresponded to unassembled 22CFP subunits expressed in excess of YFP91. Thus, the

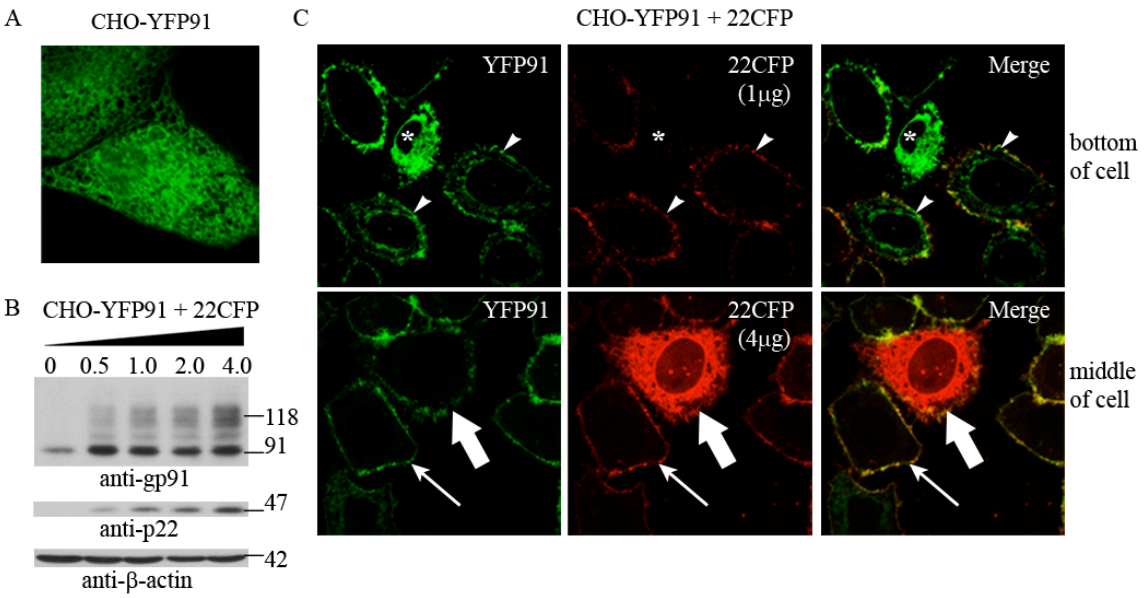

Figure 11. Heterodimers of $p22^{phox}$ and $gp91^{phox}$ traffic to the plasma membrane, while the subunit in "excess" localizes to the ER. CHO-YFP91 cells were transiently transfected with 0.5, 1.0, 2.0, or 4.0 μg of the 22CFP vector. (A) YFP91 stably expressed in CHO-YFP91 cells was imaged in living cells. A single plane z stack slice acquired from the bottom of the cell is shown. (B) Cell lysates were analyzed for $gp91^{phox}$, $p22^{phox}$, and β-actin protein expression 48 hr post transfection (n=2 experiments in which protein expression was evaluated). (C) Confocal microscopy of YFP91 (left column), 22CFP (middle column), and merged images (right column) following transient expression of 1.0 μg of 22CFP (top panel) or 4.0 μg of 22CFP (bottom panel) 72 hr post transfection of CHO-YFP91 cells. YFP91 localized to the ER in cells that lacked expression of 22CFP (*asterisks*), to the ER and plasma membrane in some cells expressing 22CFP (*arrowheads*), and to the plasma membrane but not the ER in other CHO-YFP91 cells that co-expressed 22CFP (*arrows*). 22CFP localized to the plasma membrane in most CHO-YFP91 cells (*arrows*), although present in both the plasma membrane and ER in some cells overexpressing 22CFP (*wide arrows*). Single plane z stack slices acquired from the bottom and middle of the cell are shown.

partner in excess stays in the ER while the assembled heterodimer localizes to the plasma membrane. Taken together, these results clearly illustrate a change in subunit location with their coexpression, and show that heterodimer formation is accompanied by trafficking to the plasma membrane. These results also support a requirement for heterodimer formation, rather than determinants from one of the individual subunits, to efficiently traffic flavocytochrome *b* to the cell surface.

Of interest, we also detected flavocytochrome *b* in CHO-YFP91 cells co-expressing 22CFP in intracellular vesicles near the plasma membrane (Figure 12, top panel) and in a perinuclear location (Figure 12, bottom panel). These findings suggested that a portion of flavocytochrome *b* in CHO cells resides in endocytic compartments that may recycle to the plasma membrane. The perinuclear vesicles were best seen in images collected from the middle of the cell (Figure 12, bottom panel), consistent with the perinuclear accumulation of the endocytic recycling compartment characteristic for CHO cells (Ullrich *et al.*, 1996).

4. Heterodimer formation is required for trafficking of flavocytochrome *b* to the plasma membrane

To exclude the alternative possibility that co-expression of $gp91^{phox}$ and $p22^{phox}$ and not heterodimer formation *per se* changed the subcellular distribution of the individual subunits, CHO-WT cells were transiently co-transfected with 22YFP and a H115L mutant of $gp91^{phox}$ (Biberstine-Kinkade *et al.*, 2001). This residue is believed to contribute to heme binding, and replacement with a leucine residue prevents heme incorporation and heterodimer formation with $p22^{phox}$ (Biberstine-Kinkade *et al.*, 2001).

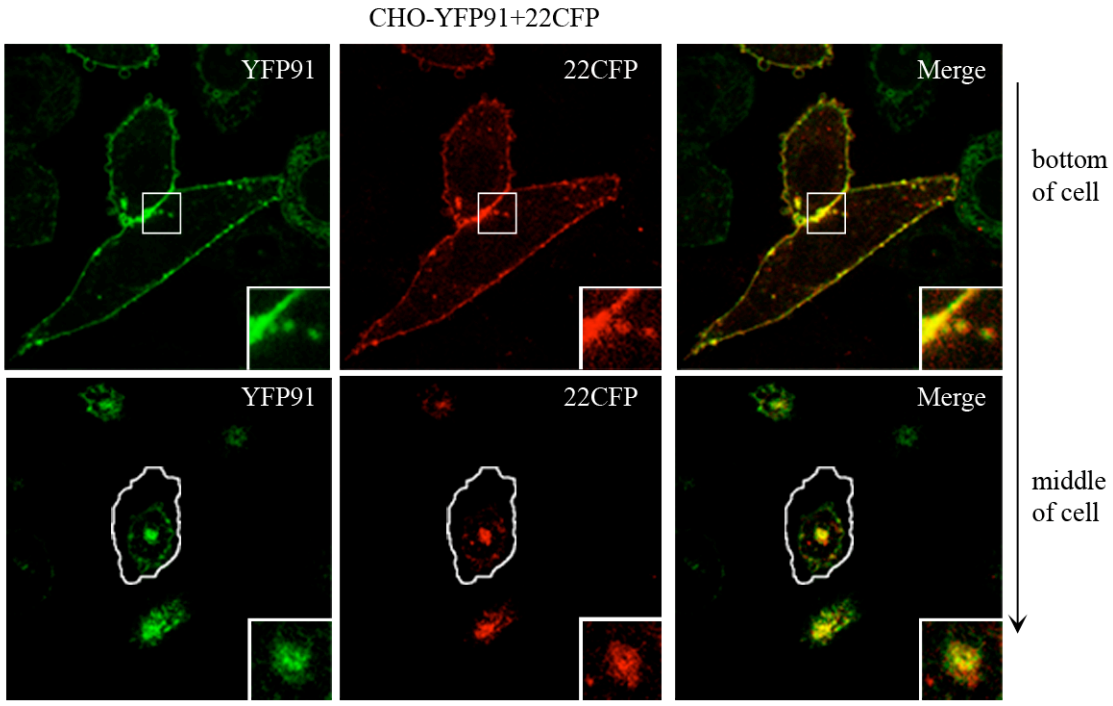

Figure 12. YFP91 and 22CFP co-localize at the plasma membrane and a perinuclear compartment in CHO cells. CHO-YFP91 cells transiently transfected with 0.5 μg 22CFP were imaged in fixed cells by confocal microscopy. YFP91 and 22CFP colocalized at the plasma membrane and vesicles near the plasma membrane (top panel, *insets*) and a perinuclear compartment (bottom panel, *insets*). Single plane z stack slices acquired from the bottom and middle of the cell are shown.

Western blot analysis showed that gp91^{phox} H115L was expressed in CHO cells predominantly as the 58 kDa and 65 kDa forms with no apparent gp91^{phox} maturation (Figure 13A), as seen previously in PLB-985 promyelocyte and COS7 cell lines (Biberstine-Kinkade *et al.*, 2001). Confocal analysis of 22YFP and gp91^{phox} H115L showed both proteins localized to a reticular compartment that resembled the ER (Figure 13B). These results support the notion that heterodimer formation is required to efficiently traffic p22^{phox} and gp91^{phox} to the plasma membrane, while the unassembled subunits remain in the ER.

5. Characterization of a CHO-91-22YFP cell line

To characterize the intracellular compartments to which flavocytochrome *b* is trafficked in CHO cells (Figure 14), we developed a CHO-91 cell line that stably expressed 22YFP (CHO-91-22YFP cells) to allow simultaneous localization of flavocytochrome *b* and tagged markers of different membrane compartments. Western blot analysis and flow cytometry showed increased gp91^{phox} maturation to the 91 kDa form and increased gp91^{phox} cell surface expression in CHO-91-22YFP cells compared to CHO-91 cells (Figures 14A and 14B). However, some gp65 was still present (Figure 14A), indicating that not all the gp91^{phox} was incorporated into flavocytochrome *b*. Confocal microscopy of CHO-91-22YFP cells showed that 22YFP localized to the plasma membrane and intracellular vesicles near the plasma membrane, as well as a perinuclear compartment (Figure 14C, left panels), similar to CHO-YFP91 cells that transiently expressed 22CFP (Figure 11). 22YFP did not colocalize with the ER marker calnexin in CHO-91-22YFP cells (Figure 14C, middle panel), as shown in images

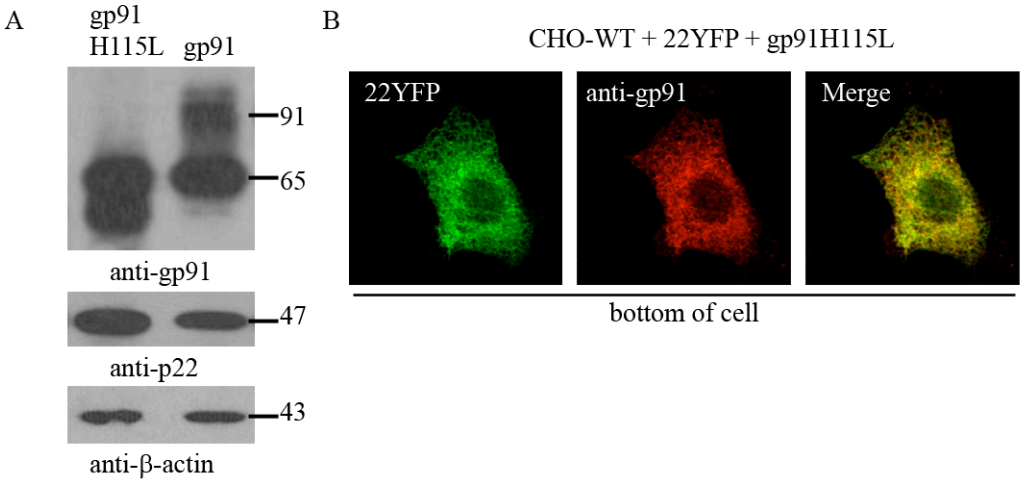

Figure 13. Heterodimer formation and not co-expression changes the subcellular distribution of $p22^{phox}$ and $gp91^{phox}$. (A) Protein expression of $gp91^{phox}$ (mAb 54.1), 22YFP (mAb NS2), and β-actin (mAb) in CHO-WT cells transiently expressing 22YFP and $gp91^{phox}$H115L or CHO-91 cells transiently expressing 22YFP. (B) CHO-WT cells transiently transfected with $gp91^{phox}$H115L and 22YFP showed 22YFP and $gp91^{phox}$H115L (detected by immunofluorescent staining) to have an ER-like distribution with no detection of plasma membrane localization.

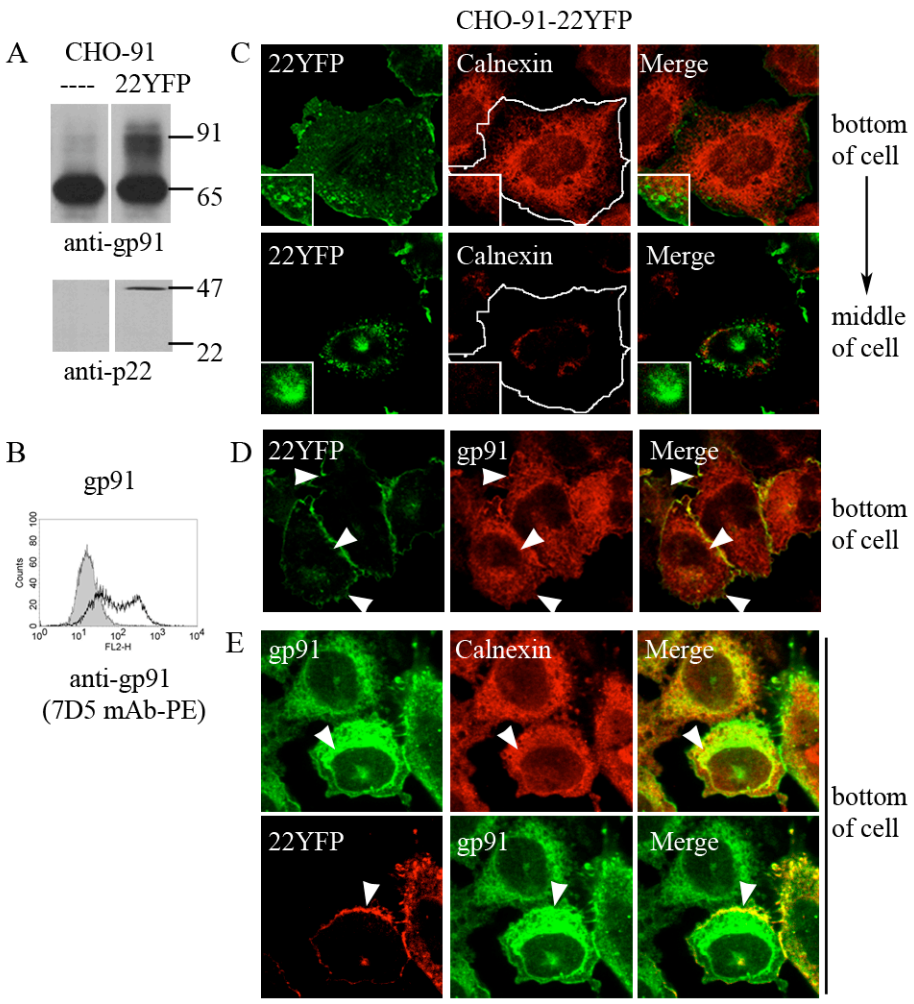

Figure 14. Characterization of model cell line, CHO-91-22YFP, to investigate trafficking of flavocytochrome *b*. (A) Immunoblots of cell lysates from CHO-91 and CHO-91-22YFP cells probed with mAb 54.1 and mAb NS2 to detect gp91^{phox} maturation and 22YFP protein expression, respectively. (B) Cell surface gp91^{phox} detected by 7D5 (mAb) using flow cytometry in CHO-91 cells (grey) and CHO-91-22YFP cells (black line). (C-E) CHO-91,22YFP cells were fixed, permeabilized and stained to detect calnexin (C), gp91^{phox} (D), or gp91^{phox} and calnexin (E). *Arrowheads* denote areas of colocalization. Single plane z stack slices acquired from the bottom and/or middle of the cell are shown.

collected from the bottom of the cell. In contrast, gp91^{phox} was present in both a reticular pattern, which colocalized with calnexin (Figure 14E, *arrowheads*), and at the plasma membrane, where it colocalized with 22YFP (Figure 14D, *arrowheads*). Taken together, these data indicate that gp91^{phox} was expressed in excess of 22YFP in the CHO-91-22YFP cell line, resulting in unassembled gp91^{phox} accumulation in the ER, while 22YFP and gp91^{phox} colocalized in the plasma membrane and intracellular compartments distinct from the ER. Thus, we used 22YFP as an indicator of flavocytochrome *b* targeting in this cell line.

6. Flavocytochrome *b* localizes to the endocytic recycling compartment

The CHO-91-22YFP cell line described above (Figure 14) was used to investigate trafficking of flavocytochrome *b*, via detection of the YFP tag on p22^{phox}. The perinuclear location of flavocytochrome *b*-containing vesicles (Figures 12 and 14) is characteristic of the endocytic recycling compartment in some cell types, including CHO cells (Maxfield and McGraw, 2004; Saraste and Goud, 2007), that is defined by the GTPase Rab11 (Ullrich *et al.*, 1996). As shown in Figure 15A, 22YFP strongly co-localized with Rab11 near the nucleus of CHO-91-22YFP cells. Transiently-expressed Rab11CFP and 22YFP also colocalized in CHO-91-22YFP cells (Figure 15B). These results suggest that a portion of flavocytochrome *b* in CHO cells resides in the endocytic recycling compartment.

Although widely used as a marker for recycling endosomes (Ullrich *et al.*, 1996; Cox *et al.*, 2000) Rab11 may also traffic between the trans-Golgi network (TGN) and the cell surface (Urbe *et al.*, 1993). Thus, to better define the Rab11-positive

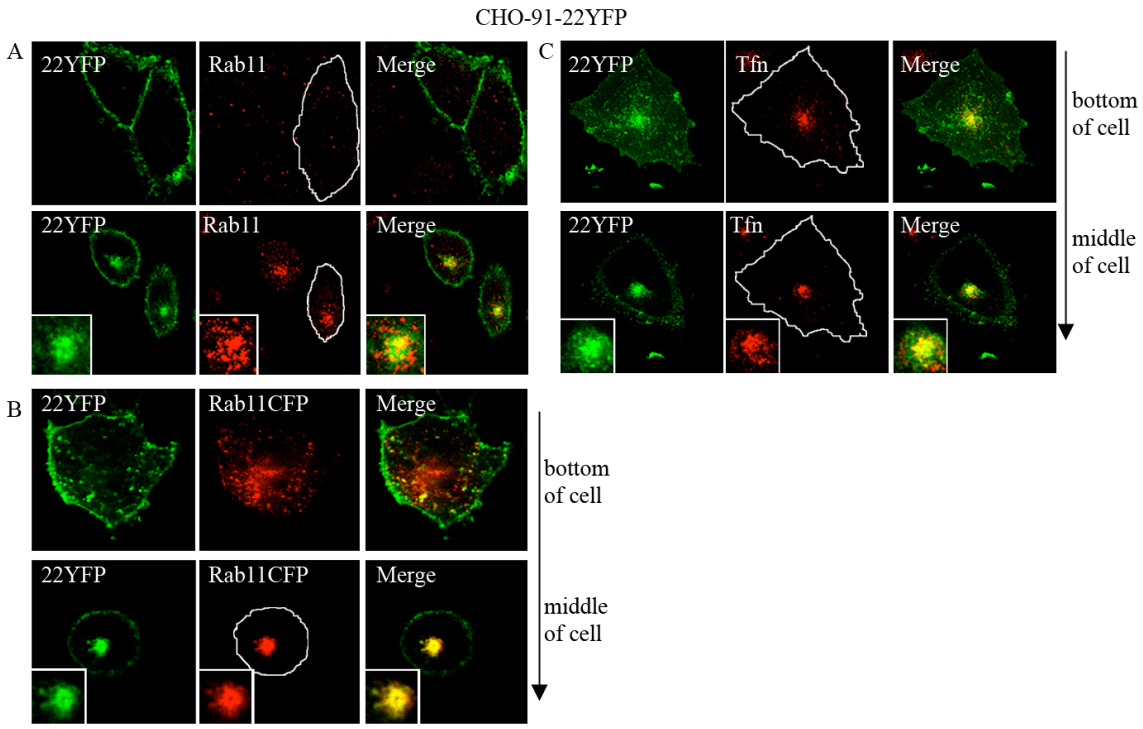

Figure 15. Flavocytochrome *b* localizes to the Rab-11 positive endocytic recycling compartment in CHO cells. (A) CHO-91-22YFP cells were fixed, permeabilized and stained for Rab11. Insets within the merged image (bottom panel) show colocalization of 22YFP and Rab11 at a perinuclear compartment. (B) CHO-91-22YFP cells transiently expressing Rab11CFP were imaged in living cells 24 hr post transfection. (C) CHO-91-22YFP cells were incubated with Alexa Fluor 647-conjugated mouse transferrin (Tfn, 20 μg/ml) for 5 min at 37°C followed by a 25 min chase at 37°C to label the endocytic recycling compartment. Living cells were imaged and colocalization of 22YFP and Tfn was evaluated in the merged image (n=2 experiments where 22YFP and Tfn colocalization was evaluated). Single plane z stack slices taken from the bottom and middle of the cell are shown.

perinuclear compartment in our studies, we also analyzed the extent to which flavocytochrome *b* colocalized with internalized transferrin, a marker for recycling endosomes that does not traffic to the Golgi. Transferrin is endocytosed upon binding to the transferrin receptor, is subsequently delivered to the recycling compartment, and then traffics back to the plasma membrane (Yamashiro *et al.*, 1984; Sonnichsen *et al.*, 2000). Recycling endosomes in CHO-91-22YFP cells were loaded with tagged transferrin, Tfn-AF647, using a 5 min pulse followed by a 25 min chase. 22YFP showed strong co-localization with Tfn-AF647 in a perinuclear location as shown in the merged image (Figure 15C, inset). In contrast, 22YFP expressed in CHO cells in the absence of $gp91^{phox}$ did not colocalize with Tfn-AF647 (Figure 16). These findings provide additional evidence that flavocytochrome *b* recycles from the plasma membrane to the endocytic recycling compartment.

7. Flavocytochrome *b* localizes to Rab5-positive early endosomes, but not Rab7-positive late endosomes or lysosomes

A recent model of endosome sorting (Seachrist and Ferguson, 2003) indicates Rab5-positive early endosomes branching into one of three pathways: 1) Rab4-positive endosomes that rapidly recycle to the plasma membrane without entering the Rab11-positive compartment, 2) the Rab11-positive endocytic recycling compartment for slow trafficking back to the plasma membrane, or 3) Rab7-positive late endosomes that subsequently fuse with lysosomes for cargo degradation (summarized in Figure 4). To determine if flavocytochrome *b* also accumulated on compartments in the degradative pathway, we evaluated the extent of flavocytochrome *b* colocalization with Rab7 and

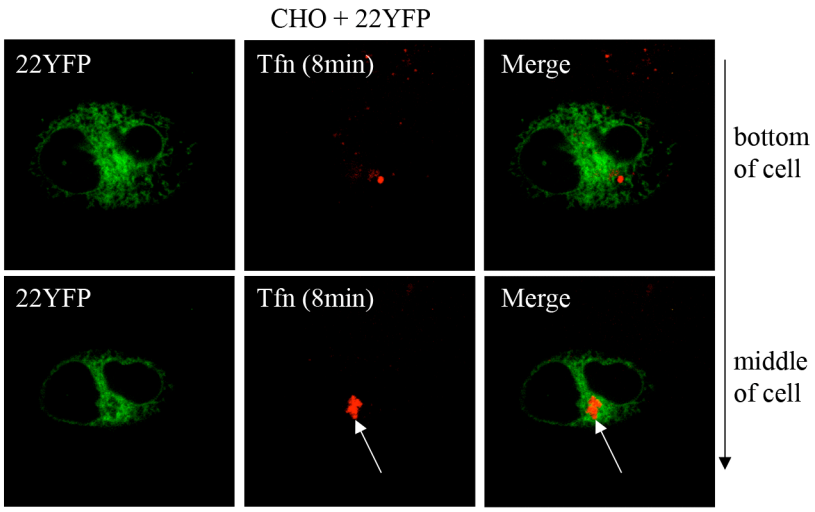

Figure 16. Unassembled 22YFP does not colocalize with the endocytic recycling compartment in CHO cells. Colocalization of 22YFP and the transferrin-labeled endocytic recycling compartment was evaluated in CHO cells transiently expressing 22YFP. Immediately following the addition of Alexa Fluor 647-conjugated mouse transferrin (Tfn, 20 μg/ml), a series of images of 22YFP and Tfn were collected over time in live cells at 37°C. Tfn was found to localize to a perinculear compartment at 8 min (*arrows*), which did not colocalize with 22YFP (merged image, *arrow*) (n=1 experiment where 22YFP and Tfn colocalization was evaluated). Single plane z stack slices taken from the bottom and middle of the cell are shown.

with lysosomes pre-loaded with Dextran. To this end, 22RED and Rab7GFP were transiently co-expressed in CHO-91 cells, using only a small amount of each plasmid (1 μg). 22RED localized to the plasma membrane in CHO-91 cells and had increased expression in the perinuclear compartment (Figure 17A), similarly to 22YFP in CHO-91-22YFP cells (Figure 14). However, 22RED did not co-localize with Rab7GFP (Figure 17A). Colocalization of flavocytochrome *b* with lysosomes was analyzed in CHO-91-22YFP cells after a 50 min incubation with fluorescently tagged Dextran (Dex-AF647) to label lysosomes. 22YFP did not colocalize with Dex-AF647 (Figure 17B), further indicating that flavocytochrome *b* does not accumulate in organelles of the degradative pathway.

8. Different combinations of fluorescently tagged and untagged $p22^{phox}$ and $gp91^{phox}$ subunits behave in a similar fashion in CHO cells

During the course of our studies, we generated a series of fluorescent-tagged $p22^{phox}$ and $gp91^{phox}$ constructs (listed in Table IV). The localization of the different combinations in CHO cells was compared by confocal microscopy to determine whether these probes could be used interchangeably. eCFP91, mCFP91 and mCIT91 (referred to as YFP91) when co-expressed with untagged $p22^{phox}$ in CHO-22 cells localized to the plasma membrane and the ERC (Figure 18A, *arrows*). In addition, mCFP91 or YFP91 co-expressed with CFP or YFP-tagged $p22^{phox}$ showed the same distribution (Figure 18B), which showed the different combinations of untagged or fluorescently tagged subunits behaved similarly in combination with their heterodimer partner.

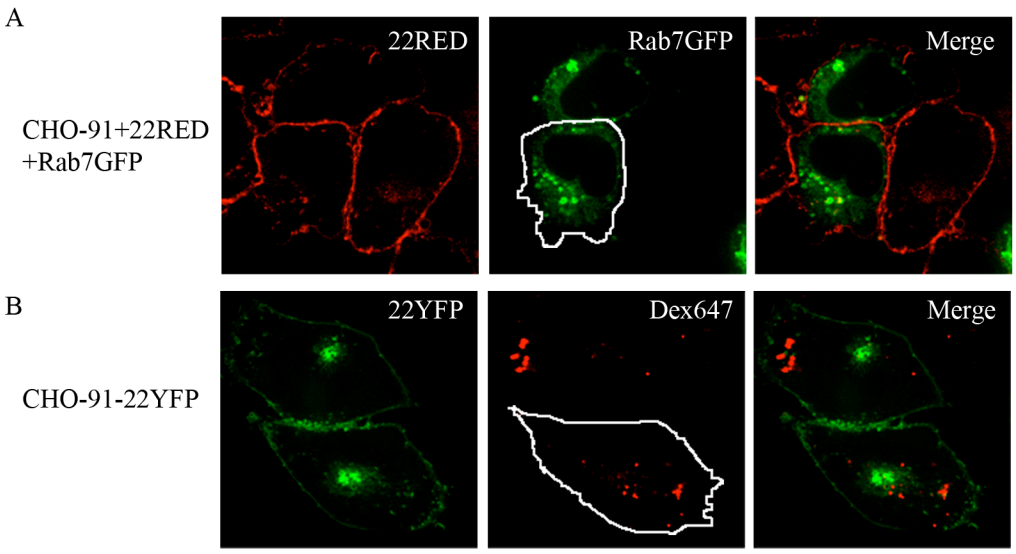

Figure 17. Flavocytochrome *b* does not appear to accumulate on late endosomes or lysosomes in CHO cells. (A) 22RED and Rab7GFP transiently expressed in CHO-91 cells did not co-localize in living cells. (B) CHO-91-22YFP cells were incubated with 10 μg/ml Alexa Fluor 647-labeled Dextran (Dex647) for 50 min at 37°C. 22YFP and Dex647-labeled lysosomes, did not appear to colocalize in live cells. (A-B) A single z stack section from the middle of the cell is shown.

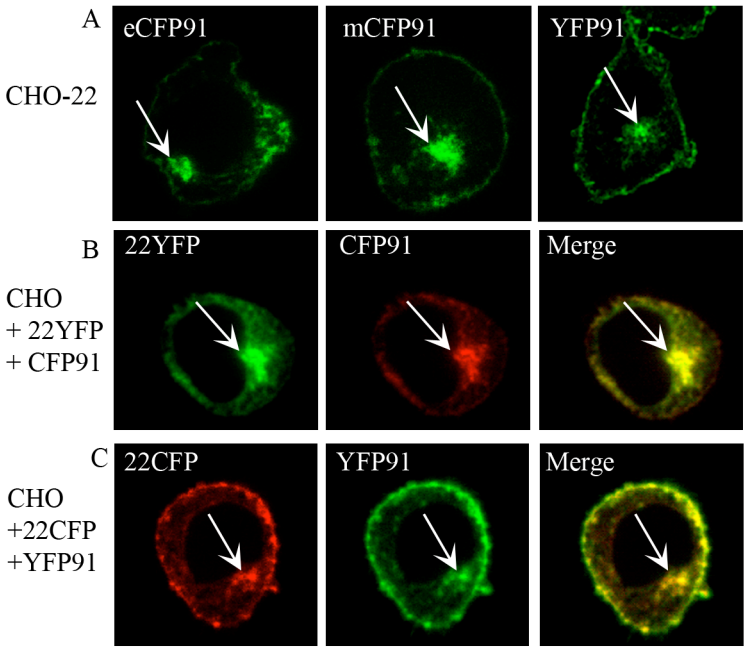

Figure 18. Different combinations of fluorescently tagged p22^{phox} and gp91^{phox} subunits behave in a similar fashion in CHO cells. CHO-WT and CHO-22 cells were transiently transfected with eCFP91, mCFP91, or YFP91. The distribution of eCFP91, mCFP91, and YFP91 in the presence of untagged or fluorescently tagged p22^{phox} was evaluated by confocal microscopy in live cells. Fluorescently tagged gp91^{phox} proteins localized to the plasma membrane and a perinuclear compartment (*arrows*) in the presence of untagged p22^{phox} (A), YFP-tagged p22^{phox} (B), and CFP-tagged p22^{phox} (C). (A-C) A single z stack section from the middle of the cells is shown.

9. Nocodazole treatment

The perinuclear localization of the Rab11-endocytic recycling compartment in Madin-Darby Canine Kidney (MDCK) cells has been shown to be dependent on the microtubule-based cytoskeleton (Casanova *et al.*, 1999). Thus, we evaluated whether localization of flavocytochrome *b* to the ERC was also dependent on microtubules. We found treatment of CHOf-22-YFP91 cells with the microtubule-depolymerizing drug Nocodazole (10 μM for 30 min) led to a dispersal of 22YFP-positive vesicles throughout the cytoplasm (Figure 19B) and loss of the prominent perinuclear distribution seen in the absence of Nocodazole (Figure 19A, *arrowheads*). A modest increase in flavocytochrome *b* expression at the cell surface was also observed (Figure 19B, *arrows*). These results suggest that trafficking of flavocytochrome *b* to the ERC is also dependent on microtubules.

10. C-terminal deletion of $p22^{phox}$ does not affect localization of flavocytochrome heterodimer to the plasma membrane and recycling endosomes

Thus far, there are no identified motifs within $gp91^{phox}$ or $p22^{phox}$ that regulate trafficking of the flavocytochrome *b* heterodimer. A current model of $p22^{phox}$ places both its N- and C-terminal domains in the cytoplasm, anchored in the membrane by a hairpin formed by two hydrophobic domains (Taylor *et al.*, 2004). The C-terminal cytoplasmic domain of $p22^{phox}$ is hydrophilic and also contains multiple proline residues, including a Pro-Xaa-Xaa-Pro SH3-binding motif around Pro156 that is a target of the tandem SH3 domains of $p47^{phox}$ during assembly of the active NADPH oxidase (Nauseef, 2004).

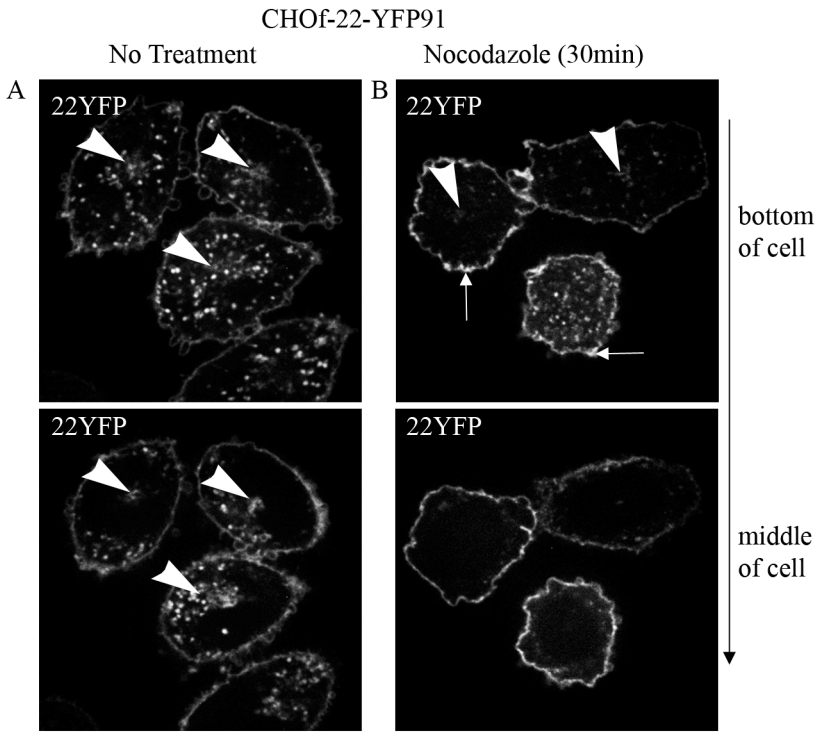

Figure 19. Nocodazole appears to decrease the endosomal distribution of flavcytochrome *b* in CHOf-22-YFP91 cells. CHOf-22-YFP91 cells, which stably express human $p22^{phox}$ and YFP-tagged human $gp91^{phox}$, were imaged by video microscopy in the absence or presence of Nocodazole (30 min, 10 μM). (A) YFP91 localizes to the plasma membrane and endosomes that cluster near the nucleus (*arrowheads*). (B) Loss of prominent perinuclear endosomal distribution of YFP91 (*arrowheads*) and modest increase in YFP91 localization to the plasma membrane (*arrows*) in Nocodazole-treated cells. Representative images collected from 1 experiment.

Since deletion of C-terminal amino acids 142 - 195 of p22^{phox} does not affect formation of the flavocytochrome *b* heterodimer (Zhu *et al.*, 2006) we tested whether the Pro-Xaa-Xaa-Pro motif or other signals in the p22^{phox} C-terminus were required for targeting of flavocytochrome *b* to the plasma membrane and/or recycling endosomes.

YFP-tagged p22^{phox} derivatives lacking amino acids 131-195 (131YFP), 149-195 (149YFP) or 172-195 (172YFP), were transiently expressed in CHO-WT and CHO-91 cells to evaluate their subcellular distribution in the absence of gp91^{phox} and in the presence of excess gp91^{phox} expression. Flow cytometry and immunoblotting with an anti-YFP antibody showed the YFP-tagged proteins were expressed at similar levels (Figures 20A and 20B) and had increasing mobility in a SDS-PAGE gel with progressive removal of the C-terminus (Figure 20B). Increased cell surface expression and maturation of gp91^{phox}, consistent with heterodimer formation, was seen with co-expression of 22YFP, 172YFP or 149YFP, but not 131YFP, (Figures 20A and 20B), as previously seen using untagged p22^{phox} truncations (Zhu *et al.*, 2006).

Confocal microscopy showed all YFP-tagged p22^{phox} mutants, in the absence of gp91^{phox}, localized to the ER (Figure 20C). When co-expressed with excess gp91^{phox}, 172YFP and 149YFP were present in both the perinuclear recycling compartment, best seen in live images (Figure 20D, *arrows*), and the plasma membrane, where they co-localized with gp91^{phox}, similar to full length 22YFP (Figure 20D, *arrowheads* in merge panels). In contrast, 131YFP remained in the ER when co-expressed with gp91^{phox} (Figure 20D), as expected from failure to form heterodimers. Thus, C-terminal amino acids 149-195 in p22^{phox} do not appear to contain localization signals required for

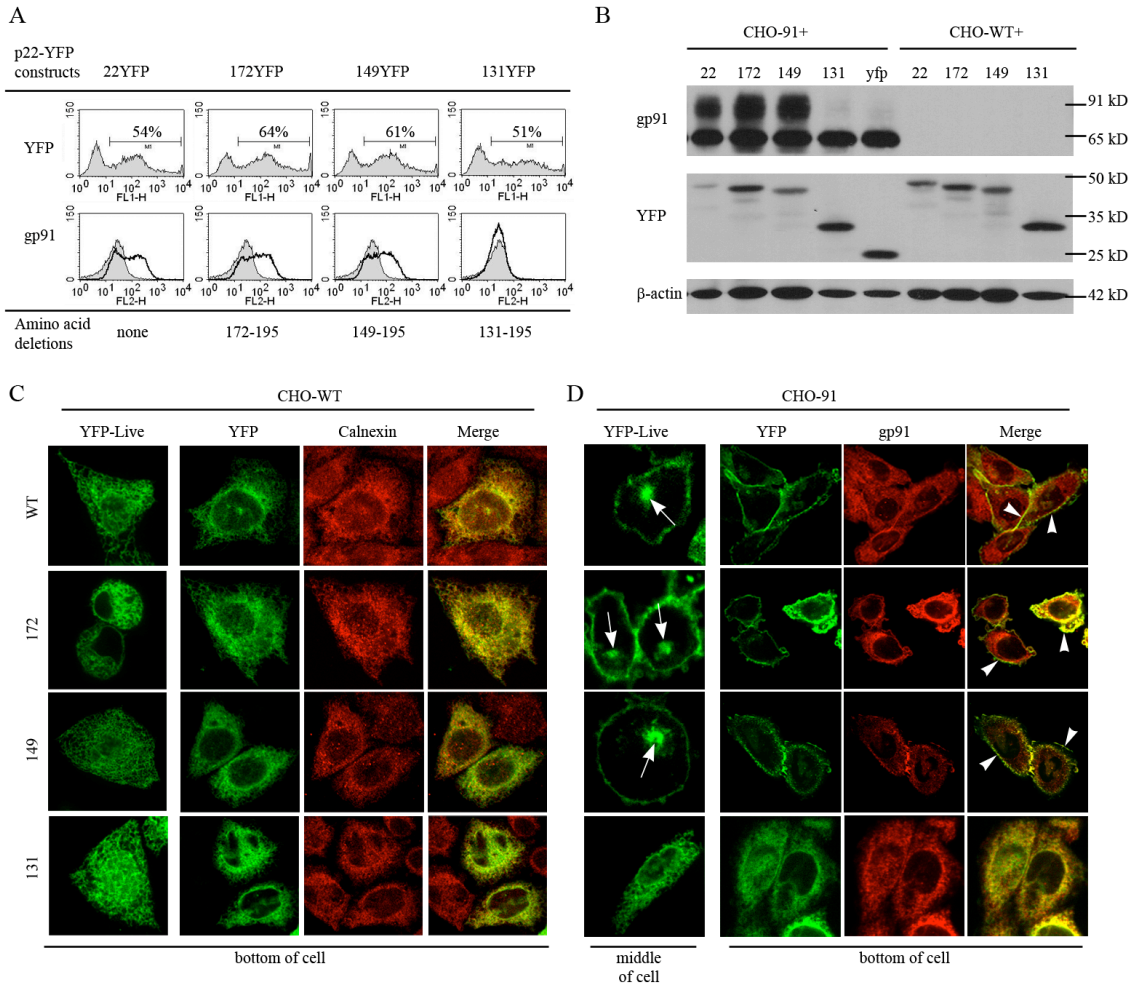

Figure 20. p22^{phox} C-terminal amino acids 149-195 are not required for trafficking of the heterodimer to the plasma membrane or to the perinuclear recycling compartment. CHO-WT or CHO-91 cells were transfected with vectors for 22YFP, 172YFP, 149YFP, or 131YFP and evaluated 24 hrs post transfection (n=2 experiments where YFP-tagged p22^{phox} C-terminal deletion proteins were evaluated). (A) **Top panel:** Flow cytometry analysis of YFP shows similar transfection efficiency of all YFP-tagged p22^{phox} constructs when transiently expressed in CHO-91 cells. **Bottom Panel:** Analysis of gp91^{phox} cell surface expression (mAb 7D5) by flow cytometry reveals increased gp91^{phox} surface expression with co-expression of 22YFP, 172YFP, and 149YFP, but not 131YFP (bottom panel, black lines). CHO-91 cells were used as the control (grey). (B) Cell lysates were evaluated for gp91^{phox} (mAb 54.1), YFP (anti-GFP), and β-actin

protein expression. (C) **Left column:** Live imaging of YFP-tagged $p22^{phox}$ derivatives transiently expressed in CHO-WT cells. **Right columns:** CHO-WT cells transiently expressing YFP-tagged $p22^{phox}$ derivatives were fixed, permeabilized, and stained for calnexin. (D) **Left column:** Live imaging of YFP-tagged $p22^{phox}$ derivatives transiently expressed in CHO-91 cells. *Arrows* show that 22YFP, 172YFP, and 149YFP associate with the endocytic recycling compartment, but 131YFP did not. Z stack slices collected from the middle of the cell are shown. **Right columns:** CHO-91 cells transiently expressing YFP-tagged $p22^{phox}$ derivatives were fixed, permeabilized, and stained for $gp91^{phox}$ (mAb 54.1). 22YFP, 172YFP, 149YFP, but not 131YFP, colocalized with $gp91^{phox}$ at the plasma membrane (*arrowheads*).

trafficking of flavocytochrome *b* to the plasma membrane or to the perinuclear endocytic recycling compartment.

II. Localization of flavocytochrome *b* in macrophages

1. Rab11 and transferrin localize to a perinuclear compartment in RAW 264.7 cells that is distinct from the Golgi

A previous report analyzing the distribution of transferrin and Rab11 in macrophages suggested Rab11-positive recycling endosomes do not accumulate to a prominent perinuclear compartment, but instead are more dispersed in this cell type (Cox *et al.*, 2000). Thus, we began our studies by determining whether Rab11 and/or transferrin localized to a perinuclear compartment in RAW 264.7 cells. RAW 264.7 cells were pulsed for 15 or 30 min with Alexa Fluor 647-conjugated human transferrin. Transferrin localized to vesicles near the cell surface following a 15 min pulse (Figure 21A, top panel), but then clustered near the nucleus following a 30 min pulse (Figure 21A, bottom panel), suggesting that transferrin does localize to a perinuclear endocytic recycling compartment in RAW 264.7 cells. In addition to transferrin, we also evaluated the distribution of endogenous Rab11 and transiently expressed fluorescently tagged Rab11 in RAW 264.7 cells. The subcellular distribution of endogenous Rab11, detected by immunofluorescence microscopy (Figure 21B), was similar to Rab11GFP and Rab11CFP detected in live cells (Figure 21C). In summary, Rab11 was found to localize to a prominent perinuclear compartment (Figure 21B and 20C), similar to transferrin (Figure 21A), and showed that RAW 264.7 cells do have a perinuclear endocytic recycling compartment.

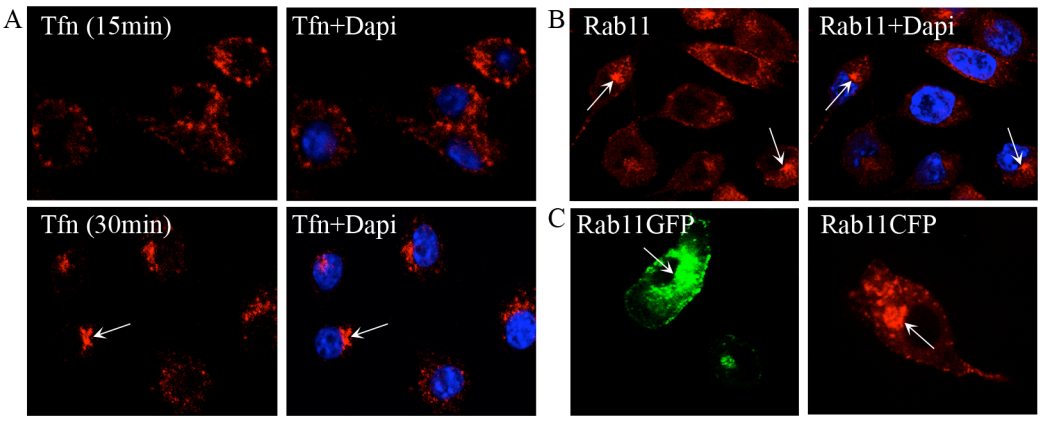

Figure 21. RAW 264.7 cells have a perinuclear Rab11-positive endocytic recycling compartment. (A) RAW 264.7 cells were incubated with Alexa Fluor 647-conjugated human transferrin for 15 or 30 min, washed, fixed in 4% paraformaldehyde for 10 min, and then stained with the nuclear dye DAPI (10 μg/ml for 7 min, RT). At 15 min (top panel), transferrin was found in vesicles near the cell surface, but at 30 min (bottom panel) transferrin accumulated in a perinuclear compartment (*arrows*). (B) In RAW 264.7 cells, Rab11, detected by immunofluorescence microscopy, localized to vesicles throughout the cell with a prominent localization near the nucleus (*arrows*). (C) Video microscopy of Rab11GFP and Rab11CFP transiently expressed in RAW 264.7 cells showed a similar distribution to endogenous Rab11 (B) and localization to a perinuclear compartment (*arrows*).

As described above, Rab11, but not transferrin has been found to traffic between Golgi compartments in addition to trafficking from the endocytic recycling compartment to the plasma membrane in polarized MDCK cells. To further characterize the endocytic recycling compartment in RAW cells, we investigated colocalization of transferrin with a GFP-tagged mutant of GAD65 (γ-aminobutyric acid) (Kanaani *et al.*, 2002) that localizes predominantly to the Golgi, and was used as our marker for the Golgi. In COS cells, the recycling compartment was shown to be distinct from the Golgi by showing that transferrin localized within the Golgi "ring," but did not colocalize with Golgi (Misaki *et al.*, 2007). We utilized this same technique to determine whether the endocytic recycling compartment was distinct form the Golgi in RAW cells.

Trafficking of Alexa Fluor 647-conjugated human transferrin in RAW 264.7 cells transiently expressing the GFP-tagged mutant form of GAD65 (referred to as mGAD65GFP) was assessed in living cells by collecting a series of images over time following addition of transferrin. Transferrin localized to vesicles near the cell surface at 8 min (Figure 22, top panel), but localized to a perinuclear compartment at 20 min (Figure 22, bottom panel). As expected, mGAD65GFP localized predominantly to the Golgi (Figure 22). Colocalization analysis of transferrin and mGAD65GFP showed transferrin localized within the ring-shaped structure of the Golgi compartment or "Golgi ring" (Figure 22, merged image, *insets*), but did not colocalize with mGAD65GFP. Taken together, similar to CHO cells, Rab11 and transferrin localize to a perinuclear compartment, which is distinct from the Golgi in RAW 264.7 cells.

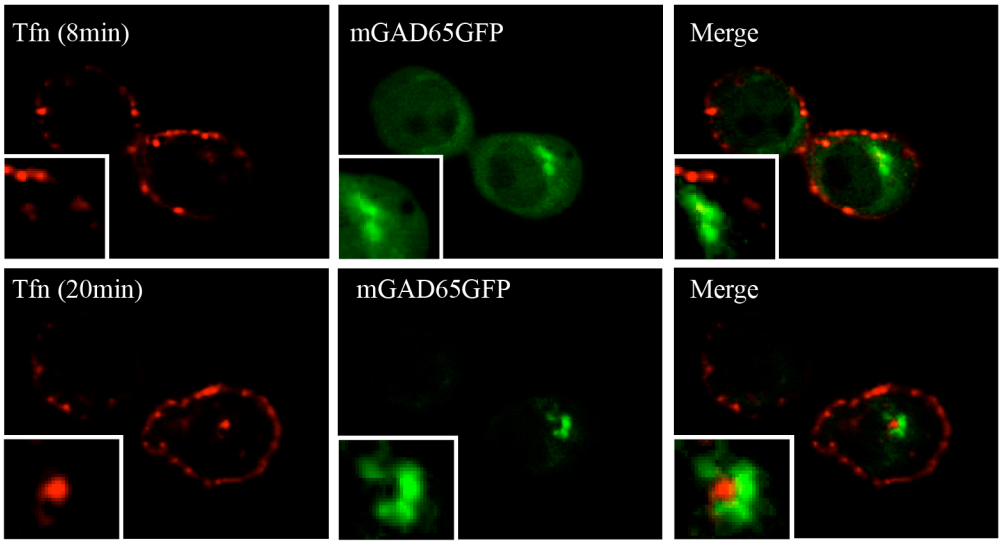

Figure 22. Transferrin labeled endocytic recycling compartment localizes to a perinuclear region that is distinct from the Golgi in RAW 264.7 cells. Alexa Fluor 647-conjugated human transferrin (Tfn, 20 μg/ml) was added to RAW cells transiently transfected with a Golgi marker mGAD65GFP, a GFP-tagged mutant form of GAD65 (γ-aminobutyric acid), and a series of images were collected over time using confocal microscopy. Transferrin localized to vesicles near the cell surface at 8 min (top panel, *insets*) and localized to a perinuclear compartment at 20 min (bottom panel, *insets*), which was found to localize within the Golgi "ring" (bottom panel, *insets*), but did not colocalize with the Golgi.

2. Flavocytochrome *b* localizes to Rab11-positive recycling endosomes in RAW 264.7 cells

We next investigated the distribution of flavocytochrome *b* in RAW 264.7 cells using antibodies specific for endogenous gp91^{phox}, and determined whether this included Rab11-positive recycling endosomes, as seen in the CHO cell model. In RAW 264.7 cells, transiently expressed Rab11GFP colocalized with endogenous gp91^{phox} on vesicles near the plasma membrane (Figure 23A, top panel, *arrowheads*) and near the nucleus (Figure 23A, bottom panel, *insets*). Of note, the distribution of gp91^{phox} was similar in adjacent cells that did not express Rab11GFP (Figure 23A, bottom panel, *arrows*) indicating that overexpression of Rab11GFP did not alter gp91^{phox} targeting.

As a second approach to examine whether flavocytochrome *b* was associated with the endocytic recycling compartment in macrophages, we performed a pulse-chase experiment using fluorescently tagged transferrin (Tfn-AF647, 5 μg/ml) and RAW-WT cells transiently expressing Rab11GFP. After a 5 min pulse with Tfn-AF647 followed by a 25 min chase, cells were fixed, permeabilized, and stained to detect endogenous gp91^{phox}. As shown in Figure 23B, Rab11GFP, gp91^{phox}, and Tfn-AF647 colocalized in the perinuclear region (*arrowheads*) and in vesicles near the plasma membrane (insets, *arrows*). Taken together with the colocalization with Rab11, these data demonstrate for the first time that a portion of macrophage flavocytochrome *b* localizes to the endocytic recycling compartment.

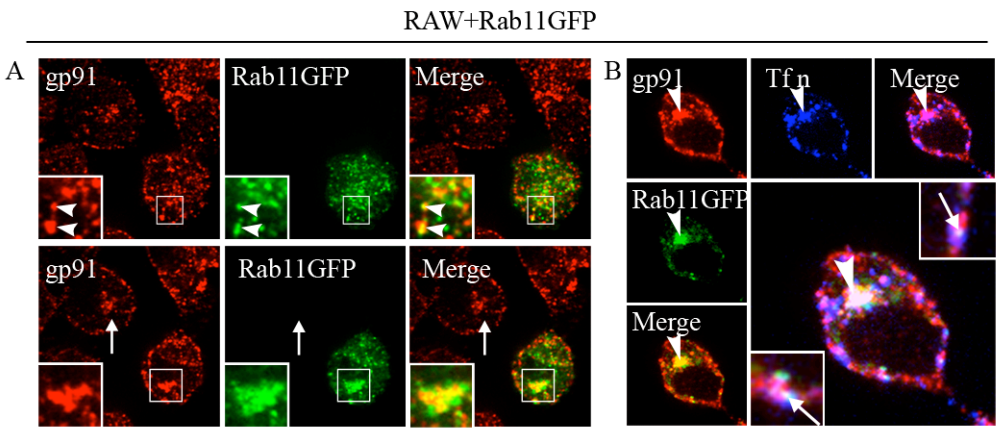

Figure 23. In macrophages, flavocytochrome *b* associates with Rab11-positive recycling endosomes. (A) RAW-WT cells transiently expressing Rab11GFP were fixed, permeabilized, and stained for gp91^{phox} (mAb 54.1) 48 hr post transfection. Colocalization of gp91^{phox} and Rab11GFP is shown in vesicles near the plasma membrane (top panel, *arrowheads*) and in the endocytic recycling compartment (bottom panel, *insets*). Localization of gp91^{phox} to the endocytic recycling compartment was not dependent on expression of Rab11GFP (top panel, *arrows*). Single plane z stack slices taken from the bottom and middle of the cell are shown. (B) RAW-WT transfected with Rab11GFP were incubated with Alexa Fluor 647-conjugated mouse transferrin (Tfn, 5 μg/ml) for 5 min at 37°C followed by a 25 min chase at 37°C to label the endocytic recycling compartment. Cells were fixed, permeabilized, and stained for gp91^{phox}. Co-localization of gp91^{phox} and Rab11GFP (top panel) and gp91^{phox} and Tfn (bottom panel) was observed at the perinuclear compartment (*arrowheads*) and near the plasma membrane (*arrows*).

3. Fcγ-receptors accumulate in the plasma membrane, but not in recycling endosomes

While it is known that some surface receptors recycle while others are targeted for degradation in lysosomes (Lodish *et al.*, 2008), the extent to which different plasma membrane proteins traverse the endocytic recycling compartment is unclear. For comparison to flavocytochrome *b*, we investigated whether the Fcγ-receptor was present in the endocytic recycling compartment in RAW 264.7 macrophages. Using both indirect immunofluorescence to detect endogenous Fcγ-receptors in RAW-WT cells and live-cell imaging to detect stably expressed FcγRIIaGFP in RAW-FcR-GFP transfectants, we detected Fcγ-receptors in the plasma membrane but not in the endocytic recycling compartment, identified in a pulse-chase experiment using Tfn-AF647 (Figure 24). These results confirm published data (Amigorena *et al.*, 1992) which suggest that Fcγ-receptors do not recycle, and as such, indicate selective accumulation of plasma membrane proteins in the endocytic recycling compartment.

4. GFP-tagged Rab5 and Rab7 validate distinct trafficking pathways in RAW 264.7 cells

The degradative pathway has been described to be distinct from the recycling pathway. As described above, Rab5 mediates trafficking of early endosomes to late endosomes (Rab7-positive) or recycling endosomes (Rab11-positive), but not lysosomes (Ullrich *et al.*, 1996). In addition, Rab7-positive endosomes traffic to lysosomes but not recycling endosomes. We evaluated whether trafficking of proteins to these subcellular pathways could be distinguished using GFP-tagged Rab7 or Rab5 in RAW 264.7 cells.

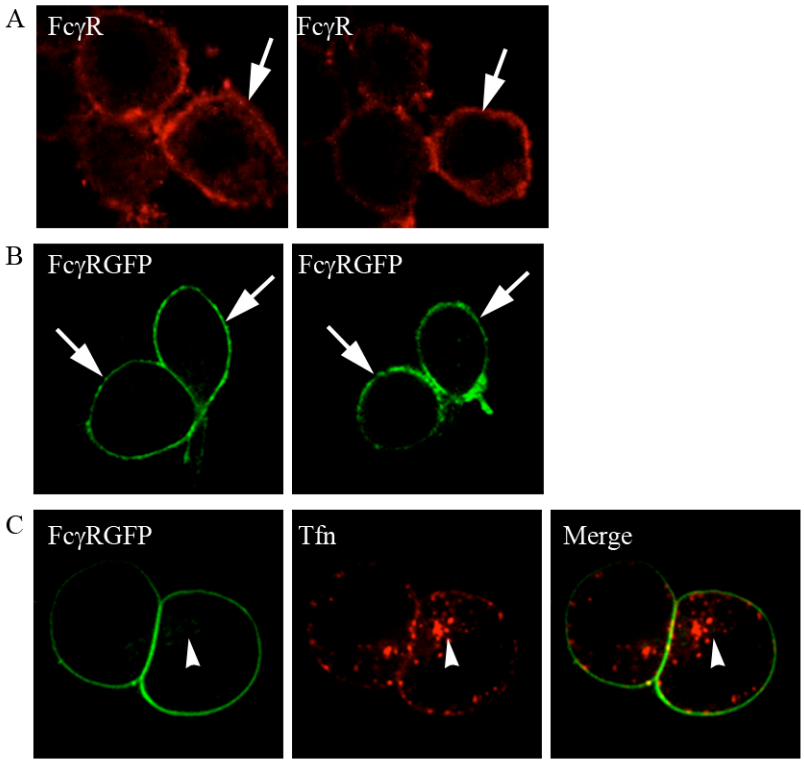

Figure 24. In contrast to flavocytochrome *b*, FcγRIIa-receptor does not accumulate in recycling endosomes near the nucleus. (A) RAW-WT cells were fixed, permeabilized, and stained to detect the Fcγ-Receptor (anti-CD16/32-PE). (B) FcγRGFP localizes to the plasma membrane in live RAW-FcγRGFP cells. Single z stack slices taken from the bottom of the cell (left) and the middle of the cell (right) are shown in (A) and (B). (C) RAW-FcγRGFP cells were labeled Alexa Fluor 647-conjugated mouse transferrin (Tfn), as described in Figure 23. Simultaneous imaging of FcγRGFP and Tfn was performed in living cells. A single z stack section from the middle of the cell is shown.

We found transferrin-labeled recycling endosomes did not colocalize with Rab7GFP (Figure 25A) and dextran labeled lysosomes did not colocalize with Rab5GFP (Figure 25B). These data further support Rab7 and Rab5 localize to distinct endocytic pathways.

5. Macrophage flavocytochrome *b* also colocalizes with the plasma membrane and early (sorting) endosomes, but not late endosomes

Flavocytochrome *b* was also present at the periphery of RAW 264.7 cells (Figures 23A and 23B). To verify that this represented targeting to the plasma membrane, we stably expressed a GFP-labeled PH domain of phospholipase C (Botelho *et al.*, 2000) to mark the inner leaflet of the plasma membrane of RAW 264.7 cells. As shown in Figure 26A, PH-GFP colocalized with endogenous gp91^{phox} at the cell surface.

In addition to Rab11-positive structures, flavocytochrome *b* was detected in other vesicular populations (Figure 23A). The extent of flavocytochrome *b* targeting to early (sorting) endosomes and late endosomes was therefore evaluated by comparison with Rab5GFP and Rab7GFP transiently expressed in RAW-WT cells. Flavocytochrome *b* exhibited modest colocalization with Rab5GFP in vesicles near the plasma membrane (Figure 26B, top panel, *insets*) and near the perinuclear compartment (Figure 26B, bottom panel, *arrows*). In contrast, the distribution of flavocytochrome *b* had little, if any, overlap with the late endosome marker Rab7GFP, which accumulated on large vesicles dispersed throughout the cell (Figure 26C, *arrowheads*), but not in the perinuclear compartment (Figure 26C, *arrow*s).

Collectively, these data indicate that flavocytochrome *b* in macrophages resides in both early endosomes and the endocytic recycling compartment, suggesting that

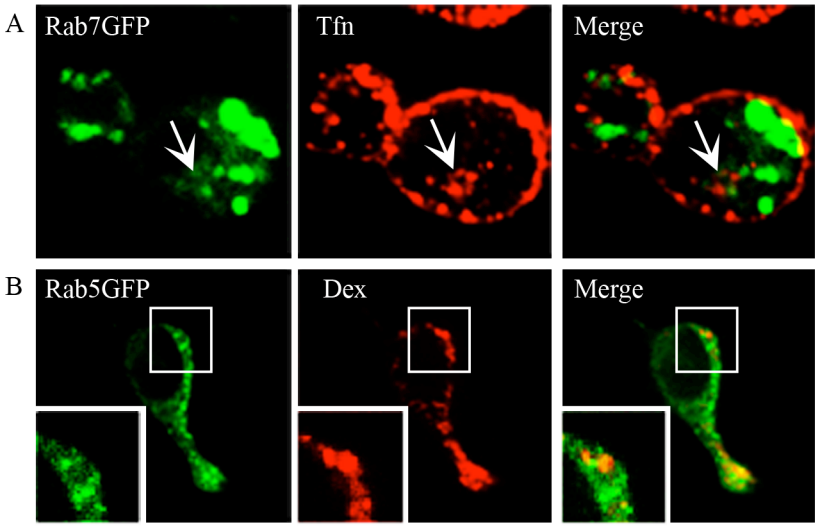

Figure 25. Validation of the specificity of Rab7 and Rab5 to label distinct endosomal pathways in RAW 264.7 cells. (A) RAW cells transiently expressing Rab7GFP were incubated with Alexa Fluor 647-conjugated mouse transferrin (Tfn, 5 μg/ml) for 40 min and then imaged in live cells using confocal microscopy. Transferrin localized to the perinuclear endocytic recycling compartment (*arrows*), while Rab7GFP did not (merged image). (B) Lysosomes in RAW cells transiently expressing Rab5GFP were labeled with Alexa Fluor 647-conjugated Dextran (60 min) and analyzed for colocalization with Rab5GFP by confocal microscopy in live cells. Rab5GFP and Dextran did not appear to colocalize (merged image, *insets*). A single z stack section from the middle of the cell is shown for (A) and (B). Experiments in both (A) and (B) were performed only once.

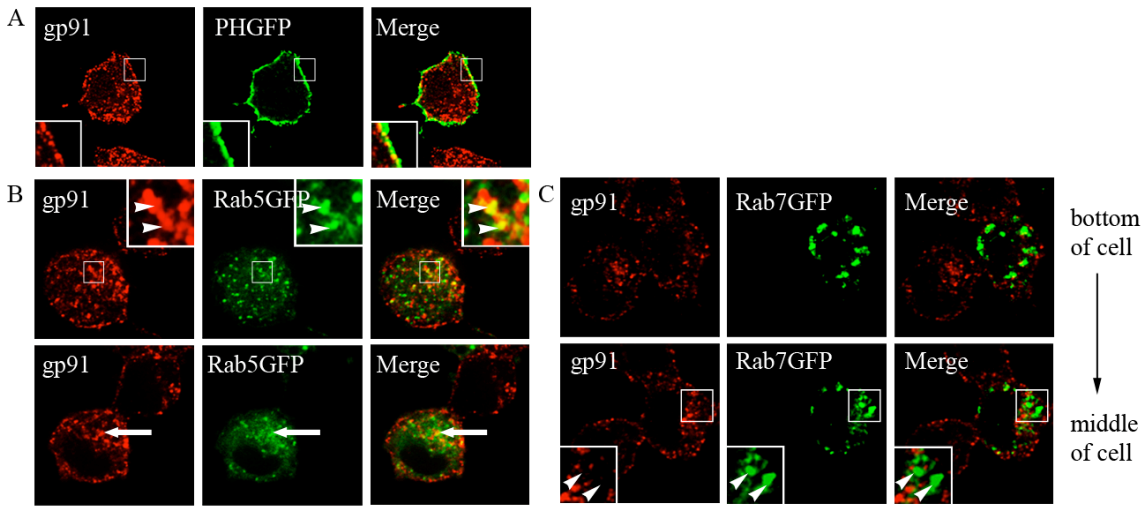

Figure 26. In macrophages, flavocytochrome *b* is present in plasma membrane and some Rab5-positive sorting endosomes, but not in Rab7-positive late endosomes. (A) RAW-PH-GFP cells were fixed, permeabilized, and stained for endogenous gp91^{phox} (mAb 54.1). Colocalization of gp91^{phox} and the plasma membrane marker, PH-GFP, was seen at the cell surface in RAW-PH-GFP cells (*insets*). A single plane z stack slice taken from near the bottom of the cell is shown (n=2 experiments where colocalization of gp91^{phox} and PH-GFP was evaluated). RAW-WT cells transfected with Rab5GFP (B) or Rab7GFP (C) were fixed, permeabilized, and stained for gp91^{phox} (mAb 54.1) 48 hr post transfection. (B) gp91^{phox} and Rab5GFP showed some colocalization in vesicles near the plasma membrane (top panel, *arrowheads*) and near the nucleus (bottom panel, *arrows*). (C) Rab7GFP accumulated on large vesicles dispersed throughout the cell, that did not colocalize with gp91^{phox} near the plasma membrane (top panel) or near the nucleus (bottom panel, *arrowheads*).

flavocytochrome *b* under homeostatic conditions undergoes recycling from the plasma membrane.

6. Unassembled fluorescently tagged gp91^{phox} and p22^{phox} subunits localize to the ER in RAW 264.7 cells, while the heterodimer does not

To visualize flavocytochrome *b* trafficking in macrophages using live cell imaging, 22YFP and YFP91 were stably expressed in RAW cells to generate RAW-22YFP and RAW-YFP91 cell lines. 22YFP and YFP91 protein expression in RAW-22YFP and RAW-YFP91 cells was examined using flow cytometry and Western blotting (Figures 27A and 27B). However, the distribution of the fluorescently tagged subunit in each of these two cell lines was reticular (Figure 27C and 27D), suggesting the fluorescently tagged subunits accumulated in the ER and were expressed in excess of their endogenous partner. Colocalization with calnexin confirmed ER localization of YFP91 in RAW-YFP91 cells (Figures 27D). To determine whether the ER-like distribution of 22YFP reflected unassembled 22YFP in excess of endogenous gp91^{phox}, CFP91 was transiently expressed in RAW-22YFP cells. Coexpression of CFP91 in RAW-22YFP cells resulted in loss of the reticular distribution of 22YFP seen in Figure 26D, and a shift to the cell surface and intracellular vesicles that had a perinuclear distribution (Figure 27E). Colocalization of 22YFP and CFP91 was detected in the plasma membrane and intracellular vesicles (Figure 27E). Taken together, these data indicate that, similar to CHO cells, unassembled monomers localize to the ER in RAW 264.7 cells while p22^{phox}/gp91^{phox} heterodimers traffic to the plasma membrane and the endocytic recycling compartment.

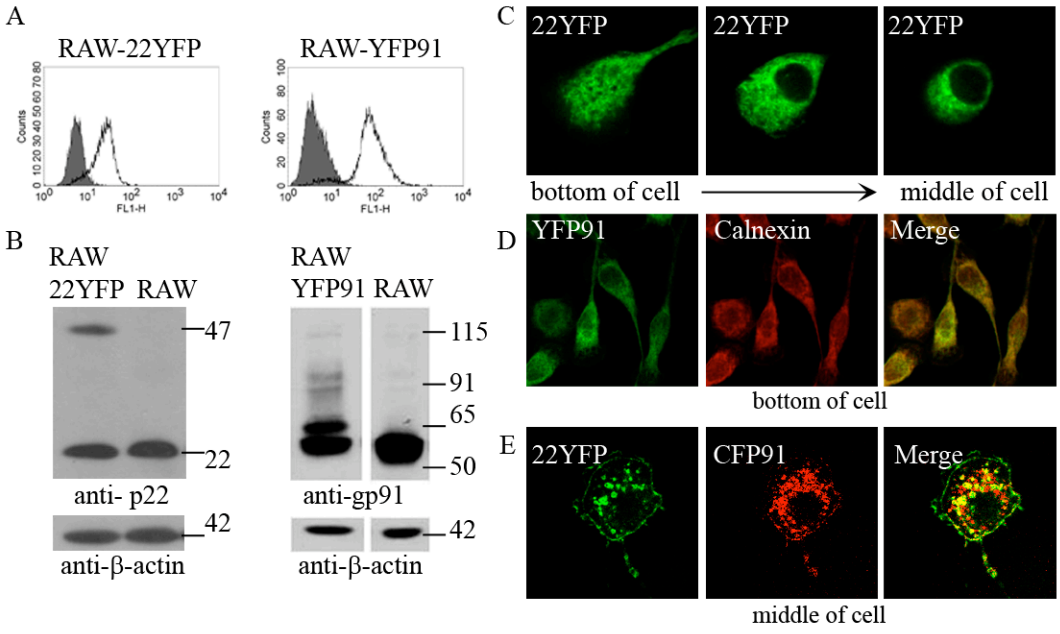

Figure 27. Unassembled fluorescently tagged flavocytochrome *b* subunits localize to the ER in RAW 264.7 macrophages while assembled subunits localize to endosomes and the plasma membrane. Protein expression and subcellular targeting of 22YFP and YFP91 were analyzed in RAW-22YFP and RAW-YFP91 cells. 22YFP and YFP91 protein expression in RAW-22YFP and RAW-YFP91 cells was examined using flow cytometry to detect YFP (A) and using Western blotting to detect $p22^{phox}$ (mAb NS2) or $gp91^{phox}$ (mAb 54.1) (B). RAW-WT cells were used as controls for analysis by flow cytometry (filled grey) and Western blot (labeled RAW). (C) Subcellular distribution of 22YFP in living cells. (D) RAW-YFP91 cells were fixed, permeabilized, and stained for calnexin (n=2 experiments where YFP91 and calnexin colocalization was evaluated. (E) Live RAW-22YFP cells transfected with CFP91 were examined 24 hrs post transfection. Single z stack slices from the bottom and/or middle of the cells are shown as indicated.

It has been shown by Western blot analysis that the monoclonal antibody 54.1 can also detect the ER-resident protein GRP 58 (Baniulis *et al.*, 2005), also known as ERp57. To determine whether immunofluorescent staining of RAW 264.7 cells can also detect this protein, we co-stained RAW 264.7 cells with mAb 54.1 and calnexin. As shown in Figure 28, immunofluorescent staining with 54.1 shows a predominant vesicular distribution with clustering near the nucleus (*arrows*), while calnexin showed a much different intracellular distribution that did not appear as punctate. In addition, immunofluorescent staining with 54.1 showed a more peripheral distribution (Figure 28, *arrowheads*) than the calnexin staining. Most importantly, immunofluorescent staining with 54.1 did not colocalize with calnexin, further establishing 54.1 as a valid antibody for localizing endogenous gp91^{phox} in RAW 264.7 cells.

7. Flavocytochrome *b* localizes to recycling endosomes in primary murine BMDMs

We next examined the localization of flavocytochrome *b* in BMDMs by confocal microscopy of live cells. To minimize potential problems in balancing expression of a fluorescently tagged subunit with endogenous flavocytochrome *b* subunits, we utilized the recently characterized p22^{phox}-deficient nmf333 mouse (Nakano *et al.*, 2008) to express 22YFP in BMDMs. The nmf333 mouse harbors a missense mutation in the p22^{phox} gene that prevents expression of the p22^{phox} subunit. nmf333 BM progenitor cells were transduced with a retroviral vector for expression of 22YFP, and then differentiated into macrophages. Western blot analysis of BMDMs (Figure 29A) confirmed the absence of p22^{phox} in mock-transduced nmf333 BMDMs, and that 22YFP was expressed.

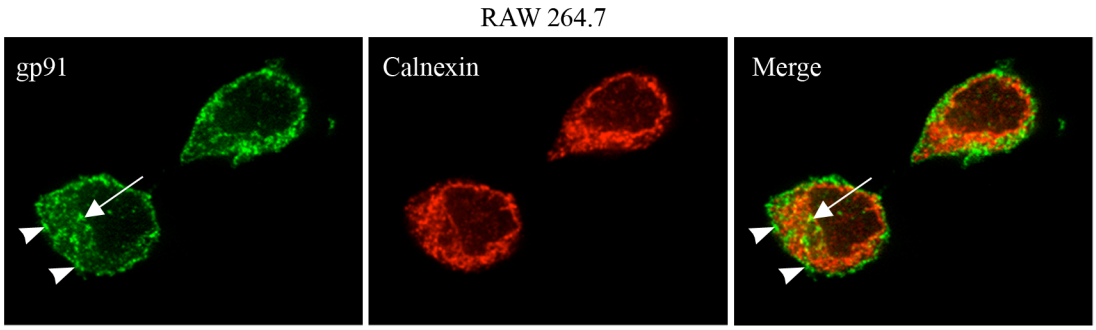

Figure 28. Endogenous gp91^{phox} does not localize to the endoplasmic reticulum in RAW 264.7 cells. Cells were fixed, permeabilized, and stained for gp91^{phox} (mAb 54.1) and calnexin (1:400 dilution). gp91^{phox} localized to vesicles near the cell surface (left, *arrowheads*) and vesicles that appeared to cluster near the nucleus (left, *arrows*), which was distinct from the intracellular distribution of calnexin (merged image, *arrowheads* and *arrows*). A single z stack section from the middle of the cell is shown.

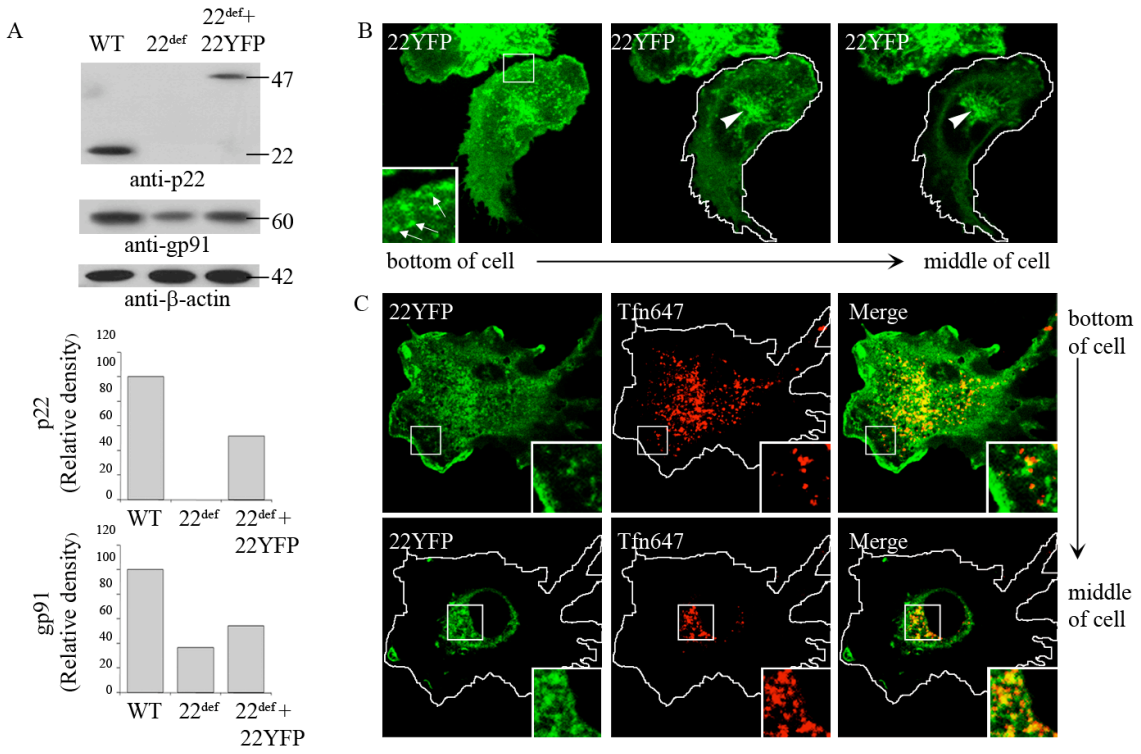

Figure 29. 22YFP expressed in p22^{phox}-deficient (p22^{def}) bone marrow derived macrophages localizes to the plasma membrane and endocytic recycling compartment. p22^{def} bone marrow (BM) cells were transduced with MSCV-22YFP and differentiated into macrophages for 6-7 days. (A) Lysates of WT, p22^{def}, and 22YFP-expressing p22^{def} BMDMs were probed to detect p22^{phox} (mAb NS2), gp91^{phox} (mAb 54.1), and β-actin (mAb). Top bar graph shows the relative density of p22^{phox} protein, normalized to β-actin. Bottom bar graph shows the relative density of gp91^{phox} protein normalized to β-actin. Data shown is representative of 3 independent experiments. (B) 22YFP expressed in p22^{phox}-deficient BMDMs was imaged in living cells. 22YFP localizes to vesicles near the plasma membrane (insets, *arrows*) and vesicles that cluster near the nucleus (*arrowheads*). (C) 22YFP-expressing p22^{phox}-deficient BMDMs were incubated with Alexa Fluor 647-conjugated mouse transferrin (Tfn647, 5 μg/ml) for 5 min at 37°C followed by a 25 min chase at 37°C to label the endocytic recycling compartment. 22YFP and Tfn647 colocalized in vesicles near the plasma membrane (top panel, *insets*) and near the nucleus (bottom panel, *insets*).

The relative level of the YFP-tagged $p22^{phox}$ was 43 +/- 14% of endogenous $p22^{phox}$ in mock-transduced wild type C57Bl/6J BMDMs (N = 3 experiments where densitometry was performed). As previously mentioned, formation of flavocytochrome *b* in phagocytic leukocytes increases the stability of each of its constituent subunits (Nauseef, 2004). A small amount of residual $gp91^{phox}$ expression was detected in nmf333 BMDMs, which increased upon expression of 22YFP by 39 +/- 12% (N = 3 experiments where densitometry was performed) (Figure 20A), consistent with the stabilization of endogenous $gp91^{phox}$ by heterodimer formation.

We utilized confocal microscopy to localize flavocytochrome *b* in nmf333 BMDMs transduced with 22YFP. As shown in Figure 29B, much of 22YFP in living macrophages was associated with intracellular vesicles (*arrows*) that appeared to cluster near the nucleus (*arrowheads*). In fixed cells, 22YFP and endogenous $gp91^{phox}$ showed a very similar distribution and colocalized at the plasma membrane, on vesicles near the plasma membrane, and on perinuclear vesicles that clustered in the middle of the cell (Figure 30A). A similar distribution was observed for endogenous $gp91^{phox}$ in WT BMDMs (Figure 30B). To verify that flavocytochrome *b* localized to the endocytic recycling compartment in primary macrophages, recycling endosomes were labeled with Alexa Fluor 647-conjugated murine transferrin, as described above. Imaging of live $p22^{phox}$-deficient BMDMs transduced with 22YFP revealed colocalization of 22YFP and transferrin in vesicles near the plasma membrane (Figure 29C, top panel, insets) and in a perinuclear distribution (Figure 29C, bottom panel, insets). These data indicate that flavocytochrome *b* is present in the endocytic recycling compartment of primary BMDMs.

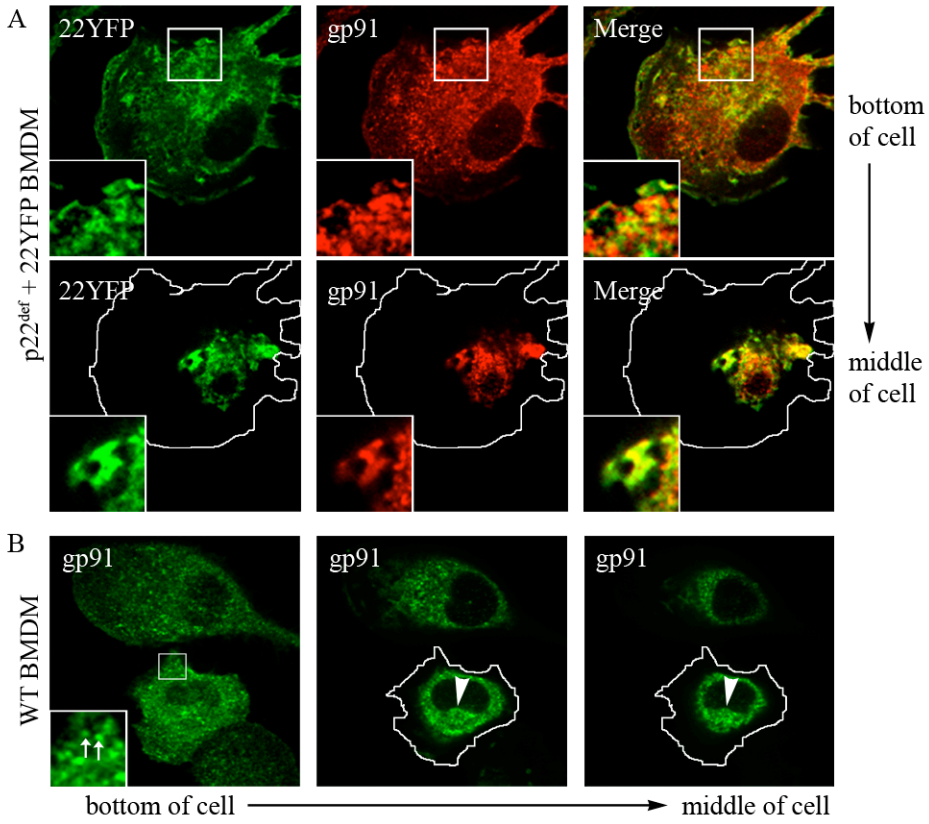

Figure 30. Endogenous gp91^{phox} in 22YFP transduced p22^{def} and WT BMDMs localizes to the plasma membrane and endosomes that cluster near the nucleus. BMDMs were fixed, permeabilized, and stained for endogenous gp91^{phox}. (A) 22YFP expressed in 22^{def} BMDMs co-localized with gp91^{phox} primarily on intracellular at vesicles near the cell surface (top panel, *insets*) and vesicles near the nucleus (bottom panel, *insets*). (B) Endogenous gp91^{phox} localizes to intracellular vesicles near the plasma membrane (inset, *arrows*) and near the nucleus (*arrowheads*).

III. Flavocytochrome *b* localizes to the phagocytic cup and vesicles near nascent phagosomes in "resting" macrophages

1. Flavocytochrome *b* trafficking during phagocytosis in BMDMs

We next investigated trafficking of flavocytochrome *b* during phagocytosis. While use of YFP- and CFP-tagged $p22^{phox}$ and $gp91^{phox}$ would have allowed simultaneous imaging of both heterodimer subunits during phagocytosis, the CFP-tagged proteins were only weakly fluorescent and not suitable for collecting a series of images over time. Thus, we evaluated colocalization of 22YFP and endogenous $gp91^{phox}$, visualized by indirect immunofluorescence, in $p22^{phox}$-deficient BMDMs expressing 22YFP after 2 and 15 min of phagocytosis of SOZ particles. 22YFP and $gp91^{phox}$ showed a very similar distribution in the phagocytic cup (Figure 31A, top panel, *arrowheads*) and nascent phagosomes (Figure 31A, top and bottom panels, *asterisks*). We also observed the presence of 22YFP and $gp91^{phox}$ in discrete patches near the phagocytic cup and near phagosomes (Figure 31A, *arrows*), which appeared vesicular. We hypothesize that these regions might be endosomes involved in trafficking of flavocytochrome *b* between phagosomes and internalized membranes.

Importantly, evaluation of immunofluorescent staining of $gp91^{phox}$ in $p22^{def}$ BMDMs lacking 22YFP (Figure 31B, *outlined in white*) showed that $gp91^{phox}$ in the absence of $p22^{phox}$ did not localize to the phagocytic cup (Figure 31B, *white arrow*) or nascent phagosomes (Figure 31B, *white arrowheads*).

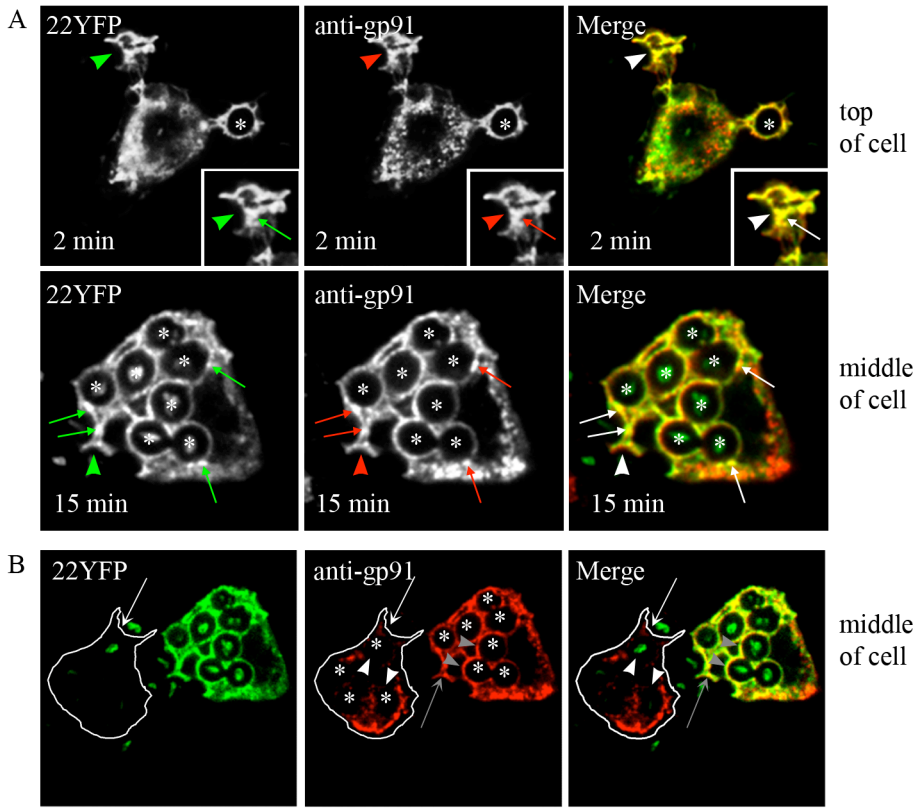

Figure 31. Flavocytochrome *b* localizes to the phagocytic cup and vesicles near nascent phagosomes in BMDMs. (A) Colocalization of 22YFP and gp91^{phox}, detected by immunofluorescence, in p22^{phox}-deficient BMDMs following 2 min (top panel) and 15 min (bottom panel) of synchronized phagocytosis. A series of z stack planes (0.16 μm) were collected. 5 single planes (total = 0.8 μm) were merged using the Z stack projection tool in ImageJ. *Arrowheads* denote phagocytic cups and *asterisks* indicate nascent phagosomes. *Arrows* indicate discrete foci of increased 22YFP and gp91^{phox} colocalization near phagocytic cups and nascent phagosomes. (B) gp91^{phox}, detected by immunofluorescence, in a p22^{phox}-deficient BMDM lacking 22YFP expression (*outlined in white*) did not localize near phagocytic cups (white *arrows*) or nascent phagosomes (white *arrowheads*) following 15 min of synchronized phagocytosis. Representative images from 2 independent experiments in which at least 10 cells were evaluated at each time point.

2. Flavocytochrome *b* colocalizes with Rab11GFP at vesicles near the phagocytic cup and sealed phagosomes

Rab11-positive recycling endosomes can be detected in the vicinity of nascent phagosomes and forming phagocytic cups (Cox *et al.*, 2000), and can deliver proteins such as TNFα to forming phagosomes (Murray *et al.*, 2005). Our finding that flavocytochrome *b* localizes to the Rab11 endocytic recycling compartment in both RAW 264.7 and BMDMs and that flavocytochrome *b* appeared to accumulate in discrete foci near the phagosome at different time points during phagocytosis suggested that recycling endosomes may serve as an intracellular reservoir from which additional flavocytochrome *b* can be delivered to the plasma membrane or phagosome. Therefore, we examined the localization of endogenous $gp91^{phox}$ and Rab11GFP during phagocytosis of SOZ particles in RAW 264.7 cells. Staining of $gp91^{phox}$ was evident on the plasma membrane, the phagocytic cup, and nascent phagosomes, as well as intracellular vesicles (Figure 32, left column), similar to BMDMs. Some $gp91^{phox}$ also appeared to be subjacent to the plasma membrane in colocalization with Rab11GFP (Figure 32, right column, *block arrows*), consistent with the role of Rab11-positive endosomes in trafficking intracellular membrane to the cell surface (Ullrich *et al.*, 1996). Interestingly, $gp91^{phox}$ was also detected on nascent phagosomes, which lacked Rab11GFP (Figure 32, *asterisks*), suggesting that some flavocytochrome *b* was targeted directly to phagocytic cups as they formed from the plasma membrane. Concordant with published data (Leiva *et al.*, 2006), Rab11GFP was also detected on vesicles near the base of forming phagocytic cups and on the membranes of newly formed phagosomes, where it colocalized with $gp91^{phox}$ (Figure 32, right column, *arrowheads and arrows,*

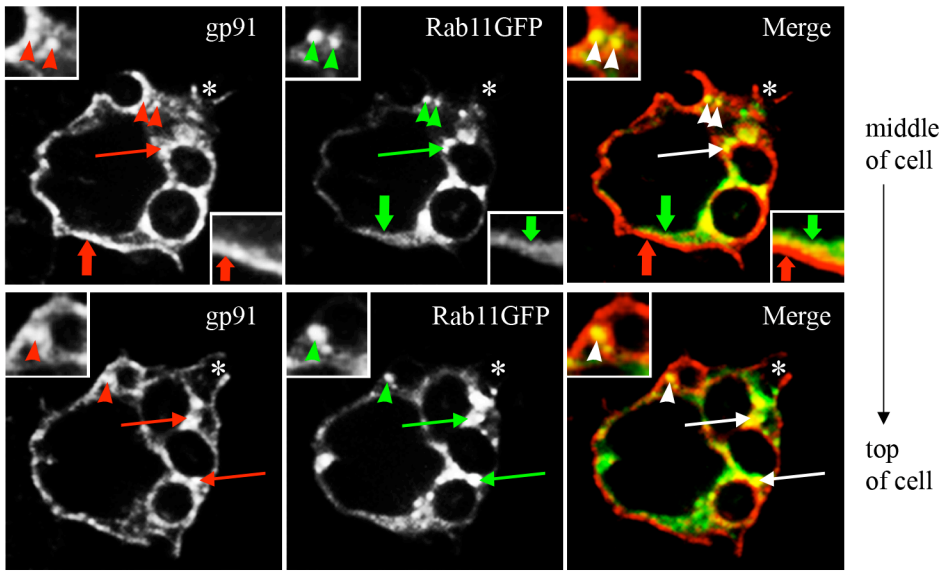

Figure 32. Flavocytochrome *b* colocalizes with Rab11GFP in or near phagocytic cups and nascent phagosomes. RAW 264.7 cells transiently expressing Rab11GFP were fixed, permeabilized, and stained to detect gp91^{phox} (mAb 54.1) 15 min after synchronized phagocytosis of serum opsonized zymosan. *Arrowheads* indicate colocalization of gp91^{phox} and Rab11GFP near a forming phagocytic cup (merged image). *Arrows* show colocalization on or near nascent phagosomes. *Wide arrows* indicate gp91^{phox} in the plasma membrane subjacent to Rab11GFP, and *asterisks* mark a recently sealed phagosome that is gp91^{phox}-positive, but Rab11GFP-deficient.

respectively). These data thus also suggest that Rab11-positive recycling endosomes may be involved in trafficking of flavocytochrome *b* between intracellular membranes and forming or nascent phagosomes.

3. Frustrated phagocytosis does not increase flavocytochrome *b* localization to the cell surface in RAW 264.7 cells

Following phagocytosis of SOZ, we found flavocytochrome *b* to modestly increase at the cell surface (Figure 32). This observation suggested that binding of phagocytic receptors may initiate signals leading to recruitment of intracellular membranes containing flavocytochrome *b* to the plasma membrane. Using immune complex coated coverslips, we sought to test whether activation of the Fcγ-receptor would increase localization of flavocytochrome *b* to the cell surface. Engagement of the Fcγ-receptor on immobilized immune complex-coated surfaces is a model system for analyzing membrane receptor mobilization and polarization to the plasma membrane (Eng *et al.*, 2007), called "frustrated phagocytosis" since the macrophage attempts to, but can not "eat" the coverslip. Immunofluorescent staining of $gp91^{phox}$ in RAW 264.7 cells following 15 or 60 min incubation on BSA-IgG-coated coverslips showed $gp91^{phox}$ did not appear to increase at the cell surface during frustrated phagocytosis (Figures 33A and 33B). Spreading of RAW 264.7 macrophages was observed (Figure 33A, *arrows*), consistent with the behavior of primary macrophages during frustrated phagocytosis (Takemura *et al.*, 1986).

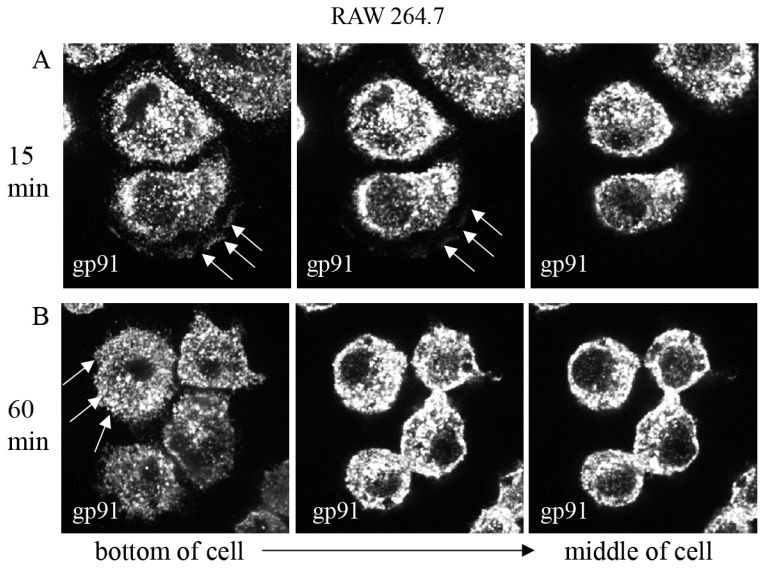

Figure 33. Frustrated phagocytosis does not increase flavocytochrome *b* localization to the cell surface in RAW 264.7 cells. Following incubation on BSA-IgG-coated coverslips for 15 min (A) or 60 min (B), $gp91^{phox}$, detected by immunofluorescence, was found mostly in vesicles that clustered near the nucleus and showed little localization to the cell surface (*arrows*) in RAW 264.7 cells. This experiment was performed only once.

IV. Flavocytocrome *b* protein expression increases in IFNγ, but not LPS, activated macrophages

1. Duration of IFNγ stimulation increases protein expression of flavocytochrome *b* subunits

Quiescent or "resting" macrophages are essential to innate immunity due to their ability to phagocytose and destroy pathogens in the absence of any required co-stimulation. However, in the presence of co-stimulatory factors, such as the T cell helper Type-1 (Th1) cytokines, IFNγ and/or TNFα, the antimicrobial activity of macrophages is greatly enhanced (Mosser and Edwards, 2008). IFNγ stimulation of both macrophages and neutrophils increases NADPH oxidase activity, which has been linked to increased protein expression of gp91^{phox} and p67^{phox} (Schroder *et al.*, 2004). 300 U/ml (~ 30 ng/ml) IFNγ is sufficient for maximum expression of the major histocompatibility complex class II (MHCII) in BMDMs (Gonalons *et al.*, 1998), and 1000 U/ml (~ 100 ng/ml) IFNγ results in maximum killing of *S. typhimurium* in BMDMs (Gordon *et al.*, 2005), suggesting 100 ng/ml is a "saturating" amount of IFNγ for these biological responses.

Thus, we evaluated the protein expression of flavocytochrome *b* and NADPH oxidase subunits p47^{phox}, p67^{phox} and p40^{phox} by Western blotting in RAW 264.7 cells stimulated with 100 ng/ml IFNγ for 24, 48, and 72 hr. As expected from previous studies showing that IFNγ increases transcription of CYBB (Newburger *et al.*, 1991; Eklund *et al.*, 1998), we observed increased gp91^{phox} expression over time (Figure 34). p22^{phox} mRNA is not tightly regulate (Newburger *et al.*, 1988), but p22^{phox} protein expression is dependent on heterodimer formation with gp91^{phox} for stability (DeLeo *et al.*, 2000). Thus, in addition to gp91^{phox}, a concomitant increase in p22^{phox} protein expression was

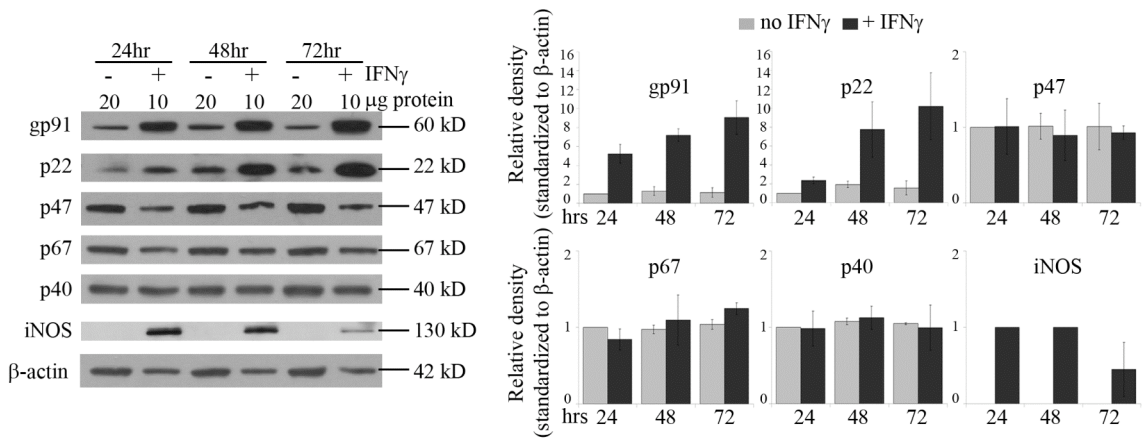

Figure 34. Duration of IFNγ activation of RAW 264.7 cells increases protein expression of flavocytochrome *b*, but not NADPH oxidase subunits p47^{phox}, p67^{phox}, or p40^{phox}. RAW 264.7 cells were stimulated with 100 ng/ml IFNγ for 24, 48, or 72 hr. Cells were harvested by trypsinization and cell lysates were analyzed for protein expression of NADPH oxidase subunits gp91^{phox} (mAb 54.1), p22^{phox} (mAb NS2), p47^{phox} (Rb poly), p67^{phox} (mAb), and p40^{phox} (Rb poly) by Western blotting. For better comparison, double the protein of lysates from cells cultured in the absence of IFNγ was loaded in each well. The density of each sample was normalized to β-actin and then the relative density of each protein from lysates cultured in the absence of IFNγ for 24 hr was calculated, with the exception of iNOS. iNOS density is reported relative to samples cultured in the presence of IFNγ for 24 hr. Densitometry was analyzed for n=3 independent experiments except for p47^{phox}, p40^{phox} and iNOS where n=2 independent experiments.

also detected (Figure 34). No change in protein expression was observed for the NADPH oxidase subunits p47^{phox}, p67^{phox}, and p40^{phox} (Figure 34). Due to the substantial increase in protein expression of flavocytochrome *b* following IFNγ stimulation, 10 μg of total protein from IFNγ stimulated samples and 20 μg of non-stimulated samples were loaded to each well for better comparison. Analysis by densitometry of 3 independent experiments showed gp91^{phox} and p22^{phox} increased, respectively, 5.2 [±1.0] and 2.4 [±0.3]-fold at 24 hr, 7.2 [±0.6] and 7.8 [±]-fold at 48 hr and 9.1 [±1.7] and 10.2 [±3.5]-fold at 72 hr (Figure 34).

IFNγ activation of macrophages also increases iNOS protein expression (Lin *et al.*, 2008), which in addition to the NADPH oxidase, enhances macrophage antimicrobial activity. Thus, iNOS protein expression in RAW 264.7 cells following IFNγ (100 ng/ml) activation for 24, 48, and 72 hr was evaluated by Western blot analysis. In the absence of IFNγ, iNOS protein expression was undetectable (Figure 34). In the presence of IFNγ, a strong signal was detected for iNOS that was similar in 24 and 48 hr IFNγ activated cells, but appeared to decrease in 72 hr IFNγ activated cells (Figure 34), consistent with a previous study (Gonalons *et al.*, 1998). Our results support differential regulation of iNOS and flavocytochrome *b* protein expression by IFNγ in RAW 264.7 cells, which has also been reported by others (Bastian and Hibbs, 1994).

IFNγ activation of macrophages is frequently assessed by evaluating the cell surface expression of MHCII (Mosser, 2003). To test whether the duration of IFNγ also increased protein expression of MHCII, MHCII surface expression was evaluated by flow cytometry. MHCII expression was undetectable in the absence of IFNγ in RAW 264.7

cells, but was induced after 24 hr of IFNγ stimulation at a dose of 100 ng/ml, which appeared to reach maximal expression at 48 hr (Figure 35), confirming previous results (Gonalons *et al.*, 1998). At 24 hr, MHCII was not expressed following activation with a low dose of 10 ng/ml IFNγ, but this dose was sufficient to increase MHCII expression by 48 hr, at which point MHCII expression was similar in cells activated with 10, 100, or 500 ng/ml IFNγ.

Next, we analyzed flavocytochrome *b* expression following 24 and 72 hr IFNγ (100 ng/ml) activation in WT C57/Bl6 and gp91^{phox}-deficient (CGD) BMDMs. Similar to RAW 264.7 cells (Figure 34), gp91^{phox} and p22^{phox} protein expression was found to increase over time in WT BMDMs (Figure 36). Densitometric analysis of one experiment found IFNγ activation to increase the protein expression of gp91^{phox} and p22^{phox} in unstimulated cells approximately 2-fold at 24 hr and dramatically increase approximately 7-fold at 72 hr (Figure 36), similar to RAW 264.7 cells.

2. Maximum increase in flavocytochrome *b* expression following 10 ng/ml IFNγ activation in RAW 264.7 cells

As mentioned above, 100 ng/ml IFNγ is a "saturating" concentration of IFNγ for MHCII expression and killing of the intracellular pathogen *S. typhimurium*, but whether flavocytochrome *b* protein expression is maximal at this concentration has not been shown. RAW 264.7 cells were stimulated with serial dilutions of IFNγ (0.1 – 100 ng/ml) to evaluate protein expression of flavocytochrome *b* at 24, 48, and 72 hr. gp91^{phox} and p22^{phox} were found to increase in RAW 264.7 cells stimulated with as little as 0.1 ng/ml IFNγ (Figure 37) and continue to increase until 10 ng/ml IFNγ, at which point,

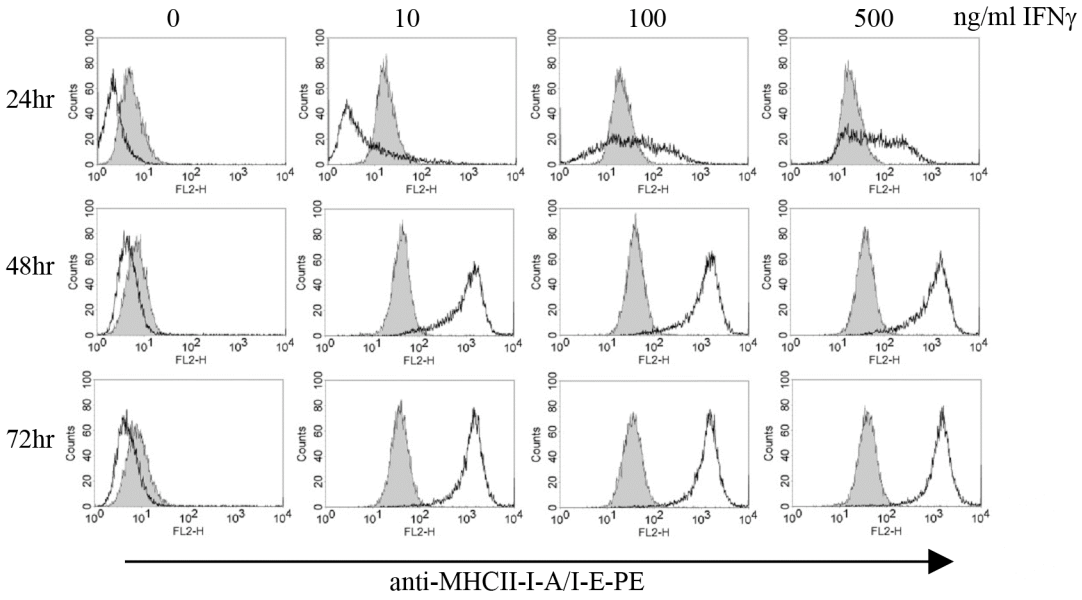

Figure 35. Increased MHCII surface expression following IFNγ stimulation is dependent on the time and dose of IFNγ stimulation in RAW 264.7 cells. Following 24, 48, or 72 hr, unactivated or IFNγ (10 – 500 ng/ml) activated RAW 264.7 cells were evaluated for the cell surface expression of MHCII (black line) by flow cytometry. The isotype control, rat IgG_{2b}, is shown in grey fill.

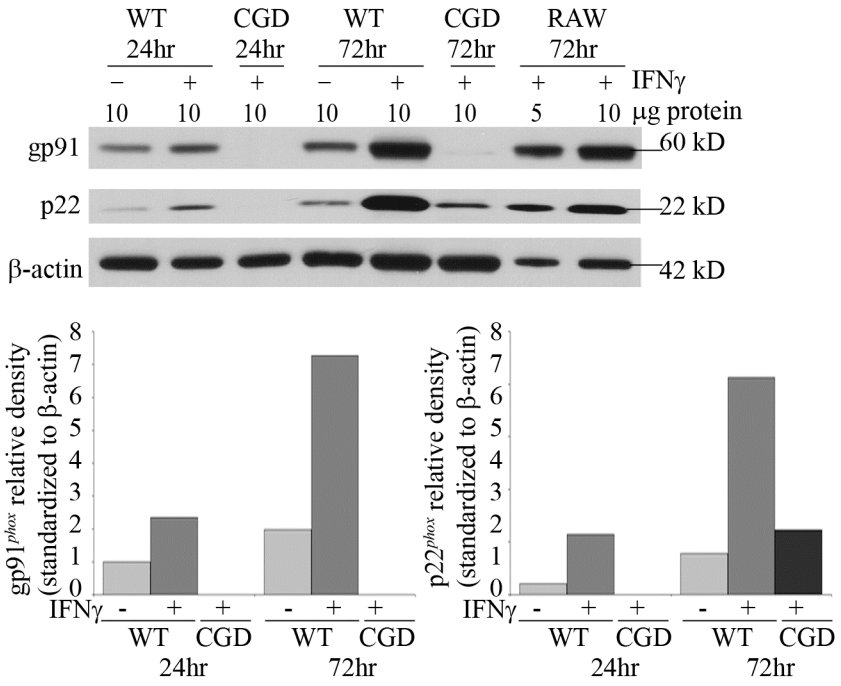

Figure 36. Duration of IFNγ activation also increases flavocytochrome *b* protein expression in BMDMs. Day 8-differentiated BMDMs (WT C57Bl/6 and CGD) were plated onto 100 mm Petri dishes in the presence (+) or absence (-) of IFNγ (100 ng/ml) in αMEM with 10% HI FCS and M-CSF (25 ng/ml) for 24 or 72 hr. BMDMs were collected using cold PBS and cell lysates were analyzed for flavocytochrome *b* protein expression using mAbs 54.1 (anti-gp91^{phox}), NS2 (anti-p22^{phox}), and anti-β-actin. This experiment was performed only once.

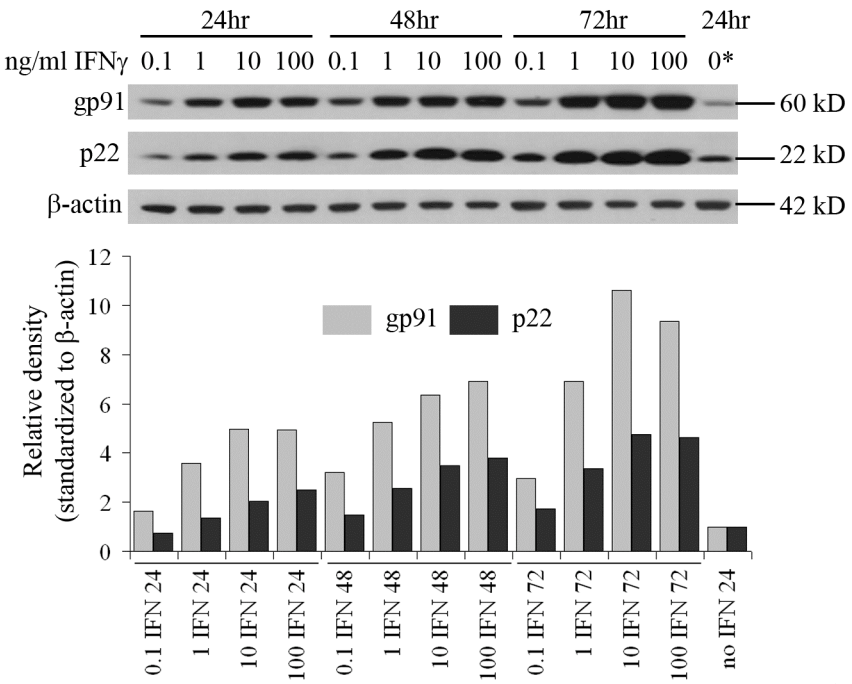

Figure 37. Maximum increase in flavocytochrome *b* protein expression following 10 ng/ml IFNγ in RAW 264.7 cells. RAW 264.7 cells were stimulated with IFNγ (0.1 - 100 ng/ml) for 24, 48 and 72 hr. Flavocytochrome *b* protein expression in cell lystates was analyzed by Western blotting using mAbs 54.1 (anti-gp91^{phox}) and NS2 (anti-p22^{phox}). Representative immunoblot from of 1 of 2 independent experiments. * denotes 20 μg protein was loaded to this lane, while 10 μg protein was added to all other lanes.

flavocytochrome *b* expression appeared to reach a plateau. We also compared flavocytochrome *b* protein expression following 100 and 500 ng/ml IFNγ and found no further increase in protein expression in cells activated with the higher dose of 500 ng/ml IFNγ (see Figure 39). Thus, similar to MHCII (see Figure 35), a marker for macrophage activation, flavocytochrome *b* expression also appeared to be reach maximum levels within the range of 10 -100 ng/ml IFNγ.

3. In contrast to IFNγ, LPS stimulation only modestly increases flavocytochrome *b* protein expression in RAW 264.7 cells

In addition to inflammatory cytokines released by cells of the adaptive and innate immune system, LPS is also known to activate macrophages (Guha and Mackman, 2001). While considerable data exist on the IFNγ stimulated increase in NADPH oxidase activity in macrophages, less is known about LPS stimulation. Notably, while LPS has been shown to increase gp91^{phox} mRNA levels approximately 2-fold after 2 hr LPS (1 μg/ml) stimulation in neutrophils (Cassatella *et al.*, 1990) little to no data exist on LPS regulation of gp91^{phox} in monocytes and/or macrophages.

Flavocytochrome *b* protein expression was evaluated in RAW 264.7 cells following LPS (20 and 250 ng/ml) stimulation at 24, 48, and 72 hr. Following 24 hr LPS stimulation, an increase in gp91^{phox} and p22^{phox} protein expression was detected, which appeared to be dose dependent (Figure 38A). gp91^{phox} and p22^{phox} protein expression appeared to continue to slightly increase at 48 and 72 hr. Densitometric analysis of one experiment found LPS stimulation (250 ng/ml) to increase the protein expression of gp91^{phox} and p22^{phox} measured in unstimulated cells by approximately 1.8- and 2.6-fold at

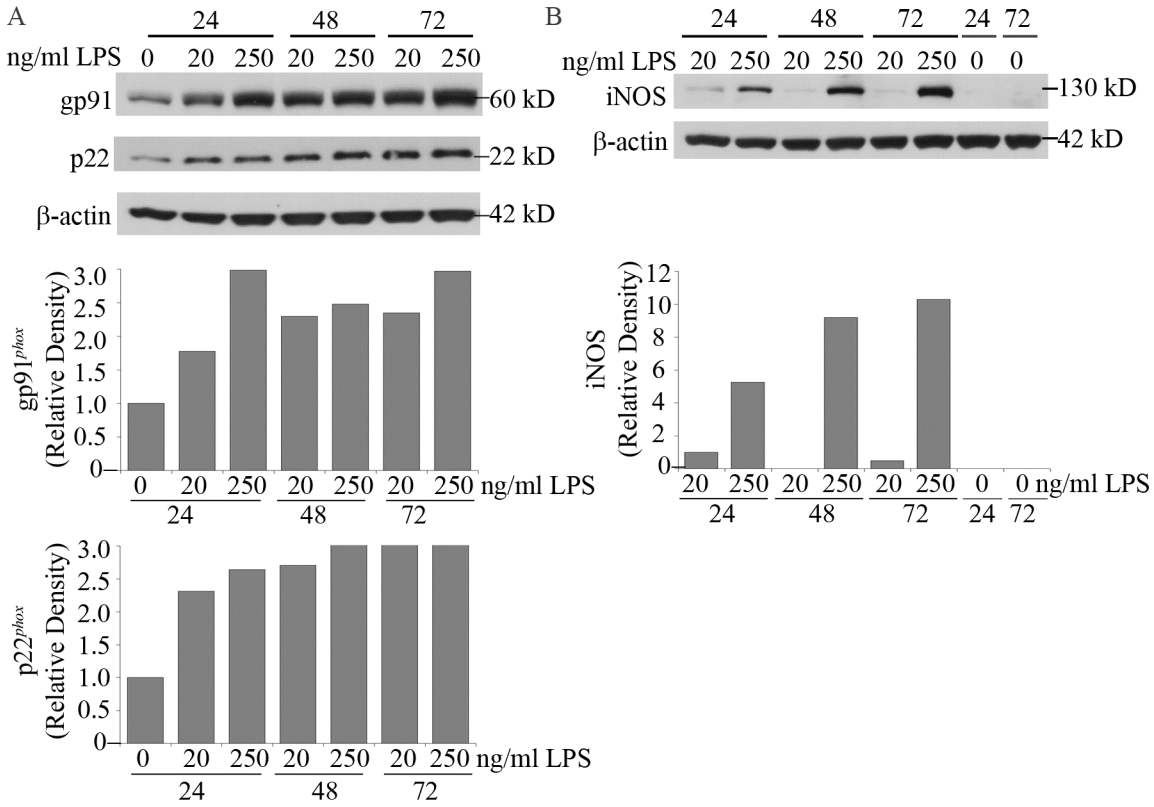

Figure 38. In contrast to IFNγ, LPS appears to only modestly increase flavocytochrome *b* expression following 24 - 72 hr in RAW 264.7 cells. Unstimulated and LPS (20 or 250 ng/ml) stimulated RAW 264.7 cells were harvested following 24, 48 and 72 hr, lysed, and analyzed for protein expression of (A) flavocytochrome *b* using mAbs 54.1 (anti-gp91^{phox}) and NS2 (anti-p22^{phox}) or (B) iNOS. Western blots and densitometry from 1 of 2 independent experiments are shown for (A) and representative Western blots and densitometry from 1 of 2 independent experiments are shown for (B).

24 hr, 2.5- and 3-fold at 48 hr, and 3- and 3.4-fold at 72 hr, respectively (Figure 38A). However, in a second experiment, 72 hr LPS (250 ng/ml) stimulation increased gp91^{phox} and p22^{phox} expression approximately 1.3- and 2.4-fold (not shown), suggesting the increase in protein expression was variable following LPS stimulation. In summary, LPS appears to increase flavocytochrome *b* protein expression, but the increase is modest compared to the 5 - 10 fold increase induced by IFNγ.

iNOS protein expression was evaluated to serve as our positive control since LPS is a potent inducer of iNOS in RAW 264.7 cells (Lin *et al.*, 2008). As expected, iNOS expression was induced following 24, 48, and 72 hr of LPS stimulation (Figure 38B).

4. Combination of IFNγ and LPS additively increases iNOS protein expression, but not flavocytochrome *b*

Next, we evaluated the protein expression of iNOS and flavocytochrome *b* following 24 - 72 hr of activation with IFNγ alone and both IFNγ and LPS since the expression of iNOS has been shown to increase synergistically following stimulation with the combination of IFNγ and LPS (Gao *et al.*, 1997; Lin *et al.*, 2008). While the protein expression of iNOS was found to be greater in cells stimulated with the combination of IFNγ (10 ng/ml) and LPS (20 ng/ml) than with IFNγ alone (Figure 39), the expression of flavocytochrome *b* did not increase with the addition of LPS (Figure 39). Thus, the combination of IFNγ and LPS did not appear to additively increase flavocytochrome *b* protein expression in RAW 264.7 cells.

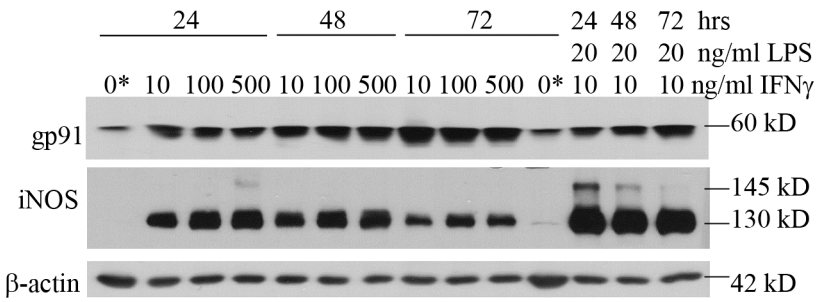

Figure 39. Combination of IFNγ and LPS additively increases protein expression of iNOS, but not flavocytochrome *b*. RAW 264.7 cells cultured in the presence or absence of IFNγ or the combination of IFNγ and LPS for 24, 48, and 72 hr were harvested, lysed, and evaluated for protein expression of (A) $gp91^{phox}$ (mAb 54.1) and (B) iNOS by Western blot analysis. * denotes 30 μg of total protein added to well, while all other wells had 10 μg protein loaded. This experiment was performed only once.

V. In macrophages, IFNγ activation increases localization of flavocytochrome *b* to the plasma membrane

1. Sustained IFNγ stimulation increases the surface localization of flavocytochrome *b* in RAW 264.7 cells

The distribution of flavocytochrome *b* in RAW 264.7 cells stimulated with 100 ng/ml IFNγ for 24 and 72 hr was evaluated by confocal microscopy. RAW 264.7 cells were fixed, permeabilized and then stained for gp91^{phox}, which we utilized as our marker for flavocytochrome *b*. While no significant change in the distribution of gp91^{phox} was seen following 24 hr IFNγ activation, a dramatic change was observed at 72 hr (Figure 40). At 72 hr, gp91^{phox} localized mostly to the cell surface (Figure 40, bottom panel, *arrowheads*), which was in marked contrast to the intracellular distribution seen in the absence of IFNγ (Figure 40, top panel) and in the presence of IFNγ for 24 hr (Figure 40, middle panel). Notably, gp91^{phox} localization to the perinuclear endocytic recycling compartment was prominent in the absence of IFNγ and following 24 hr of IFNγ (Figure 40, *arrows*), but appeared to be absent following 72 hr IFNγ activation.

The distribution of gp91^{phox} was also evaluated in RAW 264.7 cells activated with lower doses of IFNγ (5 and 10 ng/ml). As seen for 100 ng/ml IFNγ (Figure 40), 10 ng/ml IFNγ appeared to increase gp91^{phox} localization to the cell surface (Figure 41A). However, the distribution of gp91^{phox} following 5 ng/ml of IFNγ was highly variable (Figure 41B). Following 5 ng/ml IFNγ activation, 3 different distributions of gp91^{phox} were observed. Some cells showed gp91^{phox} to accumulate in a perinuclear compartment with little localization to the plasma membrane (Figure 41B, top panel), some showed gp91^{phox} to be present in the plasma membrane and endosomal compartments (Figure

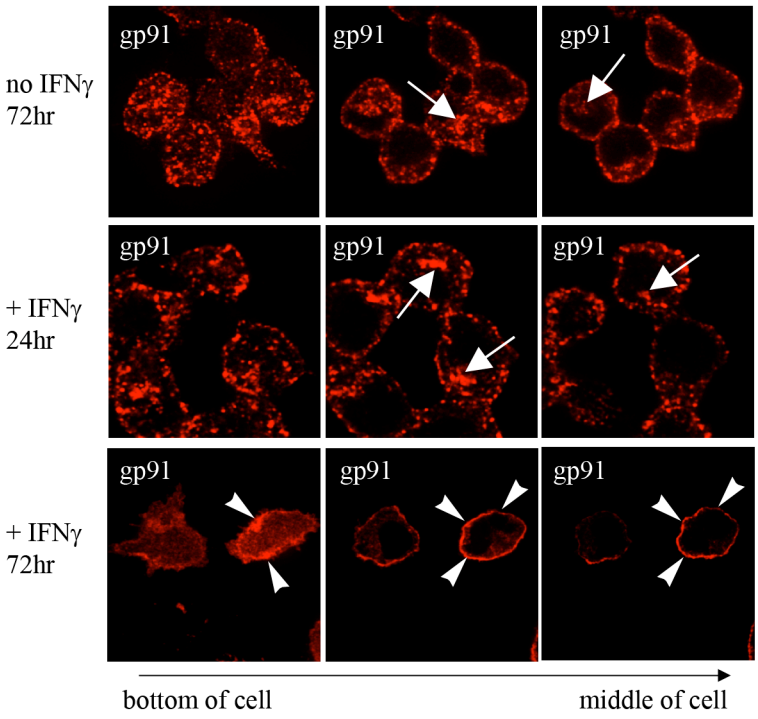

Figure 40. 72 hr IFNγ activation changes the subcellular distribution of flavocytochrome *b* in RAW 264.7 cells. RAW 264.7 cells cultured in the presence or absence of IFNγ (100 ng/ml) for 24 and 72 hr were fixed, permeabilized, and immunostained for $gp91^{phox}$ (mAb 54.1). The distribution of $gp91^{phox}$ was evaluated by immunofluorescence microscopy. $gp91^{phox}$ localized to a prominent perinuclear compartment in the absence of IFNγ and following 24 hr IFNγ stimulation (*arrows*). In contrast, following 72 hr IFNγ activation, $gp91^{phox}$ was found at the cell surface (*arrowheads*) and lacked both the perinuclear (*arrows*) and vesicular-looking distribution seen in unactivated and 24 hr IFNγ activated cells.

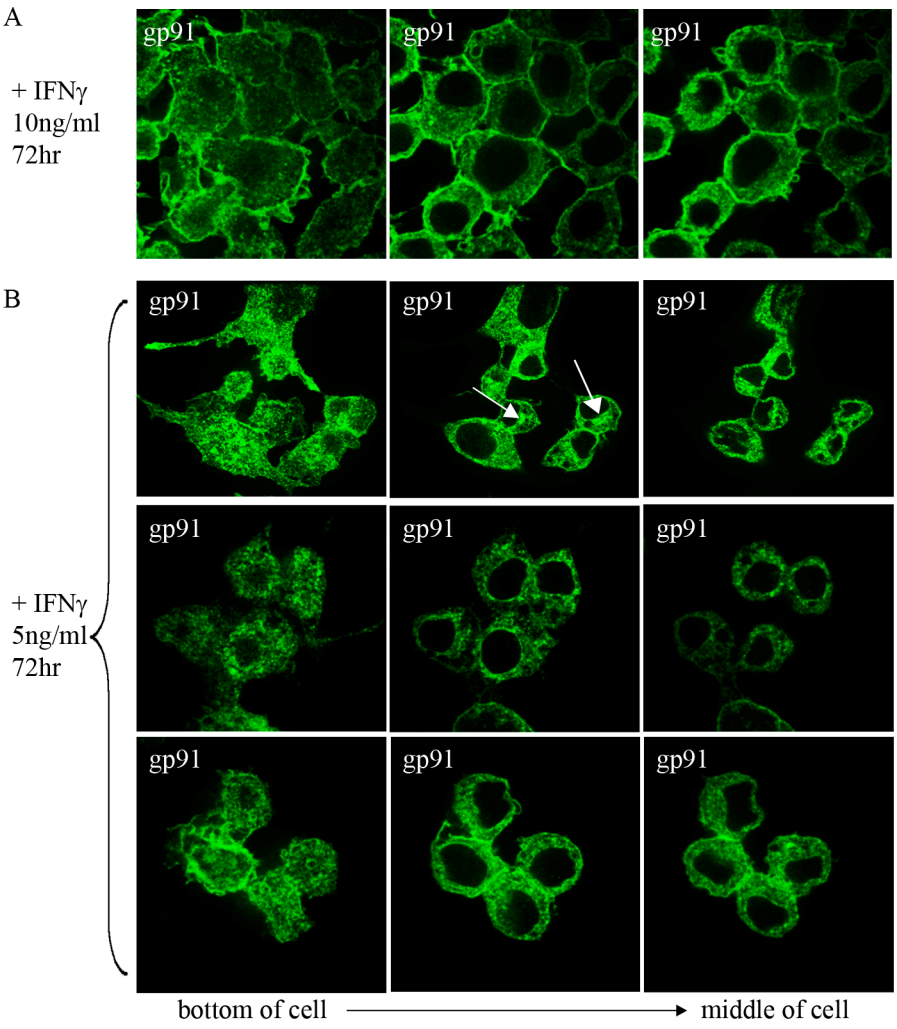

Figure 41. Similar increase in gp91^{phox} surface expression following 10 ng/ml IFNγ, but not 5 ng/ml IFNγ activation in RAW 264.7 cells. 72 hr IFNγ (5 or 10 ng/ml) activated RAW 264.7 cells were fixed, permeabilized, and the distribution of gp91^{phox} (mAb 54.1) was evaluated by immuno-fluorescence microscopy. (A) gp91^{phox} was found at the cell surface in RAW 264.7 cells activated with 10 ng/ml IFNγ. (B) Distribution of gp91^{phox} was highly variable in RAW 264.7 cells activated with 5 ng/ml IFNγ. gp91^{phox} localized either to a predominant perinuclear compartment (top panel, *arrows*), to vesicular-looking structures dispersed throughout the cell (middle panel), or to the plasma membrane and vesicular-looking structures (bottom panel). Representative images from 2 independent experiments are shown in which at least 50 cells were evaluated.

41B, middle panel), and others showed gp91^{phox} to localize mostly to the cell surface. From 2 independent experiments, it appeared that approximately 30% of cells had each of these distributions.

2. Decreased colocalization of flavocytochrome *b* with the transferrin-labeled endocytic recycling compartment following IFNγ activation in RAW 264.7 cells

We showed flavocytochrome *b* colocalizes with Rab11 and transferrin at the endocytic recycling compartment in "resting" RAW 264.7 cells and BMDMs (Figures 23 and 29). To further investigate the change in distribution of flavocytochrome *b* following IFNγ activation, colocalization of gp91^{phox} with subcellular markers for the endocytic recycling compartment and the plasma membrane was evaluated in IFNγ activated RAW 264.7 cells. To label the endocytic recycling compartment and early endosomes, RAW 264.7 cells were incubated with Alexa Fluor 647-conjugated human transferrin for 25 min. In IFNγ activated cells, gp91^{phox} did not appear to colocalize with transferrin at the endocytic recycling compartment (Figure 42, bottom panel, insets), in contrast to the colocalization observed in the absence of IFNγ (Figure 42, top panel, insets). In addition to the loss of a prominent perinuclear compartment in IFNγ activated RAW 264.7 cells, an increase in colocalization of gp91^{phox} with PH-GFP was observed (Figure 43). Changes in colocalization with these subcellular markers further suggested IFNγ induces a change in the distribution of flavocytochrome *b*.

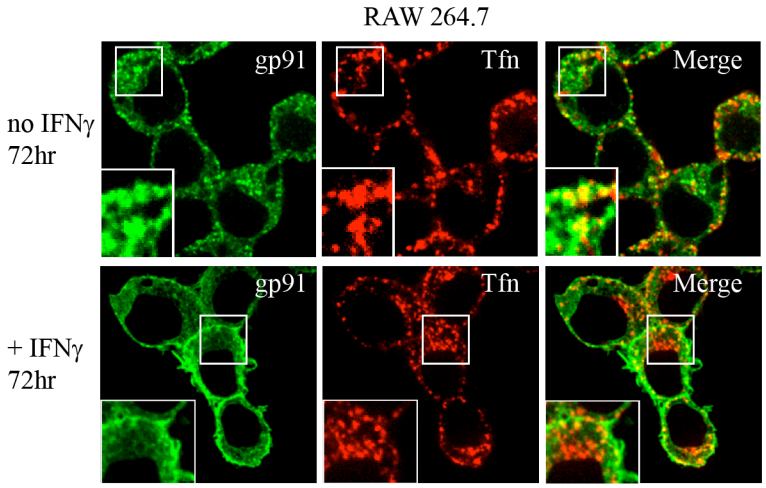

Figure 42. Loss of localization of gp91^{phox} to the transferrin-labeled endocytic recycling compartment in 72 hr IFNγ stimulated RAW 264.7 cells. RAW 264.7 cells cultured in the presence or absence of IFNγ (100 ng/ml) for 72 hr were incubated with Alexa Fluor 647-conjugated human transferrin (Tfn, 5 μg/ml) for 25 min at 37°C to label the endocytic recycling compartment and early endosomes. Cells were fixed, permeabilized, and stained for gp91^{phox}. In the absence of IFNγ, colocalization of gp91^{phox} and Tfn was observed at the perinuclear compartment (top panel, *insets*) and near the plasma membrane. In the presence of IFNγ, colocalization of gp91^{phox} and Tfn was not seen at a perinuclear compartment (bottom panel, i*nsets*), but was seen in vesicles near the plasma membrane.

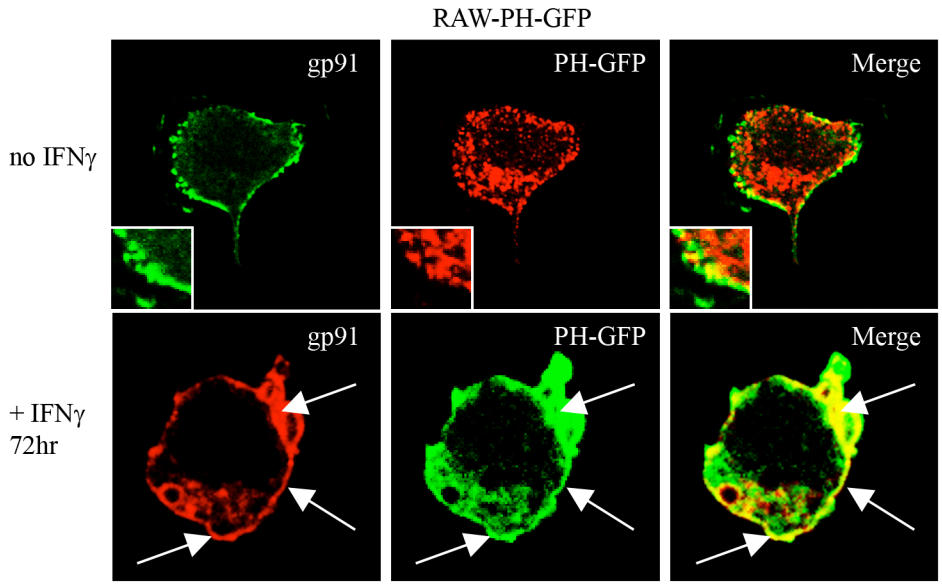

Figure 43. Increased colocalization of flavocytochrome *b* with the plasma membrane marker PH-GFP following 72 hr IFNγ activation in RAW 264.7 cells. RAW-PH-GFP cells cultured in the presence or absence of IFNγ (100 ng/ml) for 72 hr were fixed, permeabilized, and stained for endogenous $gp91^{phox}$ (mAb 54.1). In the absence of IFNγ, colocalization of $gp91^{phox}$ and the plasma membrane marker, PH-GFP, was seen at the cell surface in RAW-PH-GFP cells in discrete patches (top panel, *insets*). In the presence of IFNγ, colocalization of $gp91^{phox}$ and PH-GFP was increased and more uniform around the plasma membrane (bottom panel, *arrows*). A single plane z stack slice taken from near the bottom of the cell is shown (n=2 experiments in which colocalization of $gp91^{phox}$ and PH-GFP was evaluated).

3. IFNγ activation does not change the cell surface expression of CD16 or F4/80, or the subcellular distribution of Mac1

The change in the distribution of flavocytochrome *b* (Figure 40) could be the result of a "global" change in protein trafficking. Thus, we evaluated additional proteins known to localize to the cell surface in macrophages to see whether the surface expression of these proteins changed following IFNγ activation. The cell surface expression of FcγRIIIa (CD16) and F4/80, a marker for macrophage activation (van den Berg and Kraal, 2005), did not appear to increase following exposure to IFNγ for 24, 48, or 72 hr (Figures 44A and 44B) as detected by flow cytometry. In addition, the distribution of the integrin $\alpha_M\beta_2$, or Mac1, which has been shown to recycle in murine peritoneal macrophages using biochemical assays (Bretscher, 1992), was evaluated by immunofluorescence microscopy. Mac1 localized to the plasma membrane in unstimulated and 72 hr IFNγ stimulated RAW 264.7 cells (Figure 45). In summary, IFNγ did not change the cell surface expression of CD16 or F4/80 and did not change the distribution of Mac1.

4. Blocking TNFα did not alter the change in distribution of flavocytochrome *b* due to IFNγ in RAW 264.7 cells

The protein expression of flavocytochrome *b* was found to increase after 24 hr of IFNγ stimulation (Figure 34), but the change in the distribution of flavocytochrome *b* was not observed until 72 hr (Figure 40). Due to this delay, we hypothesized that the change in distribution of flavocytochrome *b* may be a secondary effect of IFNγ stimulation.

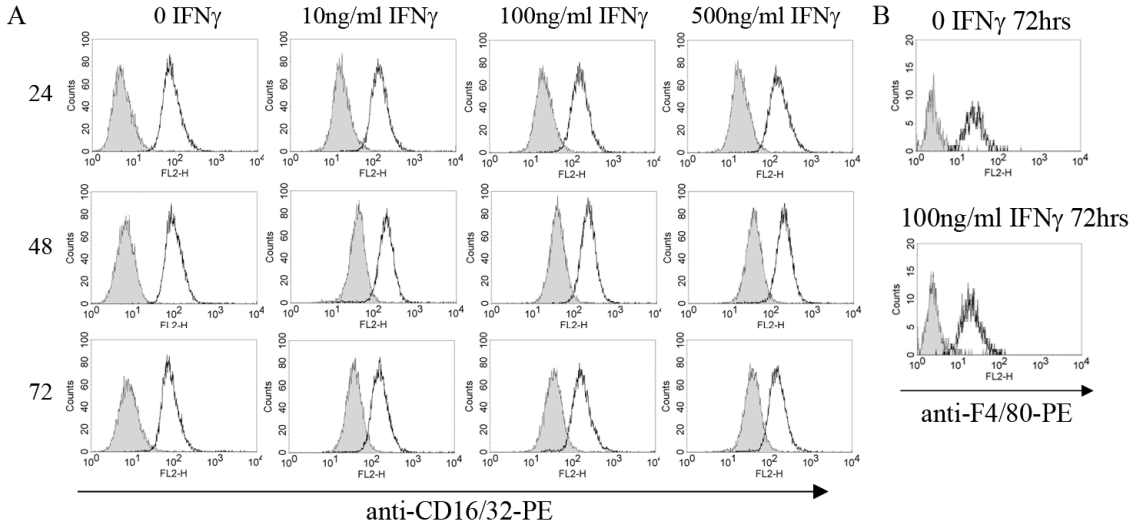

Figure 44. No increase in the surface expression of CD16 and F4/80 in response to IFNγ activation at 24 - 72 hr. Following 24, 48, or 72 hr, unactivated or IFNγ (10 – 500 ng/ml) activated RAW 264.7 cells were evaluated for the cell surface expression of (A) CD16 (black line) and (B) F4/80 (black line) by flow cytometry. Isotype controls are shown as grey fill.

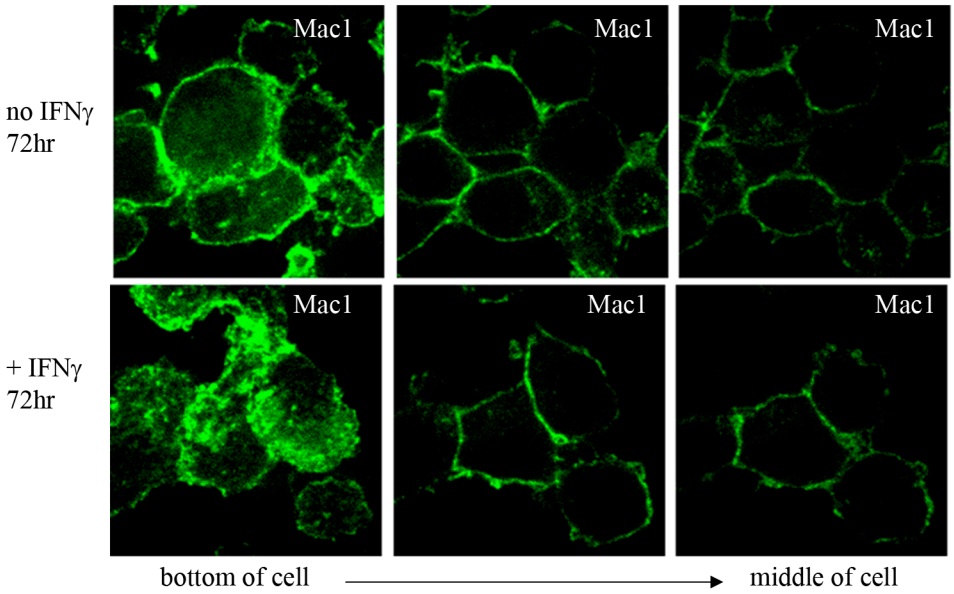

Figure 45. Mac1 does not change distribution in the presence of IFNγ (72 hr) in RAW 264.7 cells. RAW 264.7 cells cultured in the absence or presence of IFNγ (100 ng/ml) for 72 hr were fixed, permeabilized, and immunostained for Mac1 using a FITC-conjugated anti-Mac1 antibody. The distribution of Mac1 was evaluated by immunofluorescence microscopy in unactivated (top panel) and IFNγ activated cells (bottom panel).

IFNγ increases protein expression of several proinflammatory cytokines, such as TNFα (Collart *et al.*, 1986; Vila-del Sol *et al.*, 2007), IL-1β (Collart *et al.*, 1986; Marecki *et al.*, 2001), and IL-12 (Wang *et al.*, 2000). Among these cytokines, TNFα is known to increase macrophage activation (Mosser and Edwards, 2008). Recently, IFNγ-induced expression of TNFα was shown to regulate iNOS protein expression in an autocrine manner in IFNγ activated RAW 264.7 cells (Vila-del Sol *et al.*, 2007). Thus, the role of TNFα in changing the distribution of flavocytochrome *b* was evaluated by confocal microscopy in RAW 264.7 cells activated with IFNγ (100 ng/ml) in the presence or absence of a mAb against TNFα (10 μg/ml), which was added in combination with IFNγ for 72 hr. Flavocytochrome *b* localized predominantly to the cell surface in RAW 264.7 cells activated with IFNγ in the presence or absence of the TNFα blocking antibody (Figure 46). These results suggest IFNγ does not change the distribution of flavocytochrome *b* via TNFα. In addition, blocking TNFα did not change the surface expression of MHCII (Figure 47). However, it should be noted that the activity of the TNFα blocking antibody was not confirmed in our experiments, and that we did not determine whether RAW 264.7 cells were releasing TNFα under our conditions.

5. Change in distribution does not appear to be reversible within 24 hr following removal of exogenous IFNγ

The distribution of flavocytochrome *b* was found to change following 48 and 72 hr IFNγ activation (Figure 38 and not shown), which was also the time at which MHCII reached maximum surface expression. As a preliminary experiment to evaluate the

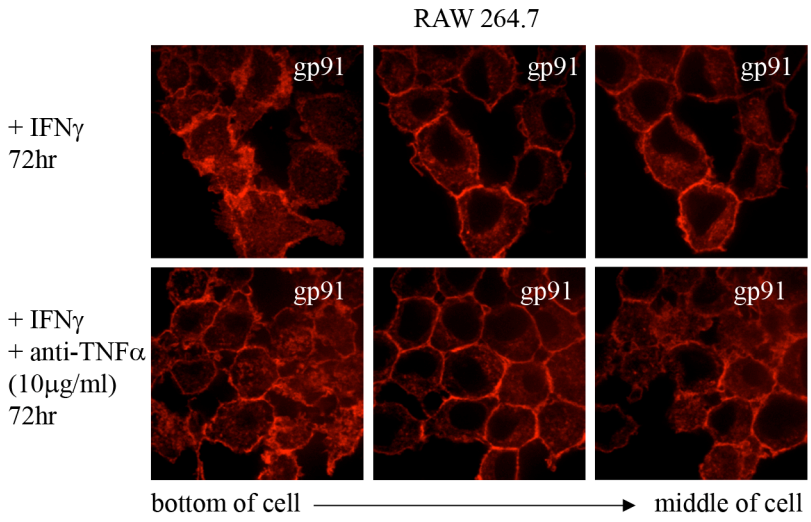

Figure 46. Blocking TNFα did not alter the change in distribution of flavocytochrome *b* following IFNγ activation in RAW 264.7 cells. RAW 264.7 cells cultured in the presence of IFNγ (100 ng/ml) or the combination of IFNγ (100 ng/ml) and a blocking antibody for TNFα (10 μg/ml) for 72 hr were fixed, permeabilized, and immunostained for $gp91^{phox}$ using the mAb 54.1. Evaluation by immunofluorescence microscopy showed $gp91^{phox}$ localized predominantly to the cell surface in IFNγ stimulated (top panel) or IFNγ stimulated in the presence of a TNFα blocking antibody (bottom panel).

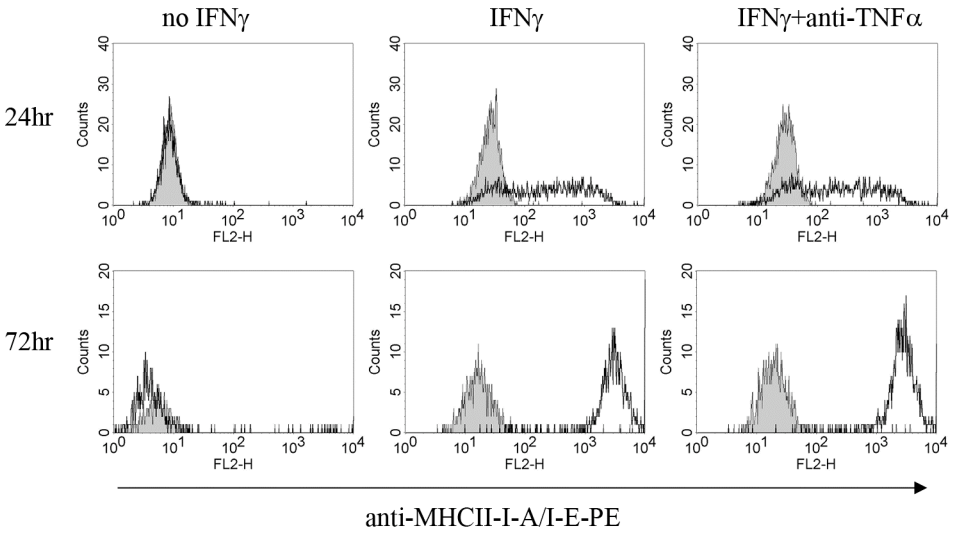

Figure 47. Blocking TNFα did not prevent the increase in MHCII surface expression in IFNγ activated RAW 264.7 cells. Following 24 or 72 hr stimulation with IFNγ (100 ng/ml) in the presence or absence of a TNFα blocking antibody (10 μg/ml), RAW 264.7 cells were evaluated for the surface expression of MHCII (black line) by flow cytometry. Isotype controls are shown as grey fill. This experiment was performed once.

mechanism responsible for this change in distribution, RAW 264.7 cells were activated with IFNγ for 48 hr, washed, and cultured for an additional 24 hr in the absence of IFNγ. Confocal microscopy showed gp91^{phox} localized mostly to the cell surface and did not show a predominant perinuclear distribution (Figure 48A). These results suggest the change in distribution could not be reversed within 24 hr by removing exogenous IFNγ, although it is possible that RAW 264.7 cells are producing endogenous IFNγ at this time point. Similar to flavocytochrome *b*, MHCII surface expression did not change after removing exogenous IFNγ for 24 hr (Figure 48B).

6. Isolation of surface gp91^{phox} by biotin labeling further establishes that IFNγ changes the distribution of flavocytochrome *b*

To quantify and compare the cell surface expression of flavocytochrome *b* in RAW 264.7 cells cultured in the presence and absence of IFNγ, we used biotin to label cell surface gp91^{phox} followed by precipitation with Neutravidin. This method was utilized since currently an antibody to detect an extracellular epitope of murine flavocytochrome *b* does not exist. In addition to the cell surface, total cell lysates were also labeled with biotin to serve as an internal control. Densitometric analysis was performed following immunoblotting for gp91^{phox} to quantify the ratio of gp91^{phox} expression at the cell surface compared to the total cell lysate in both unactivated and IFNγ activated cells. The relative amount of biotinylated cell surface gp91^{phox} was approximately 13-fold greater in cells activated by IFNγ (Figure 49). Analysis of biotinylated gp91^{phox} isolated from cell lysates showed only a 3-fold increase (Figure 48) following IFNγ stimulation compared to unactivated cells. The ratio of gp91^{phox}

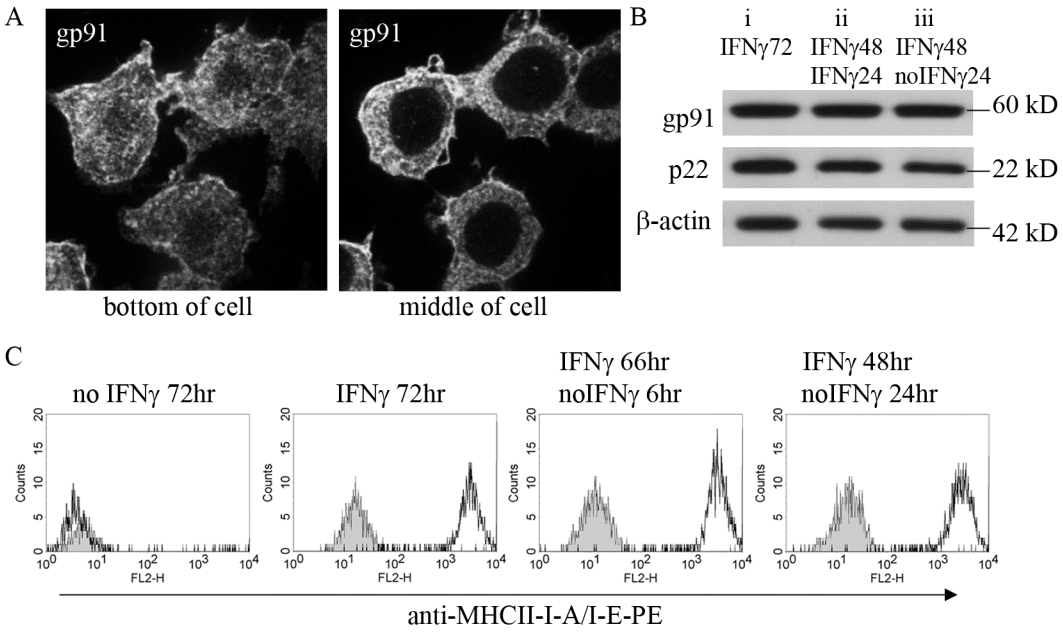

Figure 48. Change in distribution of flavocytochrome *b* following IFNγ stimulation does not appear to be reversible. (A) Immunofluorescent staining of gp91^{phox} in RAW 264. 7 cells stimulated with IFNγ for 48 hr, washed to remove exogenous IFNγ, and cultured for an additional 24 hr. (B) Western blot analysis of RAW 264.7 cells stimulated with 3 different conditions of IFNγ: 72 hr IFNγ (i), 48 hr IFNγ, then washed to remove exogenous IFNγ, and cultured for an additional 24 hr in the presence of "new" IFNγ (ii), or the absence of any additional IFNγ (iii). No change in protein expression was observed. Representative blot from 1 of 2 independent experiments. (C) Surface expression of MHCII (black line) or rat IgG_{2b} isotype control (grey fill) was evaluated in RAW 264.7 cells cultured for 72 hr under the following conditions: no IFNγ, IFNγ, IFNγ for 66 hr followed by removal of IFNγ, and IFNγ for 48 hr followed by removal of IFNγ.

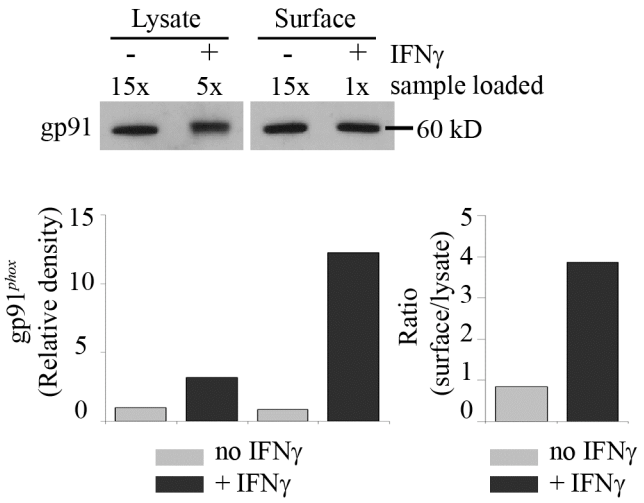

Figure 49. Isolation of surface gp91^{phox} using biotin shows IFNγ increases both the surface localization of gp91^{phox} and total gp91^{phox} expression. RAW 264.7 cells were cultured for 72 hr in the presence or absence of IFNγ (100 ng/ml). Biotinylated gp91^{phox} was isolated from the cell surface following biotinylation of living cells or biotinylation of the cell lysate. Western blot analysis was utilized to compare the amount of gp91^{phox} (mAb 54.1) isolated from the cell surface in unstimulated cells to that of IFNγ stimulated cells. Biotinylated gp91^{phox} isolated from cell lysates was used as the internal control. Sample volumes were optimized for better comparison of gp91^{phox} expression since approximately 15 times more gp91^{phox} was isolated from the surface of IFNγ stimulated cells than unstimulated cells.

expression at the surface compared to the total cell lysate cultured in the absence of IFNγ was 0.9, while a ratio of 4.5 was measured in cells cultured in the presence of IFNγ. These results indicate that IFNγ stimulation of RAW 264.7 cells increased the cell surface expression of gp91^{phox} approximately 5-fold.

7. Shift in distribution of flavocytochrome *b* in murine BMDMs following 72 hr activation

We also investigated whether IFNγ treatment changes the distribution of flavocytochrome *b* in primary murine BMDMs. Utilizing confocal microscopy, the distribution of flavocytochrome *b* in both WT (C56/BL6) and 22YFP-expressing p22^{def} BMDMs in the presence or absence of IFNγ (72 hr) was evaluated. IFNγ activated BMDMs showed an increase in gp91^{phox} and 22YFP to the cell surface (Figure 50A and 50B, bottom panels) and a loss of the prominent perinuclear compartment seen in un-activated BMDMs (Figure 50A and 50B, *arrows*). Colocalization analysis was performed in 22YFP-expressing p22^{def} BMDMs instead of colocalization of endogenous gp91^{phox} and p22^{phox} due to the lack of two antibodies of different isotypes that are sensitive enough to be used for immunofluorescent staining. Similar to wild-type BMDMs, endogenous gp91^{phox} and 22YFP in 22YFP-expressing p22^{def} BMDMs colocalized at vesicles that clustered around the nucleus in the absence of IFNγ (Figure 51A, insets) but, following 72 hr IFNγ stimulation, colocalized at the cell surface (Figures 51A and 51B). These data further establish that 72 hr IFNγ stimulation changes the distribution of the heterodimer flavocytochrome *b* in macrophages.

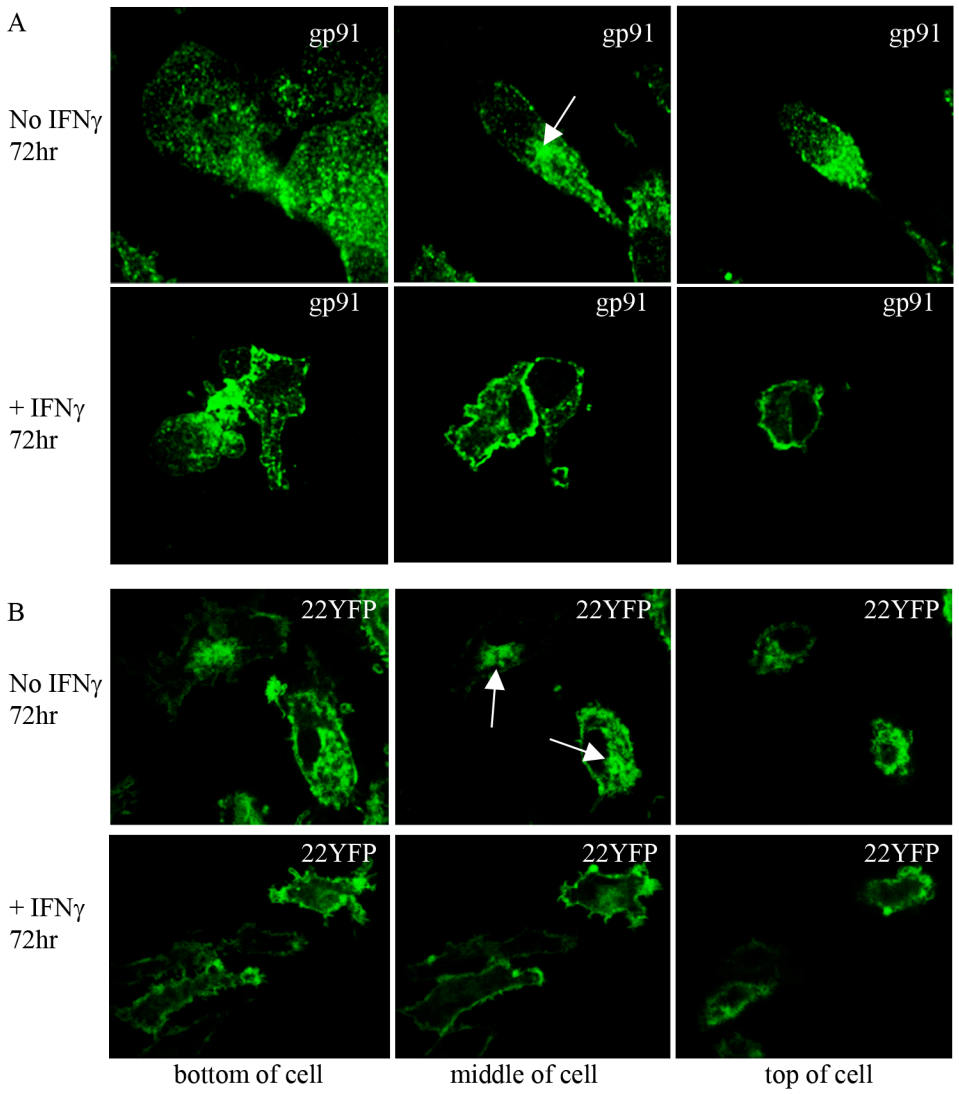

Figure 50. IFNγ activation increases localization of flavocytochrome *b* to the cell surface in wild-type (C57/BL6) and 22YFP-expressing p22^{phox}-deficient (p22^{def}) BMDMs. (A) Immunofluorescent staining of gp91^{phox} in unactivated or 72 hr IFNγ (100 ng/ml) activated WT BMDMs. (B) In both unactivated and 72 hr IFNγ activated 22YFP-expressing p22^{def} BMDMs, the distribution of 22YFP was evaluated in living cells. *Arrows* denote the location of the endocytic recycling compartment (ERC).

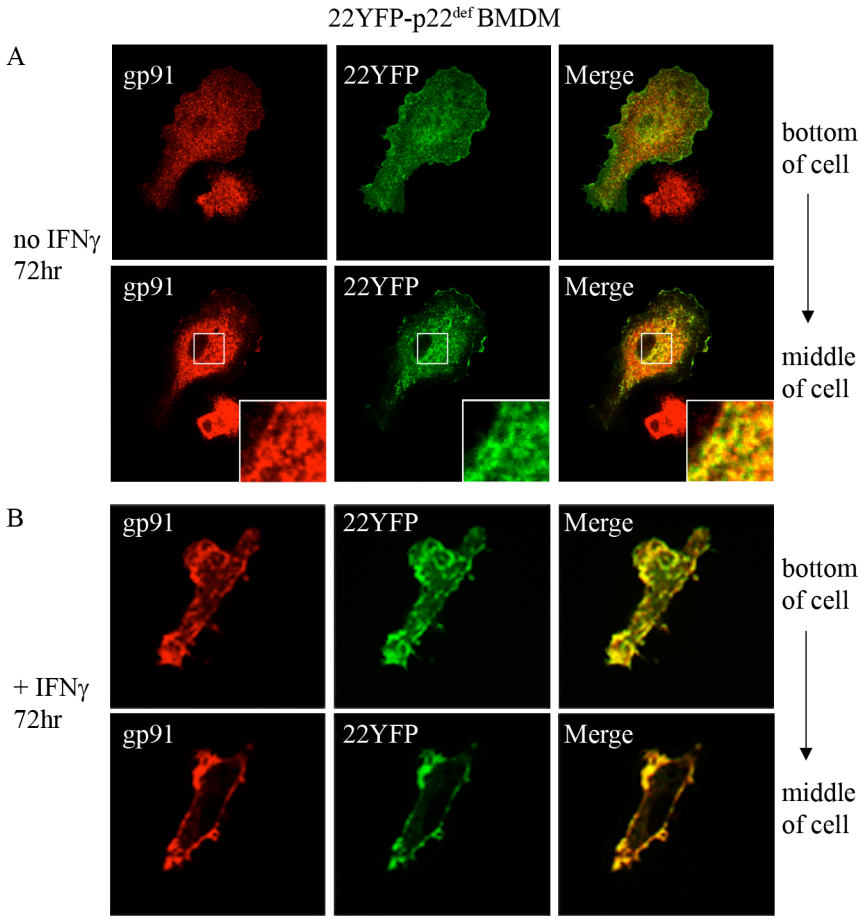

Figure 51. Colocalization of 22YFP and endogenous gp91^{phox} in BMDMs further shows IFNγ activation changes the distribution of the heterodimer flavocytochrome *b*. Colocalization of endogenous gp91^{phox}, detected by immunofluorescence, and 22YFP in 22YFP-expressing p22^{def} BMDMs was evaluated following (A) no stimulation or (B) IFNγ (100 ng/ml) stimulation for 72 hr.

8. Shift in distribution of flavocytochrome *b* is independent of p47^{phox} and Rac2 in BMDMs

Activation of the NADPH oxidase requires p47^{phox} translocation. Thus, we evaluated whether an intact oxidase was required for the redistribution of flavocytochrome *b* following IFNγ activation. Utilizing confocal microscopy, we evaluated the distribution of endogenous gp91^{phox} in BMDMs from p47$^{phox-/-}$ mice plated for 72 hr in the presence or absence of IFNγ (100 ng/ml). As shown in Figure 52A, the absence of p47^{phox} did not prevent the change in distribution of gp91^{phox} suggesting activation of the NADPH oxidase was not required.

gp91^{phox} was recently shown to be present on intracellular vesicles, by immunofluorescent staining in wild-type CD8^{+} DCs, but was localized predominantly on the cell surface in Rac2$^{-/-}$ CD8^{+} DCs (Savina *et al.*, 2009). Thus, we hypothesized that Rac2 may regulate the distribution of flavocytochrome *b* in macrophages. The distribution of endogenous gp91^{phox} in BMDMs from Rac2$^{-/-}$ mice plated for 72 hr in the presence or absence of IFNγ (100 ng/ml) was evaluated by immunofluorescence microscopy. As shown in Figure 52B, the absence of Rac2 did not prevent the IFNγ induced change in distribution of gp91^{phox}.

9. Cell surface localization of flavocytochrome *b* does not increase in RAW cell lines overexpressing flavocytochrome *b* subunits from transgenes

The change in distribution of flavocytochrome *b* correlated with a substantial increase in protein expression. To determine whether increased protein expression of flavocytochrome *b* subunits in and of itself could induce a change in the distribution of

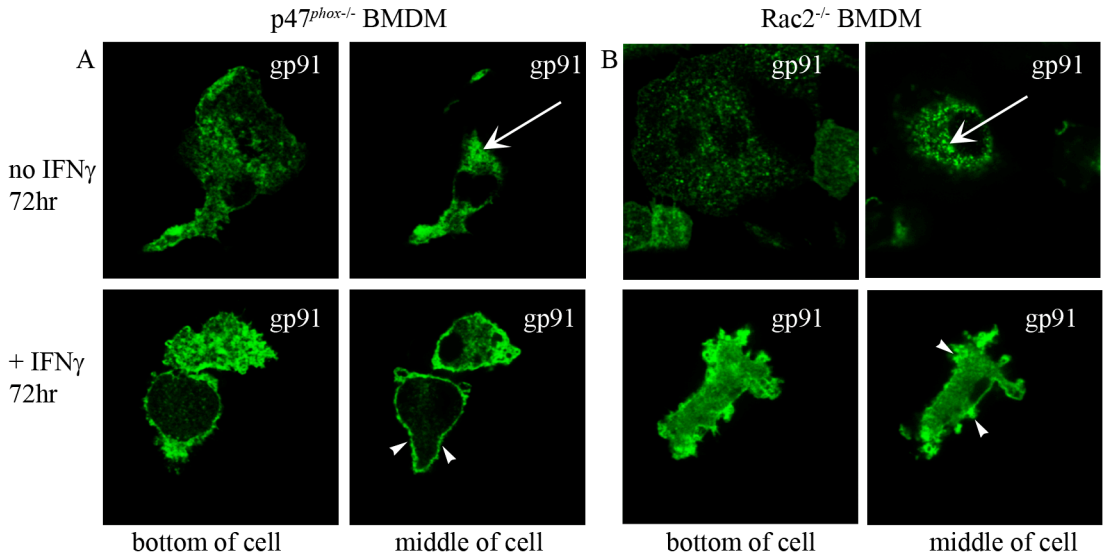

Figure 52. IFNγ-induced change in the distribution of flavocytochrome *b* in macrophages is not dependent on p47^{phox} or Rac2. Immunofluorescent staining of gp91^{phox} was evaluated by confocal microscopy in unactivated or 72 hr IFNγ (100 ng/ml) activated (A) p47$^{phox-/-}$ BMDMs or (B) Rac2$^{-/-}$ BMDMs. *Arrows* denote localization of gp91^{phox} to a prominent perinuclear compartment and *arrowheads* denote localization in the plasma membrane.

flavocytochrome *b*, we generated a RAW-91,22 cell line that stably expressed human gp91^{phox} and p22^{phox}. Western blot analysis showed stable expression of human gp91^{phox} in RAW-91,22 increased total gp91^{phox} expression by approximately 5.5-fold and p22^{phox} expression by 11-fold (Figure 53A), which closely mimicked the increase in gp91^{phox} and p22^{phox} expression following IFNγ activation in RAW cells at 72 hr (Figure 53A).

Confocal microscopy was utilized to determine whether increasing protein expression of gp91^{phox} and p22^{phox} would change the distribution of flavocytochrome *b* in RAW-91/22. As shown previously in both RAW 264.7 and bone marrow derived macrophages (Figures 23 and 30), we found gp91^{phox} in RAW-91,22 cells to localize to endosomes and the endocytic recycling compartment, shown by colocalization with transferrin (Figure 53C, *arrows*). In contrast to gp91^{phox}, p22^{phox} did not appear to localize to the ERC and showed a reticular distribution (Figure 53B), reflecting that transgenic p22^{phox} is relatively more expressed compared to transgenic gp91^{phox}.

10. Deletion of p22^{phox} C-terminal amino acids 149 - 195 does not prevent the change in distribution of flavocytochrome *b* following IFNγ activation

We found that removal of p22^{phox} C-terminal amino acids 149 - 195 did not alter flavocytochrome *b* distribution in the plasma membrane and endocytic recycling compartment in CHO cells (Figure 20). Further removal of C-terminal amino acids 131 - 195 prevented heterodimer formation of this mutant with gp91^{phox}, and this mutant was localized to the ER (Figure 20). We generated RAW-22CIT, RAW-149CIT, and RAW-131CIT cells that stably expressed CIT-tagged versions of p22^{phox} and the two C-terminal deletion mutants to investigate whether regions within the C-terminus of p22^{phox} may

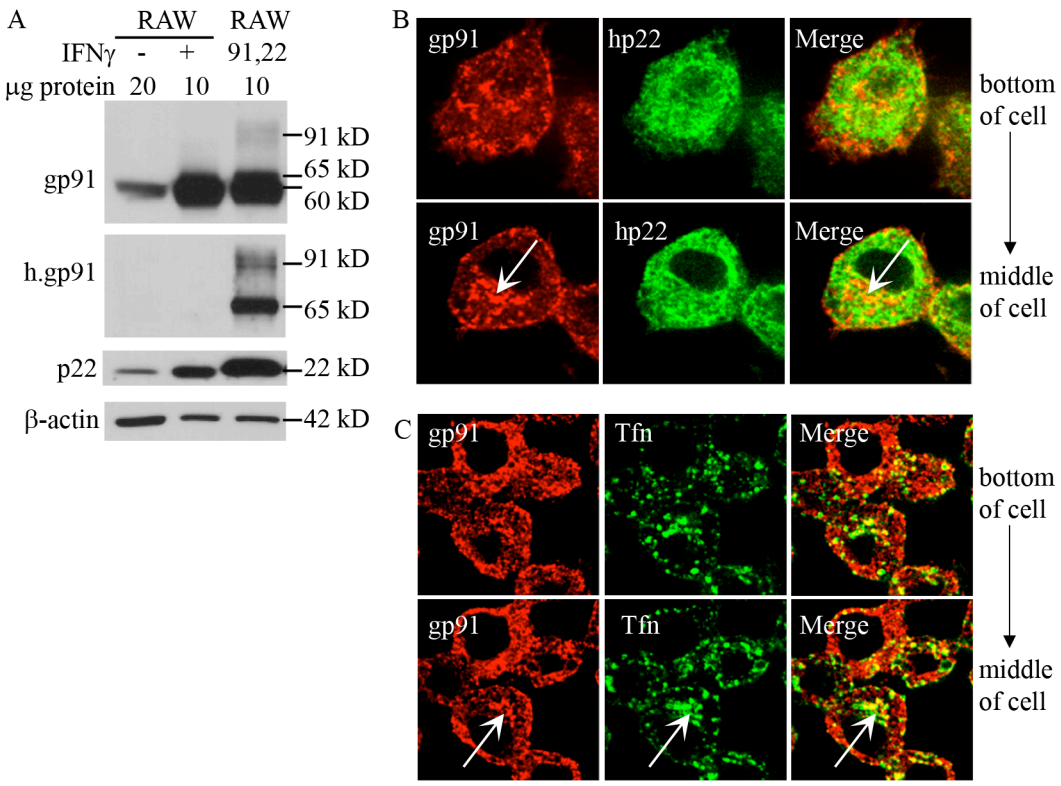

Figure 53. Increasing gp91^{phox} expression in RAW-91,22 cells does not change the distribution of flavocytochrome *b* in the absence of IFNγ. (A) Immunoblots of cell lysates from unstimulated RAW 264.7 cells and RAW,91,22 cells and from IFNγ (100 ng/ml, 72 hr) stimulated cells probed with mAbs 54.1 (anti-gp91^{phox}), CL5 (anti-human gp91^{phox}), NS2 (anti-p22^{phox}), and anti-β-actin. (B) RAW-91,22 cells were fixed, permeabilized, and stained to detect gp91^{phox} (mAb 54.1) and human p22^{phox} (mAb 44.1). (C) RAW-91,22 cells were incubated with Alexa Fluor 647-conjugated human transferrin for 25 min at 37°C, then fixed, permeabilized and stained for gp91^{phox} (mAb 54.1). *Arrows* denote localization to the endocytic recycling compartment.

regulate the change in distribution of flavocytochrome *b* following IFNγ activation. In the absence of IFNγ, 22CIT, 149CIT, and 131CIT localized to the ER (Figure 54A) in RAW-22CIT, RAW-149CIT and RAW-131CIT cell lines. This suggested the fluorescently tagged 22CIT and 149CIT subunits were expressed in excess of endogenous gp91^{phox} (Figure 27). However, 131CIT is incapable of heterodimer formation (Figure 20) and thus is expected to be in the ER. In the presence of IFNγ, endogenous gp91^{phox} expression increases dramatically (Figure 34). Thus, we hypothesized that in IFNγ stimulated cells, the otherwise "excess" 22CIT or 149CIT derivative would no longer be expressed in excess of gp91^{phox} and would be incorporated into flavocytochrome *b* heterodimers. As shown in Figure 54B, 22CIT and 149CIT were found to localize to the cell surface in IFNγ activated RAW cells, suggesting amino acids 149 - 195 were not required for the change in distribution of flavocytochrome *b* to the plasma membrane. Importantly, 131CIT, which lacks the ability to form heterodimers with gp91^{phox}, remained in the ER in IFNγ activated RAW-131CIT cells, establishing that the change in distribution of 22CIT and 149CIT to the plasma membrane was dependent on heterodimer formation with endogenous gp91^{phox}.

VI. In contrast to IFNγ, LPS stimulation does not increase flavocytochrome *b* localization to the plasma membrane

1. LPS stimulation does not increase surface localization of flavocytochrome *b*

We also investigated the distribution of flavocytochrome *b* in RAW cell macrophages following stimulation with LPS alone or LPS in combination with IFNγ.

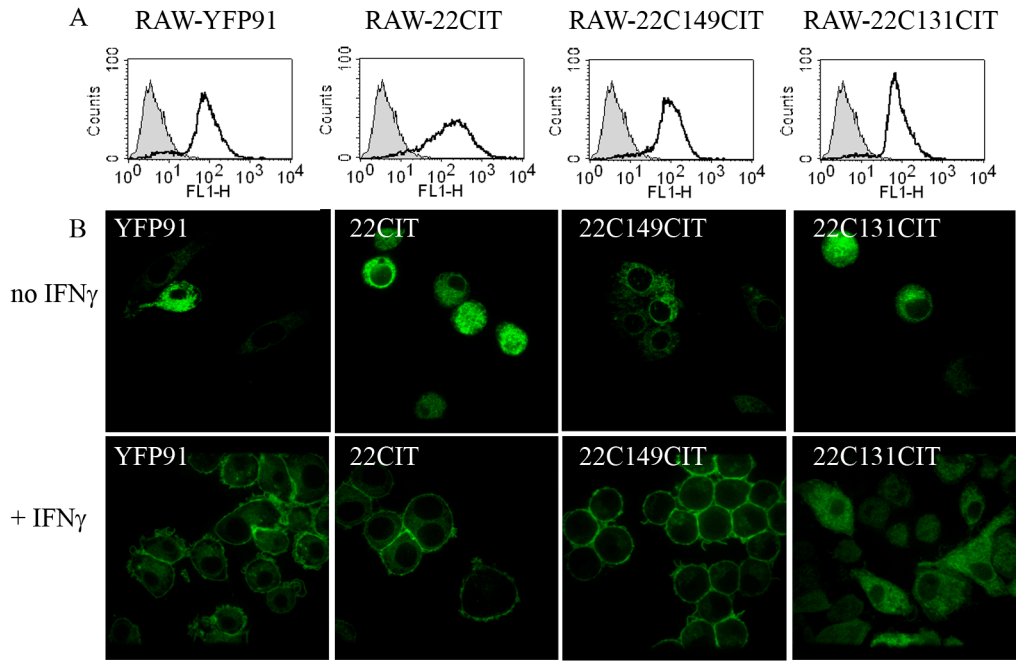

Figure 54. Deletion of p22^{phox} C-terminal amino acids 149-195 does not prevent the change in distribution following IFNγ activation in RAW 264.7 cells. (A) Protein expression, assessed by fluorescent intensity of YFP/CIT using flow cytometery, of fluorescently tagged flavocytochrome *b* subunits stably expressed in RAW-YFP91 (black line), RAW-22CIT (black line), RAW-22C149CIT (black line), and RAW22C131CIT (black line) was similar. RAW 264.7 cells (grey fill) were used as the negative control. (B) In the absence of IFNγ stimulation, fluorescently tagged gp91^{phox} and p22^{phox} subunits localized to the ER (top panel). In the presence of IFNγ, fluorescently tagged subunits, YFP91, 22CIT, and 22C149CIT localized to the cell surface (bottom panel) but 22C131CIT resided in the ER.

RAW 264.7 cells activated with LPS for 24 or 72 hr were evaluated by confocal microscopy. Following 24 or 72 hr of LPS stimulation, flavocytochrome *b* appeared to lose the prominent perinuclear distribution (Figure 55, top panel, *arrow*) and was localized to vesicles that were more dispersed throughout the cell (Figure 55, middle and bottom panels). Notably, there was no apparent increase of flavocytochrome *b* in the plasma membrane. LPS stimulation appeared to increase cell spreading, which may be of relevance to the more dispersed distribution for flavocytochrome *b* since stabilization of microtubules has been shown to disperse Rab11-positive endosomes (Yoon *et al.*, 2005). In addition, MHCII surface expression did not change in response to LPS (Figure 56A). To confirm that our LPS preparation was active, TLR4 surface expression was evaluated in RAW 264.7 cells that were either unstimulated or stimulated for 24 hr with 250 ng/ml LPS or 100 ng/ml IFNγ. As expected (Nomura *et al.*, 2000), 250 ng/ml LPS decreased TLR4 expression, while no change was observed in IFNγ activated or unstimulated cells (Figure 56B), establishing the activity of our LPS preparation.

2. Addition of LPS to IFNγ activated macrophages reverses the predominant surface distribution of flavocytochrome *b* seen in macrophages activated with only IFNγ

A standard protocol for generating classically "primed" macrophages involves stimulating cells with both IFNγ and LPS (Mosser and Zhang, 2008), which prompted us to investigate the distribution of flavocytochrome *b* in RAW 264.7 cells stimulated with IFNγ (10 ng/ml) and LPS (250 ng/ml) for 24 and 72 hr. Following 24 hr stimulation with IFNγ and LPS, flavocytochrome *b* showed a predominant perinuclear distribution

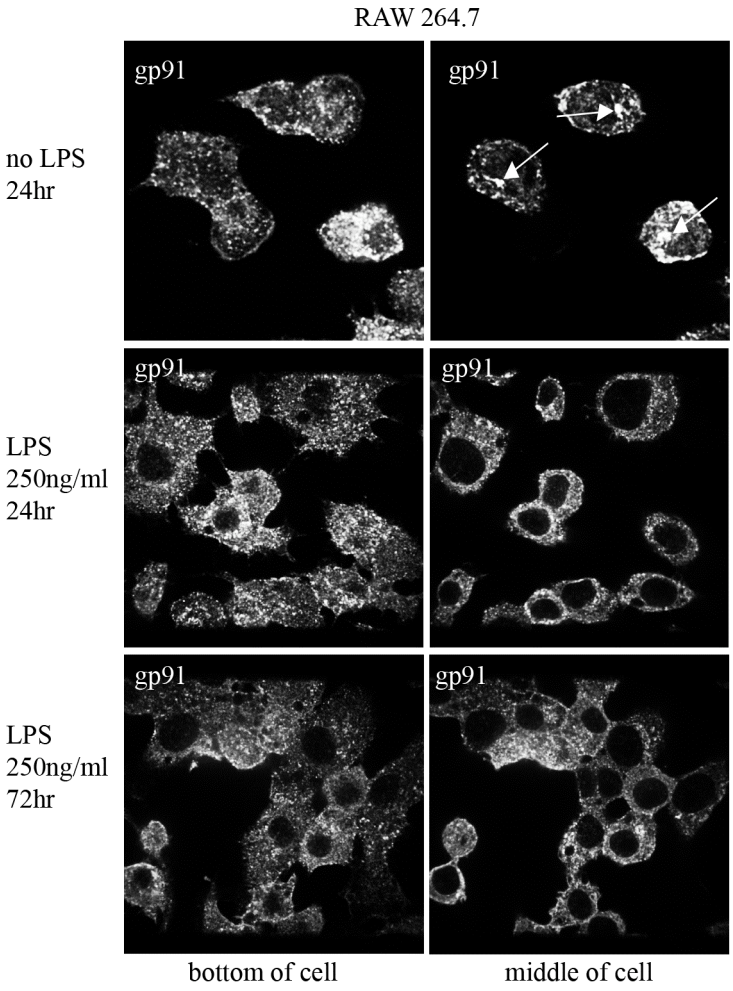

Figure 55. LPS stimulation does not appear to increase the cell surface expression of flavocytochrome *b* in RAW 264.7 cells. Unstimulated or LPS (250 ng/ml) stimulated RAW 264.7 cells were fixed, permeabilized, and stained for gp91^{phox} (mAb 54.1). The distribution of gp91^{phox} was evaluated in unstimulated cells (top panel), 24 hr LPS stimulated cells (middle panel), and 72 hr LPS stimulated cells (bottom panel). *Arrows* denote the perinuclear endocytic recycling compartment. Representative images from 2 independent experiments.

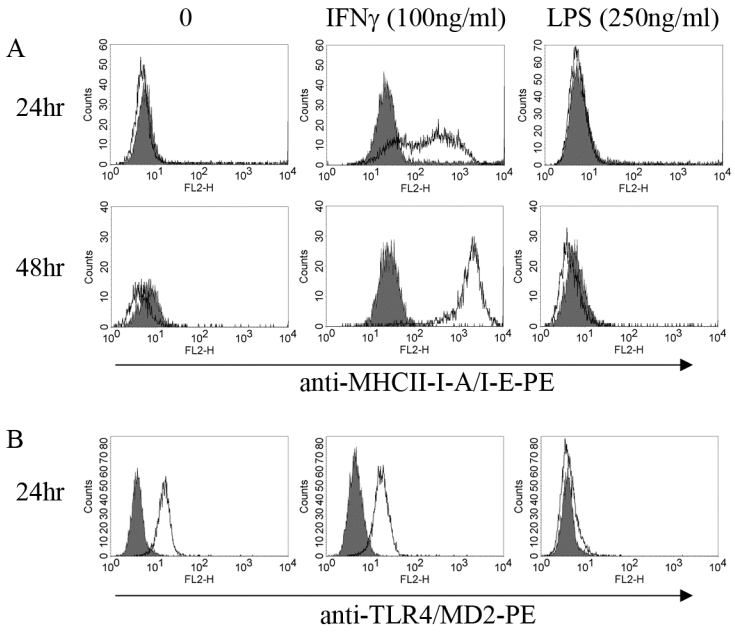

Figure 56. In contrast to IFNγ, LPS does not increase MHCII surface expression. RAW 264.7 cells were stimulated with IFNγ (100 ng/ml) or LPS (250 ng/ml) for 24 or 48 hr. Surface expression of (A) MHCII (black line) and (B) TLR4 (black line) was evaluated by flow cytometry. Isotype controls are shown as dark grey fill.

(Figure 57, middle panel, *arrows*) and localized to vesicles throughout the cytosol, similar to the distribution of 24 hr IFNγ activated cells (Figure 57, top panel). Interestingly, in contrast to IFNγ alone, many of the cells treated with the combination of IFNγ and LPS for 72 hr appeared to be dead (not shown) and not many cells were found on the coverslips (approximately less than 10% cells compared to IFNγ stimulated only). In addition, the cells present on the coverslips were filled with large vacuoles (Figure 57A, bottom panel); thus, we could not evaluate the distribution of flavocytochrome *b*. We hypothesize that the simultaneous administration of IFNγ and LPS for 72 hr caused the cells to die due to cytotoxicity related to high LPS and/or "over"-activation (Ma *et al.*, 2003).

In addition, we examined the distribution of flavocytochrome *b* in RAW cells activated with IFNγ (100 ng/ml) for 72 hr with LPS (250 ng/ml) added only for the last 24 hr. As shown previously, flavocytochrome *b* localized predominantly to the cell surface in IFNγ (72 hr) activated RAW 264.7 cells (Figure 57B, top panel). In marked contrast, flavocytochrome *b* showed an endosomal or vesicular-looking distribution in cells stimulated with both LPS and IFNγ and little presence in the cell surface (Figure 57B, bottom panel). Similar to LPS alone (Figure 55), flavocytochrome *b* appeared dispersed in vesicles and did localize to a prominent perinuclear compartment in cells stimulated with the combination of IFNγ and LPS for the last 24 hr. These results suggest LPS can reverse the change in distribution of flavocytochrome *b* following IFNγ activation.

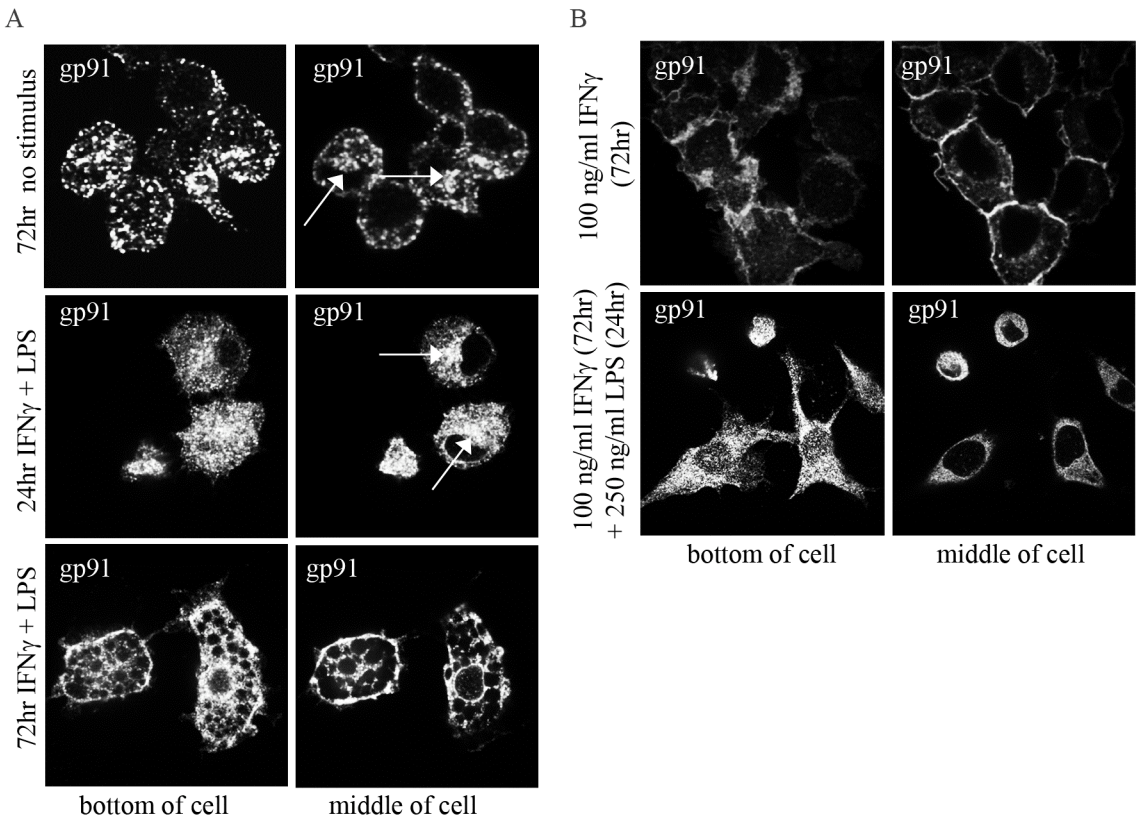

Figure 57. LPS in the presence of IFNγ appears to reverse the change in distribution of flavocytochrome *b* due to IFNγ alone. Unstimulated or stimulated with IFNγ (100 ng/ml) and/or LPS (250 ng/ml) RAW 264.7 cells were fixed, permeabilized, and stained for $gp91^{phox}$. (A) **From top to bottom:** Localization of $gp91^{phox}$ in cells that were unstimulated, stimulated for 24 hr, or stimulated for 72 hr with both IFNγ and LPS. (B) Localization of $gp91^{phox}$ in cells stimulated with IFNγ only for 72 hr or stimulated with IFNγ for 72 hr with the addition of LPS for the last 24 hr. Representative images from 2 independent experiments in which at least 50 cells were analyzed, except for (A) bottom panel, in which only 20 cells were analyzed.

VII. Flavocytochrome *b* localization to phagocytic cups is more visible in IFNγ activated RAW 264.7 cells and BMDMs

1. IFNγ pre-stimulation of RAW 264.7 cells appears to increase presence of flavocytochrome *b* in the phagocytic cup and nascent phagosomes

We next performed synchronized phagocytosis assays to evaluate whether the enhanced surface expression of gp91^{phox} following 72 hr IFNγ activation would increase localization of flavocytochrome *b* to phagosomes. Following 5 min of phagocytosis of SOZ, flavocytochrome *b* presence in phagocytic cups was evaluated in RAW 264.7 cells plated in the absence of IFNγ (72 hr) or in the presence of IFNγ for 24 or 72 hr, by immunofluorescence microscopy. gp91^{phox} was present in phagocytic cups in unstimulated cells (Figure 58A, left panel), which did appear to be increasingly more visible after 24 (Figure 58A, middle panel) and then 72 hr (Figure 58A, right panel) of IFNγ stimulation. Further evaluation in nascent phagosomes present 15 min after initiation of phagocytosis showed localization of gp91^{phox} in vesicles that appeared to cluster near phagosomes in the absence of IFNγ (Figure 58B, left panel, *asterisks*), but in 24 hr IFNγ stimulated cells gp91^{phox} showed less of a "patchy" distribution and more of a uniform "ring" around the phagosome (Figure 58B, middle panel, *asterisks*), which appeared even more evident in cells stimulated with IFNγ for 72 hr (Figure 58B, right panel, *asterisks*). However, it was difficult to assess whether the increase in the visibility of gp91^{phox} in phagocytic cups and nascent phagosomes was due to IFNγ-induced changes in the distribution of flavocytochrome *b* or simply reflected the marked increase in gp91^{phox} protein expression in IFNγ stimulated cells.

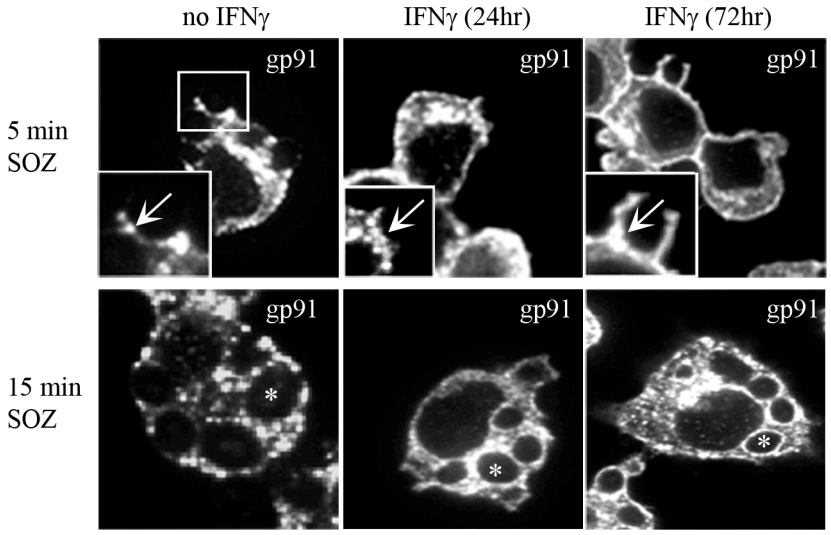

Figure 58. Localization of gp91^{phox} to phagocytic cups and nascent phagosomes appears more visible in IFNγ pre-stimulated RAW 264.7 cells. RAW 264.7 cells were fixed, permeabilized, and stained to detect gp91^{phox} (mAb 54.1) following 5 or 15 min synchronized phagocytosis of serum opsonized zymosan. **Top panel (5 min):** Localization of gp91^{phox} to phagocytic cups (*arrows*) was evaluated in unstimulated, 24 hr IFNγ stimulated, and 72 hr IFNγ stimulated cells. **Bottom panel (15 min):** Localization of gp91^{phox} to nascent phagosomes (*asterisks*) was evaluated in unstimulated, 24 hr IFNγ stimulated, and 72 hr IFNγ stimulated cells. Shown are representative images from 2 independent experiments in which at least 50 cells were evaluated. Single z stack sections from the middle of the cell are shown.

2. More uniform distribution of 22YFP in phagocytic cups in IFNγ activated 22YFP-expressing p22^{def} BMDMs

Next, we evaluated trafficking of flavocytochrome *b* during phagocytosis in unstimulated and IFNγ (72 hr) pre-stimulated BMDMs. We utilized our 22YFP-expresssing p22^{phox}-deficient BMDMs to evaluate localization of flavocytochrome *b*, using 22YFP, during phagocytosis in living cells. Localization of 22YFP in p22^{phox}-deficient BMDMs was evaluated following 5 and 20 min of phagocytosis of SOZ particles by video microscopy. As described previously in fixed cells (Figure 31), 22YFP was found in phagocytic cups (5 min) and nascent phagosomes (20 min) in unstimulated BMDMs (Figure 59, top panel) and appeared to cluster in discrete patches near the cup and phagosomes. In IFNγ pre-stimulated BMDMs, 22YFP appeared more uniform in phagocytic cups (Figure 59, bottom panel, left image) and less punctate, but no difference in the localization of 22YFP on nascent phagosomes (Figure 59, bottom panel, right image) was observed. Thus, flavocytochrome *b* localization to phagocytic cups appeared to increase in both BMDMs and RAW 264.7 cells activated with IFNγ, but a more uniform localization to nascent phagosomes was only observed in IFNγ activated RAW 264.7 cells.

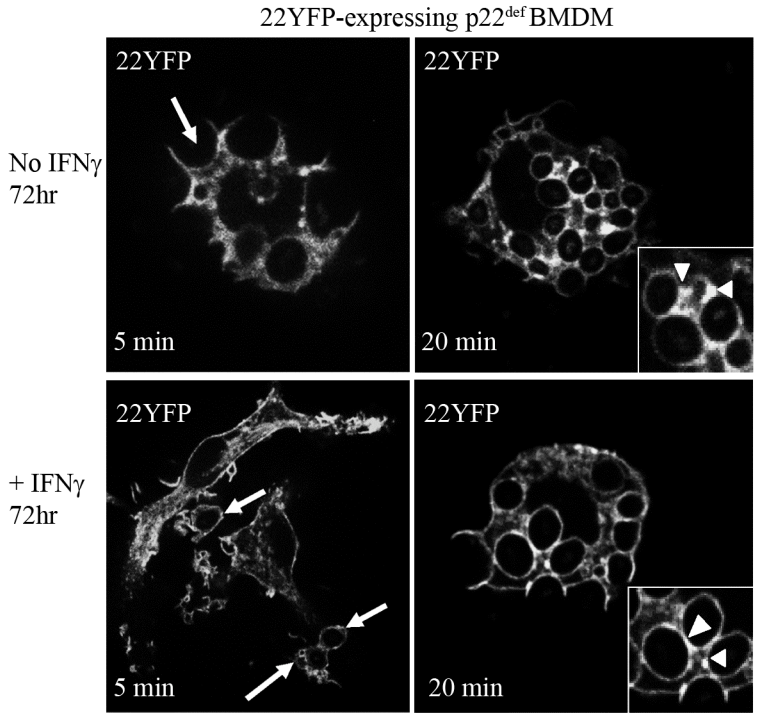

Figure 59. More uniform localization of 22YFP to phagocytic cups in IFNγ activated 22YFP-expresing p22^{def} BMDMs. Localization of 22YFP in 22YFP-expressing p22^{phox}-deficient BMDMs following 5 min (left panel) and 20 min (right panel) of synchronized phagocytosis in unstimulated cells (top panel) and 72 hr IFNγ (100 ng/ml) activated cells was assessed by confocal microscopy in living cells. *Arrows* denote phagocytic cups and *arrowheads* indicate discrete foci of increased 22YFP colocalization near nascent phagosomes. Single plane z stack sections from the middle of the cells are shown.

VIII. Increase in NADPH oxidase activity is dependent on the duration and dose of IFNγ stimulation in RAW 264.7 cells and BMDMs

1. Duration of IFNγ stimulation increases SOZ and PMA stimulated superoxide production in RAW 264.7 cells

IFNγ was first identified as the macrophage activating factor based on its ability to enhance secretion of hydrogen peroxide by macrophages (Nathan *et al.*, 1983), although surprisingly few studies have systematically analyzed the effects of dose and time dependency of IFNγ stimulation on NADPH oxidase activity and its correlation with $gp91^{phox}$ expression. Thus, we measured NADPH oxidase activity under our conditions, and found that superoxide release by IFNγ activated RAW 264.7 cells and BMDMs was generally correlated with $gp91^{phox}$ expression. Unexpectedly, we also found IFNγ activated macrophages produced superoxide in the absence of exogenous stimulus.

Importantly, we wanted to know the optimal conditions of IFNγ stimulation for enhancing NADPH oxidase activity in macrophages. Thus, we evaluated the effect of the duration and concentration of IFNγ on NADPH oxidase activity in macrophages. We assessed both the kinetics of the release of superoxide and total superoxide produced following SOZ or PMA stimulation using the chemiluminescent substrate luminol.

Following SOZ stimulation, little superoxide was detected in unactivated cells, but increased in 24 hr IFNγ activated cells and continued to rise at 48 hr, but seemed to plateau, since 72 hr IFNγ activated cells did not produce much more superoxide (Figure 60A). In contrast to SOZ, 24 hr IFNγ activated cells produced little superoxide in response to PMA (Figure 60B), but the response gradually increased in 48 hr IFNγ activated cells and continued to increase substantially in 72 hr IFNγ activated cells

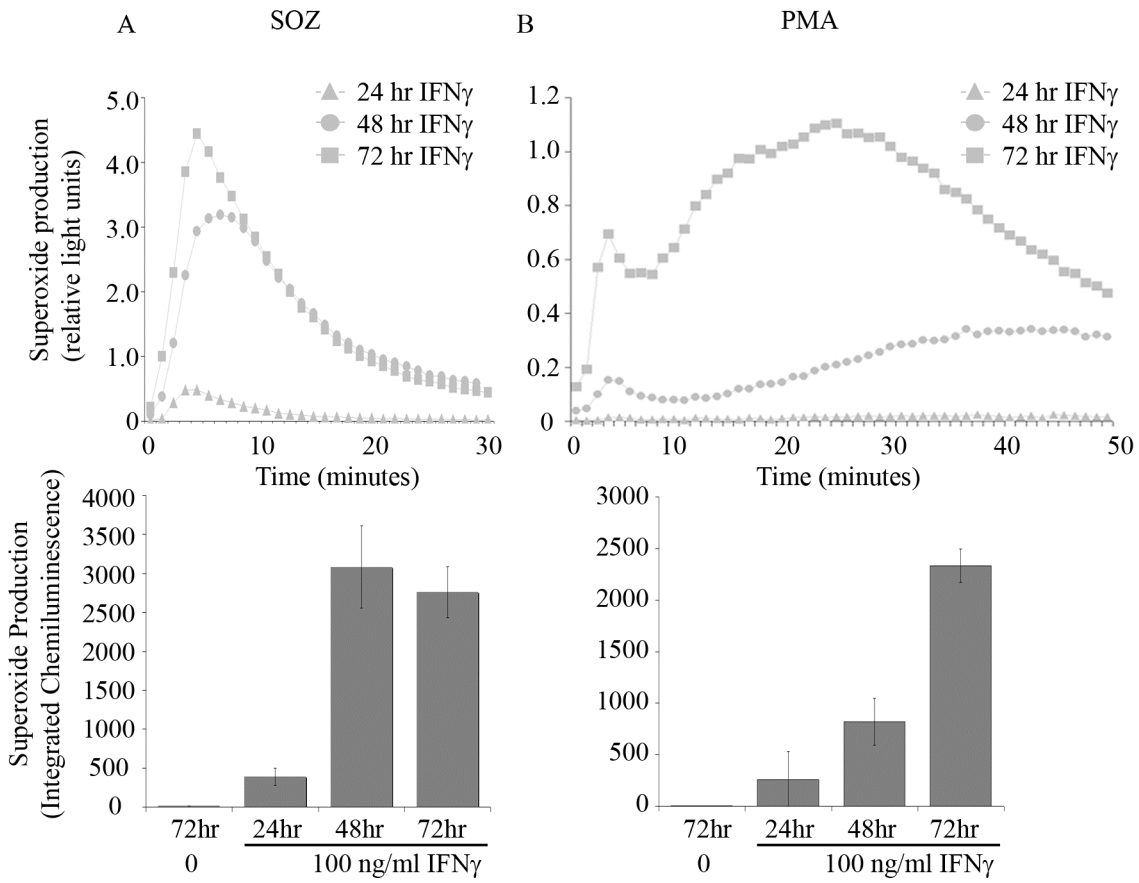

Figure 60. Duration of IFNγ stimulation increases SOZ and PMA stimulated superoxide in RAW 264.7 cells. RAW 264.7 cells cultured in the presence or absence of IFNγ (100 ng/ml) for 24, 48 or 72 hr were evaluated for NADPH oxidase activity by luminol. (A) SOZ stimulated superoxide production was measured for 30 min. (B) PMA stimulated superoxide production was measured for 50 min. Bar graphs show average +/- standard deviation of 4 (A) or 3 (B) independent experiments.

(Figure 60B). Evaluation of total superoxide released from unactivated and IFNγ activated cells following SOZ and PMA stimulation showed IFNγ activation increased superoxide production in RAW 264.7 cells, respectively, by 33- and 86-fold at 24 hr, 260- and 273-fold at 48 hr and 230- and 780-fold at 72 hr (N = 4 independent experiments for SOZ and N = 3 for PMA). In addition to the total increase in PMA stimulated superoxide production following 72 hr IFNγ activation, a change in the kinetics in response to PMA was observed in which the curve appeared to shift to the left (Figure 60B), suggesting a quicker response to PMA in the 72 hr IFNγ activated macrophages. In summary, we found prolonged IFNγ stimulation of RAW 264.7 cells increases both flavocytochrome *b* protein expression and NADPH oxidase activity.

2. Maximum increase in NADPH oxidase activity following 10 ng/ml IFNγ activation in RAW 264.7 cells

We next investigated the effect of the concentration of IFNγ on NADPH oxidase activity in RAW 264.7 cells. PMA and SOZ stimulated superoxide production was measured in RAW 264.7 cells stimulated with 0.1 – 100 ng/ml IFNγ for 24, 48 or 72 hr. We found that, similar to flavocytochrome *b* protein expression, NADPH oxidase activity increased in response to IFNγ in a dose-dependent manner in response to IFNγ. In response to SOZ or PMA, superoxide production seemed to plateau in cells activated with 10 ng/ml IFNγ (Figures 61A and 61B), the same concentration at which we observed flavocytochrome *b* protein expression to reach its maximum (Figure 37). Thus, we found that a dose of at or above 10 ng/ml IFNγ (100 U/ml) results in maximum flavocytochrome *b* protein expression and NADPH oxidase activity, which is

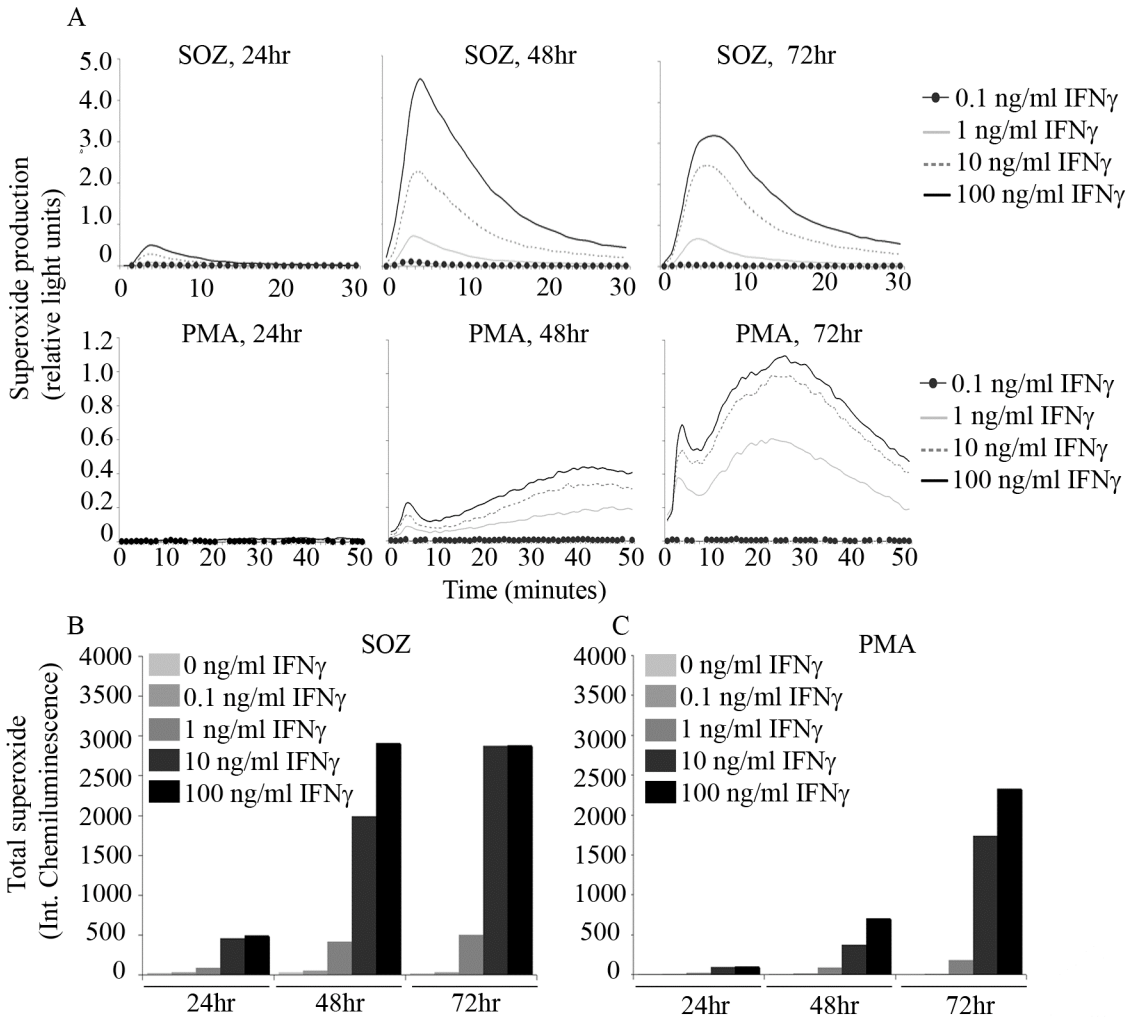

Figure 61. IFNγ dose response to SOZ and PMA stimulated superoxide in RAW 264.7 cells. RAW 264.7 cells were activated with increasing concentrations of IFNγ (0.1 – 100 ng/ml) for 24, 48, or 72 hr. NADPH oxidase activity in unactivated and IFNγ activated cells was assessed by luminol. (A) SOZ stimulated superoxide production was measured for 30 min (B) PMA sitmulated superoxide production was measured for 50 min. Bar graphs show mean of 2 independent experiments.

within the range of IFNγ (30 – 100 ng/ml) previously described to be a "saturating" concentration for IFNγ-induced MHCII cell surface expression (Gonalons *et al.*, 1998) and for enhanced killing of *S. typhimurium* (Gordon *et al.*, 2005).

3. SOZ and PMA stimulated superoxide is inhibited by SOD, but not NO inhibitor L-NMMA

Luminol can permeate the cell membrane and thus, allows for the detection of intracellular and extracellular superoxide production; however, the reaction requires a peroxidase (Dahlgren and Karlsson, 1999). Extracellular superoxide can be measured by adding exogenous HRP, but intracellular superoxide requires endogenous expression of a peroxidase. Neutrophils have azurophilic granules containing MPO (see Table II), which allows for intracellular detection of superoxide. It is generally believed that mature macrophages lack expression of MPO; thus, we can not compare the amount of intracellular vs. extracellular superoxide produced in IFNγ activated macrophages. However, we can confirm luminol is detecting extracellular superoxide by utilizing SOD, which catalyses the dismutation of superoxide to hydrogen peroxide and, when added exogenously, can prevent the detection of extracelluar superoxide by luminol due to the conversion to hydrogen peroxide. Superoxide production was measured in 72 hr IFNγ (0.1 - 500 ng/ml) activated RAW 264.7 cells stimulated with SOZ (Figure 62A) or PMA (Figure 62B) in the presence or absence of SOD. Luminol-enhanced chemiluminescence following SOZ or PMA stimulation was substantially reduced in the presence of SOD, suggesting that we are detecting predominantly extracellular superoxide release by macrophages in the absence of SOD (Figures 62A and 62B).

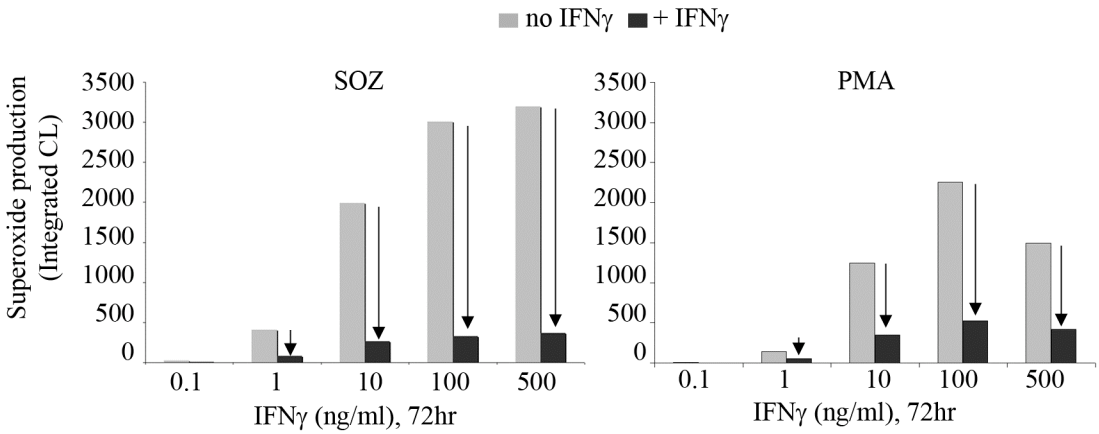

Figure 62. SOZ and PMA stimulated superoxide in IFNγ activated RAW 264.7 cells is reduced by superoxide dismutase (SOD). Superoxide production following SOZ (left panel) or PMA (right panel) stimulation in the presence (black bars) or absence (grey bars) of SOD was evaluated in RAW cells activated with 0.1 – 500 ng/ml IFNγ for 72 hr. Bar graphs are representative of 1 of 2 independent experiments. *Arrows* denote the decrease in superoxide detected by luminol in the presence of SOD.

As mentioned previously, IFNγ increases gene expression of iNOS and iNOS activity (Mosser and Edwards, 2008). Luminol has been suggested to also detect other ROS, including peroxynitrite (Radi *et al.*, 1993), which is generated from the combination of NO and superoxide. To determine whether luminol was detecting NO in our system, we also measured superoxide production in the presence of a NO inhibitor, N^G-monomethyl-L-arginine (L-NMMA). In contrast to SOD, blocking NO activity did not substantially decrease SOZ stimulated superoxide production in IFNγ (72 hr) activated RAW 264.7 cells (Figure 63).

4. SOZ and PMA stimulated superoxide production in IFNγ activated BMDMs is dependent on $gp91^{phox}$, $p22^{phox}$, and $p47^{phox}$

$gp91^{phox}$ (NOX2) is one member of a family of NADPH oxidases (NOXs) that are found in many tissues and contribute to a wide range of physiological functions such as vascular tone and angiogenesis, but all are capable of producing superoxide (Nauseef, 2008). It was of interest to determine whether the increase in superoxide production following IFNγ was specific to NOX2 and likewise dependent on $gp91^{phox}$, $p22^{phox}$, and $p47^{phox}$. Comparison of SOZ stimulated superoxide production in 72 hr IFNγ activated wild-type BMDMs to $gp91^{phox}$-, $p22^{phox}$-, and $p47^{phox}$-deficient BMDMs (Figures 64A, 64B, and 64C) showed superoxide production was dependent on all three of these NADPH oxidase subunits.

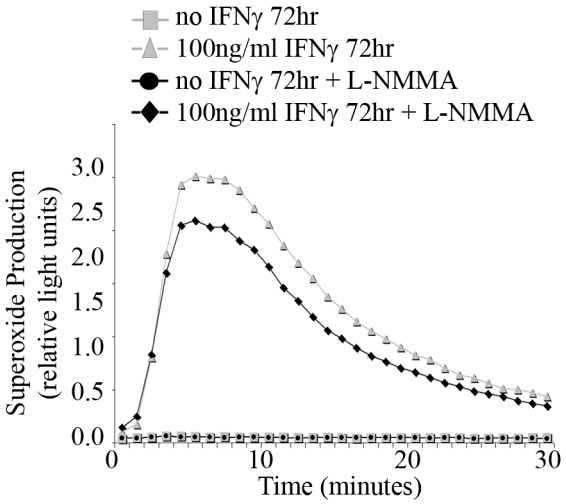

Figure 63. In contrast to SOD, the NO inhbitor L-NMMA did not dramatically decrease SOZ stimulated superoxide production in IFNγ activated RAW 264.7 cells. SOZ stimulated superoxide was measured in 72 hr IFNγ stimulated (100 ng/ml) RAW 264.7 cells in the presence or absence of L-NMMA (500 μM final). This experiment was performed one time.

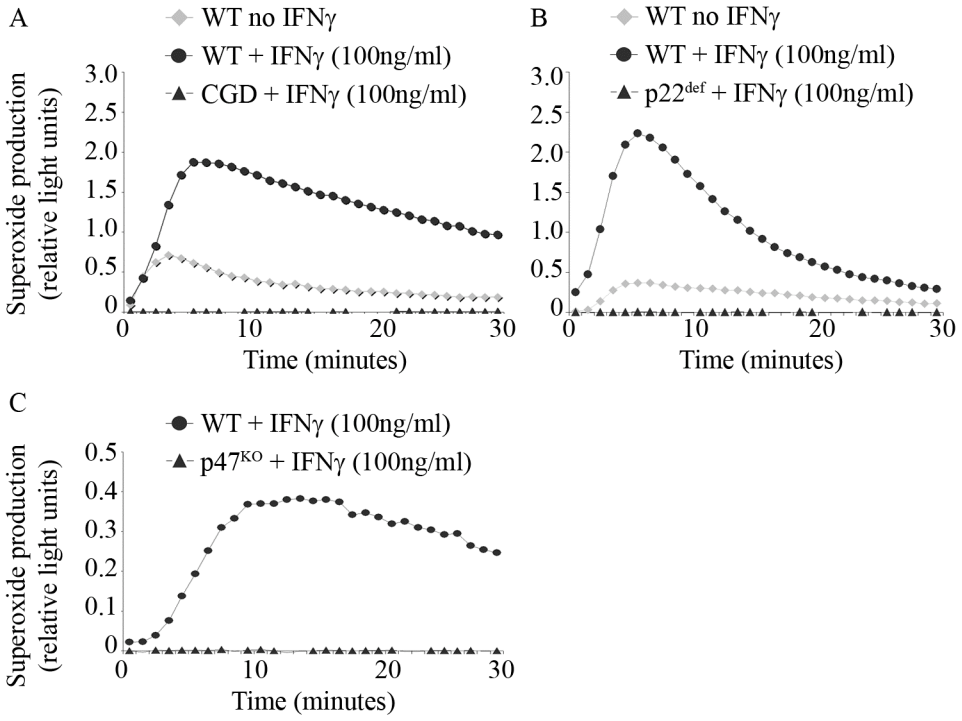

Figure 64. Increase in SOZ stimuated superoxide in 72 hr IFNγ activated BMDMs is dependent on gp91^{phox}, p22^{phox}, and p47^{phox}. SOZ stimulated superoxide production in (A) wild-type and gp91^{phox}-null (CGD) BMDMs or (B) wild-type and p22^{phox}-deficient BMDMs in the presence or absence of IFNγ (100 ng/ml) for 72 hr in αMEM, 10% HI FCS, and M-CSF (25 ng/ml). (C) SOZ stimulated superoxide in wild-type and p47^{phox}-knockout BMDMs was measured following 72 IFNγ (100 ng/ml) stimulation in αMEM and 10% HI FCS (no M-CSF). In (C) only, 2.5x10^4 cells were plated in each well vs. 1x10^5 cells used for all other experiments.

5. LPS alone or in combination with IFNγ did not appear to increase NADPH oxidase activity in RAW 264.7 cells

We observed a small increase in flavocytochrome *b* protein expression in LPS stimulated RAW 264.7 cells (Figure 38). Thus, we investigated whether LPS also increased NADPH oxidase activity. RAW 264.7 cells were stimulated for 24 and 48 hr with LPS (250 ng/ml) or IFNγ (100 ng/ml), and superoxide production was evaluated in SOZ stimulated cells. In comparison to unstimulated cells, 24 and 48 hr LPS stimulation only resulted in a 7- and 31-fold increase in SOZ stimulated superoxide production, while IFNγ activation resulted in a 31- and 237-fold increase (Figure 65). Our results confirm a previous report by C. Nathan (Nathan *et al.*, 1983) that LPS alone is a less potent activator of the NADPH oxidase than IFNγ is in macrophages.

As mentioned earlier, the combination of IFNγ and LPS are used frequently to generate "classically" activated macrophages (Mosser and Edwards, 2008). Thus, we also investigated NADPH oxidase activity in RAW cells activated with the combination of IFNγ and LPS. The addition of LPS (20 ng/ml) to two different concentrations of IFNγ (10 and 100 ng/ml) did not additively increase superoxide production in RAW 264.7 cells stimulated with SOZ (Figures 66A and 66B, bottom panels) and did not appear to change the kinetics of superoxide release (Figures 66A and 66B, top panels). However, as described above (page 140), the combination of IFNγ and LPS did appear to kill the cells by 72 hr since the number of cells harvested following the combination of IFNγ (10 ng/ml) and LPS (20 ng/ml) were reduced approximately 80% and the combination of IFNγ (10 ng/ml) and LPS (250 ng/ml) approximately 90% from those cells treated with IFNγ (10 ng/ml) alone at 72 hr.

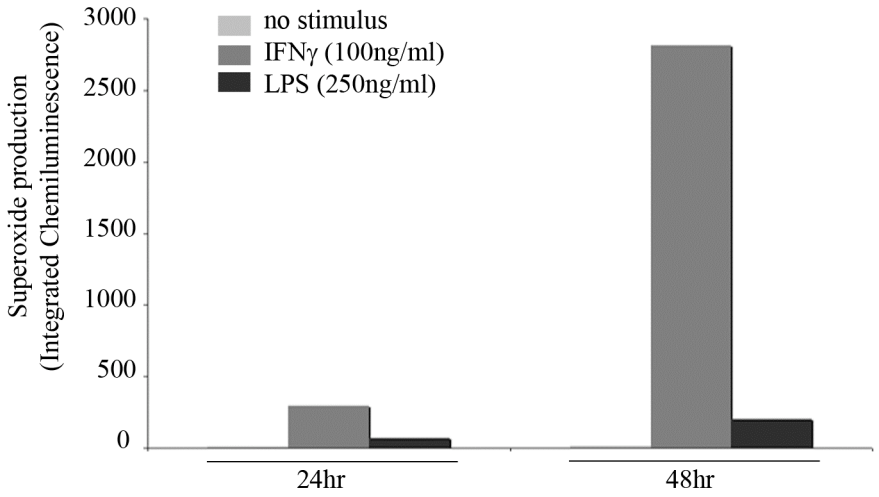

Figure 65. In contrast to IFNγ, LPS does not dramatically increase SOZ stimulated superoxide production in RAW 264.7 cells. SOZ stimulated superoxide production was measured in RAW 264.7 cells cultured for 24 or 48 hr with no stimulus, IFNγ (100 ng/ml), or LPS (250 ng/ml). Integrated chemiluminescence detected for 30 min is shown. This experiment was only performed one time.

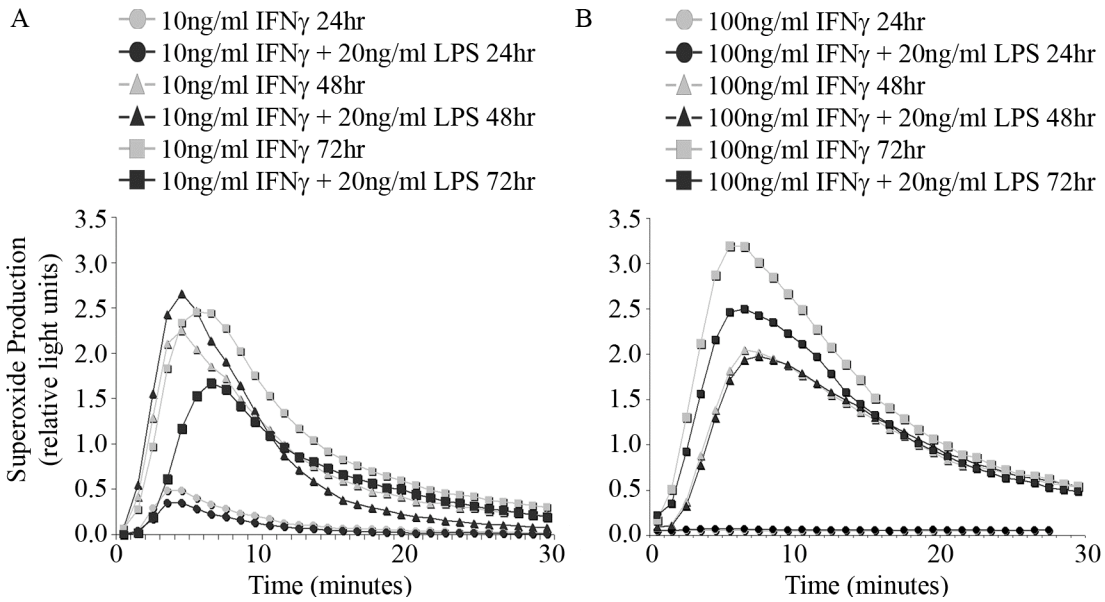

Figure 66. Combination of IFNγ and LPS does not additively increase SOZ stimulated superoxide production in RAW 264.7 cells. SOZ stimulated superoxide production was measured in RAW 264.7 cells activated with (A) 10 ng/ml IFNγ or (B) 100 ng/ml IFNγ with or without 20 ng/ml LPS for 24 - 72 hr. Each experiment was performed only once.

6. Blocking TNFα did not appear to decrease SOZ or PMA stimulated superoxide production

We also investigated whether TNFα played a role in inducing NADPH oxidase activity in IFNγ activated cells. SOZ and PMA stimulated superoxide production was evaluated in unstimulated RAW 264.7 cells and cells stimulated with IFNγ in the presence of absence of a blocking antibody for TNFα. In comparison to unstimulated cells, the increase in NADPH oxidase activity in IFNγ activated cells did not appear to be altered in the presence of a low (200 ng/ml) or a high (10 μg/ml) concentration of TNFα blocking antibody (Figure 67). These data suggest TNFα does not contribute to IFNγ-induced NADPH oxidase activity in macrophages. However, as described above, it should be noted the activity of the blocking antibody was not tested.

IX. Extracellular superoxide detected by luminol and NBT in the absence of exogenous stimulus in IFNγ stimulated RAW 264.7 cells and BMDMs

1. Superoxide production detected by luminol in IFNγ activated RAW 264.7 and BMDMs in the absence of exogenous stimulus

Unexpectedly, we also found that IFNγ activated cells produced superoxide in the absence of any exogenous stimulus, as evidenced by detection of ROS in cells suspended in buffer alone (PBSG). Following 24 hr of IFNγ activation, little superoxide was detected in the absence of an added stimulus (Figure 68), but dramatically increased in 48 and 72 hr IFNγ activated RAW 264.7 cells and BMDMs (Figure 68). ROS detected by chemiluminescence in the absence of exogenous stimulus ranged from 7 - 20% of that detected following SOZ stimulation. Similar to the SOZ and PMA stimulated superoxide

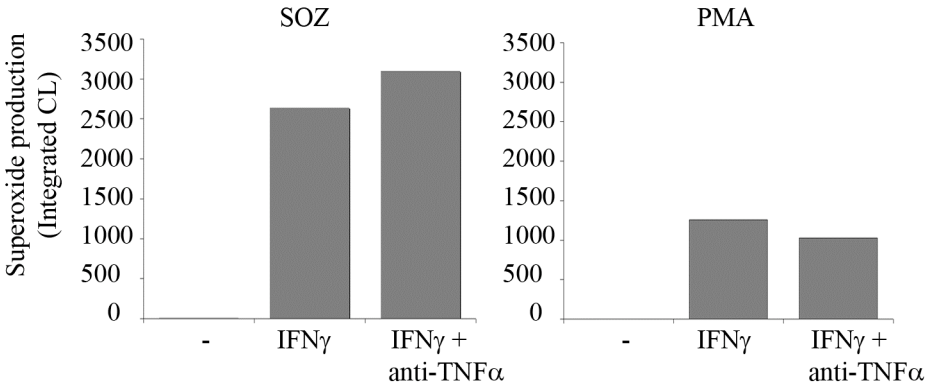

Figure 67. Blocking TNFα did not appear to decrease SOZ or PMA stimulated superoxide production in IFNγ activated RAW 264.7 cells. (A) SOZ stimulated superoxide production in RAW cells activated with IFNγ (100 ng/ml) in the presence or absence of anti-TNFα (200 ng/ml) for 72 hr. (B) PMA stimulated superoxide production in RAW 264.7 cells activated with IFNγ (100 ng/ml) for 72 hr in the presence or absence of anti-TNFα (10 μg/ml). Each experiment was performed once.

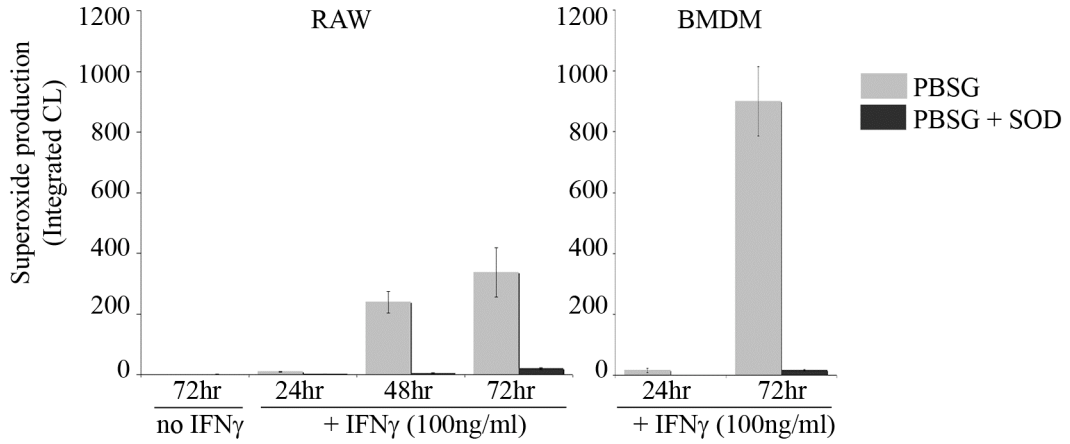

Figure 68. Extracellular superoxide in the absence of exogenous stimulus is detected by luminol in IFNγ activated RAW 264.7 cells and BMDMs. RAW 264.7 cells and BMDMs were activated with IFNγ (100 ng/ml) for 24, 48, or 72 hr. NADPH oxidase activity in unactivated or IFNγ activated cells was assessed by luminol in the absence of any exogenous stimulus (labeled as PBSG for buffer only). In addition, superoxide production was evaluated in the presence of SOD. Relative light units were monitored for 30 min. Total superoxide is shown (integrated chemiluminescence) and is the mean of 5 independent experiments (left panel) or 2 independent experiments (right panel).

in IFNγ activated cells (Figure 62), superoxide production in the absence of stimulus was also inhibited by SOD (Figure 68).

2. Dose dependent production of superoxide in the absence of exogenous stimulus in IFNγ activated RAW 264.7 cells

To further investigate the induction of superoxide production by IFNγ, we evaluated superoxide production in response to increasing concentrations of IFNγ (0.1 - 500 ng/ml). As shown in Figure 69, a dose dependent increase in superoxide production was observed which appeared to reach a plateau at a concentration of 100 ng/ml IFNγ (Figure 69). Next, we also evaluated whether the production of superoxide in the absence of stimulus in IFNγ activated BMDMs was dependent on $p22^{phox}$. As shown in Figure 70, no superoxide was detected in $p22^{phox}$-deficient BMDMs in the presence or absence of exogenous stimulus (SOZ), showing the ROS detected in IFNγ activated cells is due to the NADPH oxidase.

3. Superoxide detected at the cell surface by NBT in IFNγ activated BMDMs in the absence of exogenous stimulus

Nitroblue tetrazolium (NBT) assays were performed to further investigate the production of superoxide in the absence of exogenous stimulus in IFNγ activated BMDMs. Similar to luminol, superoxide was also detected by NBT, in the absence of stimulus in 72 hr IFNγ activated wild-type BMDMs, but not unactivated BMDMS or IFNγ activated $gp91^{phox}$-deficient BMDMs (Figure 71), further establishing the ROS detected was dependent on $gp91^{phox}$ and IFNγ stimulation. Interestingly, 72 hr IFNγ

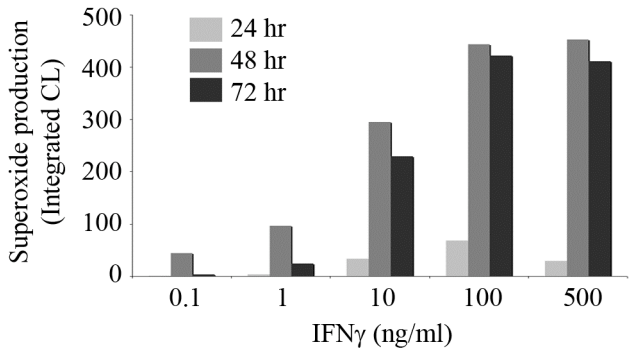

Figure 69. Dose and time-dependent increase in superoxide produced in the absence of exogenous stimulus following IFNγ stimulation in RAW 264.7 cells. RAW 264.7 cells were activated with increasing concentrations of IFNγ (0.1 – 100 ng/ml) for 24, 48, or 72 hr. NADPH oxidase activity in unactivated and IFNγ activated cells was assessed by luminol in the absence of any exogenous stimulus. Relative light units were monitored for 30 min. Total superoxide from 1 experiment is shown (integrated chemiluminescence), which is representative of 3 independent experiments.

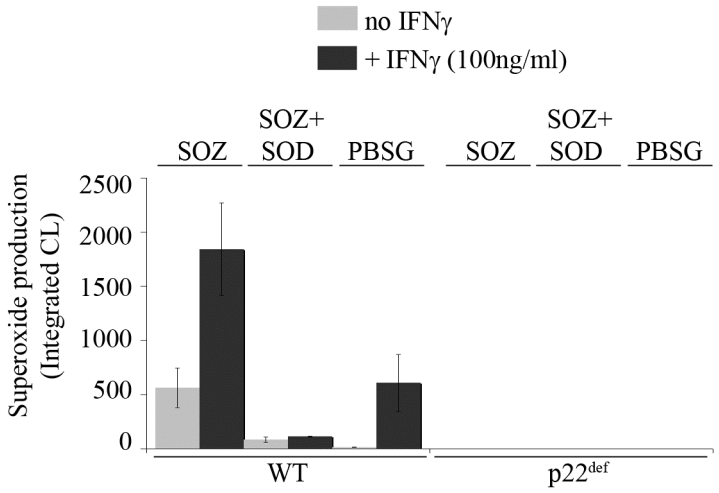

Figure 70. Superoxide production in the absence of exogenous stimulus is p22^{phox} dependent. Superoxide production is increased following IFNγ activation in BMDMs. BMDMs were plated on 100 mm Petri dishes in the absence or presence of IFNγ (100 ng/ml) in MEM, 10% HI FCS, and M-CSF (25 ng/ml) for 72 hr. Cells were collected using cold PBS, and superoxide was measured using luminol in the presence or absence of SOZ with or without SOD, or PBSG alone (i.e. no stimulus). Average of 2 independent experiments is shown.

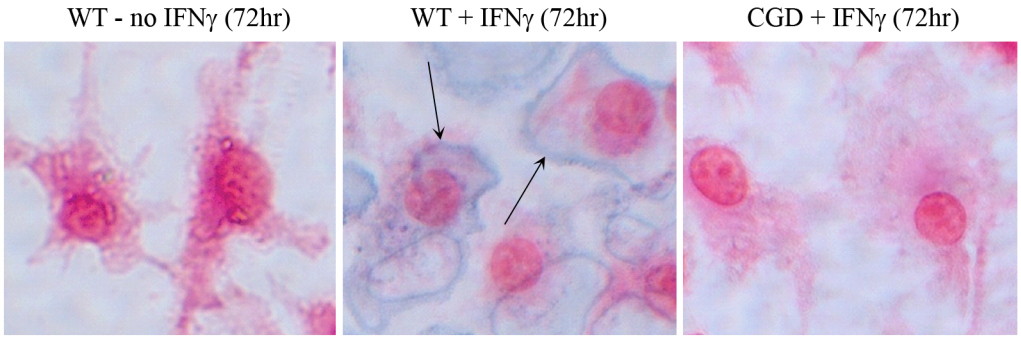

Figure 71. IFNγ activated BMDMs show NBT-positive superoxide production at the plasma membrane in the absence of exogenous stimulus. Day 6 differentiated BMDMs (wild-type and gp91^{phox}-null CGD) were plated in the absence or presence of IFNγ (100 ng/ml) in MEM and 10% HI FCS (no M-CSF) for 72 hr onto 8-well chamber slides. Following 72 hr, nitroblue tetrazolium (NBT) was added to cells without any exogenous stimulus and incubated for 30 min at 37°C. Cells were then counterstained with safrinin, and the conversion of NBT to insoluble purple formazan deposits was evaluated by microscopy. *Arrows* denote localized production of superoxide.

activated BMDMs showed localized production of superoxide at the cell surface (Figure 71, *arrows*), which was the same location where we found flavocytochrome *b* (Figure 40).

DISCUSSION

I. Macrophage NADPH Oxidase flavocytochrome *b* localizes to the plasma membrane and Rab11-positive recycling endosomes

In these studies, we show for the first time that the NADPH oxidase flavocytochrome *b* is localized to both the plasma membrane and the endocytic recycling compartment in macrophages. We used a combination of fluorescently tagged probes for gp91^{phox} and p22^{phox} and indirect immunofluoresence of the corresponding endogenous proteins to examine the subcellular distribution of each subunit in living and fixed cells. While our study is the first to show localization of macrophage flavocytochrome *b* to recycling endosome compartments, human peripheral blood monocytes also contain intracellular vesicles enriched in flavocytochrome *b*, but the nature of these structures and whether they recycle remains to be determined (Ginsel *et al.*, 1990; Calafat *et al.*, 1993). Of note, FcγRs did not accumulate in recycling compartments, thereby indicating selectivity in this process despite the fact that these receptors decline in the membranes of nascent phagosomes following ingestion of IgG-coated particles (Pitt *et al.*, 1992). Additional results from our experiments demonstrate that individual subunits of flavocytochrome *b*, either when expressed alone or when one subunit is expressed in excess of its partner, remain in the ER, thereby confirming previous studies in neutrophils which demonstrated that heterodimer formation is an essential prerequisite of, and provides an important signal for, efficient trafficking to more peripheral membrane compartments (Yu *et al.*, 1999; DeLeo *et al.*, 2000; Zhu *et al.*, 2006). Similar data were obtained using murine RAW 264.7 macrophages, primary BMDMs, and the CHO cell

model system. Our demonstration that a portion of the flavocytochrome *b* in macrophages is present in Rab11-positive endosomes suggests that the endocytic recycling compartment may act as a reservoir of flavocytochrome *b* which cycles between this compartment and the cell surface.

This study is also the first to indicate a relationship between relative expression levels of gp91^{phox} and p22^{phox} and their accumulation in different subcellular compartments. In CHO cells, where each flavocytochrome *b* subunit is relatively stable in the absence of its partner, both gp91^{phox} and p22^{phox} accumulated in the endoplasmic reticulum when expressed individually. In addition, a small fraction of gp91^{phox} is present in its mature 91 kDa glycosylated form and traffics to the cell surface (Biberstine-Kinkade *et al.*, 2002; Zhu *et al.*, 2006). These data suggest that some maturation and trafficking to the cell surface of unassembled gp91^{phox} occurs as an inefficient default pathway, or, alternatively, it is possible that another protein is capable of directing some gp91^{phox} to the cell surface in CHO cells in the absence of p22^{phox}. Titration experiments in CHO cells showed that when co-expressed at similar levels, p22^{phox} and gp91^{phox} no longer accumulate in the ER, and instead colocalize at the cell surface and in the endocytic recycling compartment. However, in both CHO cells and macrophages, if one subunit is overexpressed compared to its partner, the "excess" subunit remains in the ER. Previous studies examining localization of p22^{phox} and gp91^{phox} in transfected cells have not addressed the importance of the ratio of the two subunits or clearly shown that the location of the heterodimer may be distinct from the location of the individual subunits (Ambasta *et al.*, 2004; Murillo and Henderson, 2005).

In neutrophils, specific granules carrying flavocytochrome *b* can serve as a storage pool and a mechanism by which flavocytochrome *b* is recruited to the plasma membrane and phagosomes. Our findings localizing flavocytochrome *b* to Rab11-positive and Rab5-positive endosomes in macrophages suggest recycling endosomes may serve a similar function. Macrophages have the capacity to rapidly ingest many large particles or microbes, and it has long been known that cell surface area increases during phagocytosis (Hackam *et al.*, 1998; Cox *et al.*, 1999; Di *et al.*, 2003). Membrane compartments mobilized for expansion of the cell surface include but are not limited to Vamp3- and/or Rab11-positive endosomes (Bajno *et al.*, 2000; Cox *et al.*, 2000; Allen *et al.*, 2002; Murray *et al.*, 2005; Leiva *et al.*, 2006; Manderson *et al.*, 2007). However, the nature of the compartments mobilized in response to any one stimulus remains controversial, and the extent to which vesicles fuse directly with forming phagosomes as compared with the 'uninvolved' plasma membrane is not well defined (Di *et al.*, 2003; Rogers and Foster, 2008). Thus, it is also possible that fusion of recycling endosomes with the cell surface provides a mechanism to replenish plasma membrane flavocytochrome *b* during phagocytosis or macrophage activation as has been described for TNFα (Murray *et al.*, 2005; Manderson *et al.*, 2007). Alternatively, it is also possible that recycling endosomes remove flavocytochrome *b* from the membranes of phagosomes as they mature. In either case, it is interesting to hypothesize that macrophages, which unlike neutrophils are long-lived cells, may utilize this compartment to retain and conserve the use of flavocytochrome *b*.

S. typhimurium is a facultative intracellular pathogen of macrophages. An essential aspect of virulence is the ability of *S. typhimurium* to introduce bacterial effector

proteins into the cytosol of host cells using Type III secretion (T3SS) that disrupt membrane trafficking and prevent phagosome maturation. Previous studies by us and others have shown that effectors of the *S. typhimurium* pathogenicity island-2-encoded T3SS are also required to prevent accumulation of NADPH oxidase components, including flavocytochrome *b*, on *S. typhimurium* compartments in primary murine and human macrophages (Gallois *et al.*, 2001; Vazquez-Torres *et al.*, 2001). Although the mechanisms of action of T3SS effectors are not well defined, it is attractive to predict that targeting Rab11 may allow selective depletion of flavocytochrome *b* from the *S. typhimurium* phagosome as has recently been reported for CD44 (Smith *et al.*, 2005).

II. IFNγ increases flavocytochrome *b* localization to the cell surface

During an infection, macrophages become activated by cytokines, such as IFNγ or TNFα, or bacterial LPS, to enhance antimicrobial killing, referred to as "classical" activation. Notably, activated macrophages have an increased ability to kill intracellular pathogens, which has been linked to an increased ability to release superoxide (Nathan *et al.*, 1983) and increased expression of $gp91^{phox}$ (Newburger *et al.*, 1988). In resting macrophages, we found flavocytochrome *b* localized mostly inside the cell to recycling endosomes. We next examined whether IFNγ activation affected the distribution of macrophage flavocytochrome *b*. We also investigated the change in protein expression of NADPH oxidase subunits and NADPH oxidase activity following stimulation with IFNγ, LPS, or a combination of the two in macrophages.

In IFNγ activated RAW 264.7 macrophages, the protein expression of $gp91^{phox}$ and $p22^{phox}$ was found to continually increase from 24 - 72 hr following IFNγ activation

and to plateau at a concentration of 10 ng/ml IFNγ (100 U/ml). We detected no change in the protein expression of NADPH oxidase subunits $p47^{phox}$, $p67^{phox}$, or $p40^{phox}$. In neutrophils, IFNγ downregulates $p47^{phox}$ approximately 50% following 2 hr IFNγ stimulation (Cassatella *et al.*, 1990; Amezaga *et al.*, 1992), and the protein expression of $p67^{phox}$ during differentiation of the promyelocytic cell line HL-60 increases approximately 3- to 4-fold following 4 days IFNγ stimulation (Gupta *et al.*, 1992). Thus, the regulation of $p47^{phox}$ or $p67^{phox}$ protein expression by IFNγ may be different between neutrophils and macrophages. In comparison to IFNγ, LPS only modestly increased $gp91^{phox}$ and $p22^{phox}$ expression by 3-fold, which was dependent on the dose and duration of LPS stimulation.

NADPH oxidase activity was evaluated in both RAW 264.7 cells and murine bone marrow derived macrophages following activation with IFNγ, LPS, or the combination. As expected, IFNγ activation increased NADPH oxidase activity, as detected by luminol-enhanced chemiluminescence, in both cell types. The increase in NADPH oxidase activity correlated with increased $gp91^{phox}$ and $p22^{phox}$ protein expression. In the presence of SOD, luminol-detected superoxide was reduced 75 - 90%, indicating that the signal largely reflected extracellular superoxide. In contrast to IFNγ alone, LPS alone or in combination with IFNγ did not increase NADPH oxidase activity in RAW 264.7 cells.

As mentioned, LPS only resulted in a modest increase in both the protein expression of $gp91^{phox}$ and $p22^{phox}$ and NADPH oxidase activity. These results support previous reports that LPS alone is not a major activator of the NADPH oxidase in macrophages (Nathan *et al.*, 1983). In our experiments, the simultaneous activation with

LPS and IFNγ did not additively enhance superoxide production and in fact appeared cytotoxic to cells following 72 hr.

We found that inhibition of TNFα using a blocking antibody did not substantially decrease NADPH oxidase activity in IFNγ activated cells. TNFα is described as the second most important cytokine (IFNγ being the first) for "classical" activation of macrophages (Mosser and Edwards, 2008). Pre-treatment of human monocytes with TNFα has been shown to increase PMA stimulated superoxide approximately 2- to 5-fold (Gauss *et al.*, 2007) and BMDMs greater than 10-fold (Phillips *et al.*, 1990). TNFα secretion by activated macrophages is generally thought to require LPS stimulation (Mosser, 2003); however, recently it was shown that IFNγ (2.5 ng/ml) activation alone can increase TNFα secretion in a time-dependent manner in RAW 264.7 cells (Vila-del Sol *et al.*, 2007). Taken together, our results suggest IFNγ-induced TNFα secretion does not contribute to increased NADPH oxidase activity in IFNγ activated RAW 264.7 cells, but further studies are required since we did not measure TNFα secretion and the activity of the blocking antibody in our experiments.

Remarkably, in addition to the overall increase in flavocytochrome *b* protein expression, a shift in the distribution of flavocytochrome *b* was observed following 72 hr IFNγ activation in both RAW 264.7 and primary murine BMDMs. This shift resulted in a substantial increase in the presence of flavocytochrome *b* in the plasma membrane and a marked decrease of endosomal flavocytochrome *b*. Importantly, overexpressing $gp91^{phox}$ and $p22^{phox}$ from transgenes in RAW-91,22 cells did not increase localization of flavocytochrome *b* to the cell surface in the absence of IFNγ. These data suggest IFNγ induces a change in distribution of flavocytochrome *b* independent of the change in

protein expression. Interestingly, addition of LPS for only the last 24 hr of 72 hr of IFNγ activation cells appeared to reverse the predominant surface localization of flavocytochrome *b* seen in 72 hr activated cells with IFNγ alone. These results suggest LPS stimulation may also regulate trafficking of flavocytochrome *b* either by inhibiting signaling pathways leading to the IFNγ-induced change or by activating an additional pathway.

Our finding that IFNγ activation results in increased localization of flavocytochrome *b* to the plasma membrane suggests IFNγ may increase antimicrobial defense by mobilizing flavocytochrome *b* to the cell surface. Localization of flavocytochrome *b* to the plasma membrane would strategically place flavocytochrome *b* at the site where a phagocyte would first encounter a pathogen and would allow for immediate incorporation into a newly forming phagosome. We evaluated whether the shift in distribution of flavocytochrome *b* would enhance its relative incorporation into newly forming phagosomes. While localization of flavocytochrome *b* on phagocytic cups and nascent phagosomes was more visible and appeared less "patchy" in IFNγ activated macrophages compared to unactivated, we could not conclude that the IFNγ-induced change in distribution increased the amount of flavocytochrome *b* in nascent phagosomes relative to the total amount in the cell. However, it still remains possible that during an infection with a live pathogen, increased trafficking of flavocytochrome *b* to a phagosome could occur in IFNγ activated macrophages and warrants further studies.

Increased localization of flavocytochrome *b* in the plasma membrane could enable macrophages to release superoxide directly into the extracellular environment or into newly forming phagosomes. In neutrophils, little flavocytochrome *b* is found in the

plasma membrane, but upon activation, specific granules and secretory vesicles fuse with the plasma membrane (and phagosomes depending on the stimulus) and deliver flavocytochrome *b* to the cell surface. IFNγ activated macrophages have increased NADPH oxidase activity, as detected by luminol. The majority was shown to be SOD-sensitive, suggesting we are detecting predominantly extracellular superoxide release by macrophages under our conditions. Note that since luminol-enhanced chemiluminescence requires a peroxidase (Dahlgren and Karlsson, 1999), we added exogenous HRP. In contrast to neutrophils, macrophages are generally believed to have little to no expression of myeloperoxidase (MPO) and thus, our studies may be limited in their ability to detect intracellular superoxide. However, Adachi and colleagues (Adachi *et al.*, 2006) recently showed that IFNγ stimulation of RAW 264.7 cells and human monocytes increased localization of MPO at the cell surface, by immunofluorescence microscopy, suggesting MPO was being secreted at the cell surface. Additional investigations evaluating NADPH oxidase activity using luminol-based assays in IFNγ activated macrophages in the absence of HRP could determine whether MPO is being secreted and contributing to luminol-detected ROS. Taken together, we hypothesize that the increase in surface expression of gp91^{phox} and p22^{phox} in IFNγ activated cells may serve as a new "priming" mechanism for increasing NADPH oxidase activity at the cell surface in macrophages.

Notably, we found macrophages exposed to IFNγ for sustained periods produced superoxide in the absence of an exogenous stimulus. Most interesting was that localized production of superoxide in the absence of an exogenous stimulus was detected at the cell surface in BMDMs activated with IFNγ for 72 hr, but not 24 hr. This time course

correlated with the IFNγ-induced increase in surface localization of flavocytochrome *b*. These results further support our hypothesis that redistribution of flavocytochrome *b* to the cell surface is important for endowing macrophages with the capacity to produce superoxide at the cell surface.

p47^{phox} activation is required for NADPH oxidase activity. Evaluation of NADPH oxidase activity and the distribution of flavocytochrome *b* in p47$^{phox-/-}$ BMDMs activated with IFNγ showed p47^{phox} was required for IFNγ-induced NADPH oxidase activity, but was not required for the change in distribution of flavocytochrome *b*, confirming that ROS production is mediated by the assembled NADPH oxidase complex and also suggesting the redistribution of flavocytochrome *b* was not regulated by NADPH oxidase assembly.

In resting macrophages, it is known that the entire plasma membrane is completely turned over every 33 min and that this turnover is enhanced following IFNγ activation (Cohn, 1978; Mellman *et al.*, 1983). To our knowledge, the change in the "global" rate of endocytosis due to IFNγ has not been shown to enhance or concentrate localization of a plasma membrane protein to the cell surface independent of increased protein expression in macrophages. IFNγ activation has been reported to decrease localization of the Tfn-Receptor (Hamilton *et al.*, 1984) to the cell surface, and it is interesting to speculate that the increase in flavocytochrome *b* localization to the plasma membrane might be specific to proteins important in antimicrobial activity.

The redistribution of flavocytochrome *b* occurred following prolonged exposure to IFNγ, suggesting IFNγ does not directly regulate the change in distribution of flavocytochrome *b*. IFNγ is known to control gene expression, which may indirectly

regulate the trafficking of flavocytochrome *b*. Changes in gene expression following dendritic cell (DC) maturation regulate trafficking of MHCII (van Niel *et al.*, 2008). During DC maturation, the synthesis of MHCII is downregulated yet the cell surface expression increases. The increase in surface expression of MHCII is due to changes in trafficking regulated directly by ubiquitination. In immature DCs, ubiquitination of MHCII targets MHCII to MVBs (multi-vesicular bodies) which traffic to lysosomes for degradation, but upon DC maturation, ubiquitination ceases and MHCII stays at the cell surface (Shin *et al.*, 2006; van Niel *et al.*, 2006). Ubiquitination ceases due to changes in gene expression of a ubiquitin E3 ligase, MARCH1, which is down regulated upon DC maturation (De Gassart *et al.*, 2008). While a role in ubiquitination of flavocytochrome *b* has not been investigated, the studies in MHCII provide one mechanism of how changes in gene expression can lead to changes in trafficking of a surface protein. Notably, there are many other possibilities and future goals will be to identify the mechanism by which IFNγ changes the trafficking of flavocytochrome *b*.

CONCLUSIONS

We generated functional fluorescently tagged gp91^{phox} and p22^{phox} subunits and in combination with immunofluorescence microscopy characterized the subcellular distribution of flavocytochrome *b* in "resting" macrophages. We developed a CHO cell model in which trafficking of flavocytochrome *b* was evaluated by live imaging. Additionally, we established a system for investigating trafficking of flavocytochrome *b*, using p22^{phox}-deficient primary bone marrow derived macrophages for expression of a fluorescently tagged p22^{phox} probe. Utilizing these approaches, we showed for the first time that flavocytochrome *b* localizes primarily to the Rab11-positive endosome recycling compartment in "resting" macrophages (Figure 72). We also found flavocytochrome *b* to localize to Rab5-positive early endosomes and the plasma membrane, suggesting flavocytochrome *b* is internalized from the cell surface and recycles through these endosomal compartments before trafficking back to the cell surface (Figure 72). These findings expand our knowledge of the subcellular distribution and trafficking of flavocytochrome *b* in macrophages.

Our data suggests that recycling endosomes, which are in close proximity to the phagocytic cup and to nascent phagosomes, might be involved in targeting flavocytochrome *b* to phagocytic cups and/or recycling flavocytochrome *b* from phagosomes back to the plasma membrane. Currently, it is not known how flavocytochrome *b* is targeted to phagosomes. While the plasma membrane is an obvious source, we showed that little flavocytochrome *b* resides in the plasma membrane in "resting" macrophages and thus, Rab11-positive recycling endosomes may be

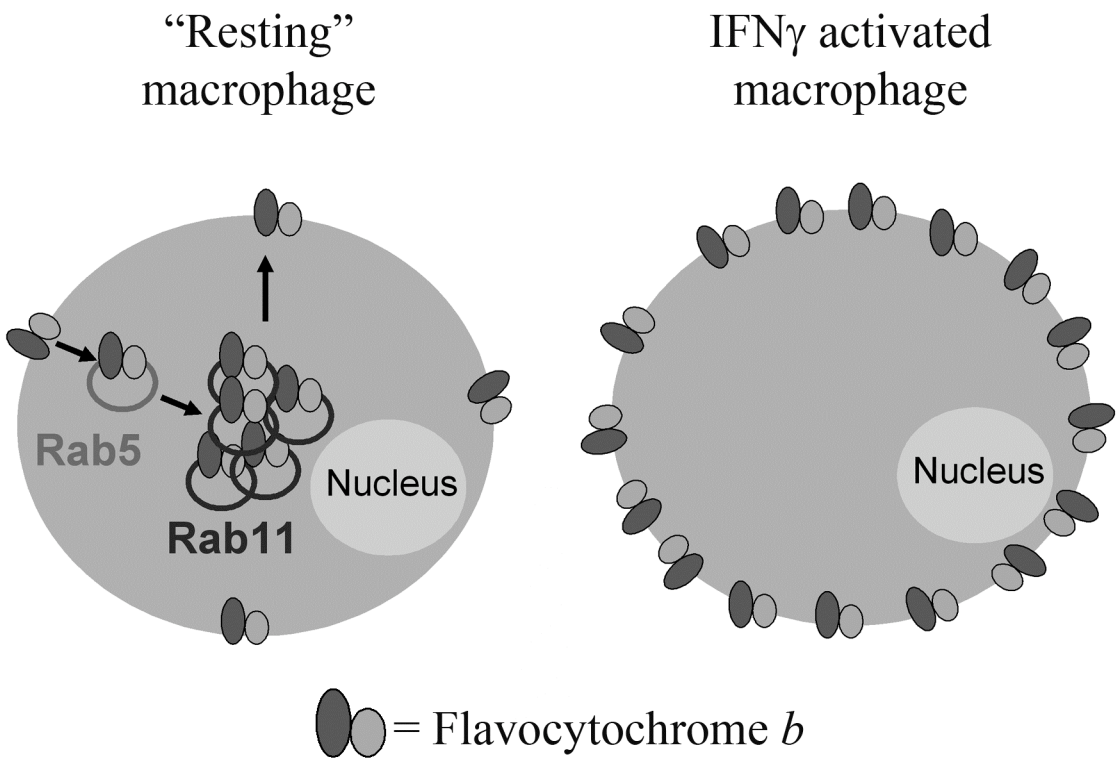

Figure 72. A model illustrating the subcellular distribution of flavocytochrome *b* in "resting" and IFNγ activated macrophages. **Left panel:** Flavocytochrome *b* is found in the plasma membrane and Rab5-positive endosomes, but appears to predominantly localize to the Rab11-positive endocytic recycling compartment in "resting" macrophages. Localization of flavocytochrome *b* to these endocytic compartments suggests flavocytochrome *b* is internalized from the cell surface, traffics to early Rab5-positive endosomes, and then to the Rab11-positive endocytic compartment before trafficking back to the cell surface (*arrows*). **Right panel:** The amount of flavocytochrome *b* increases and its distribution shifts from endocytic compartments to the cell surface following sustained IFNγ (72 hr) activation.

important for trafficking of flavocytochrome *b* to phagosomes during phagocytosis. Thus, our data suggests recycling endosomes may be one mechanism by which macrophages localize superoxide production for microbial killing.

We found the distribution of flavocytochrome *b* changed from a prominent perinuclear compartment in "resting" macrophages to a predominant localization to the plasma membrane following sustained IFNγ activation (Figure 72). This shift in distribution strategically positions flavocytochrome *b* at the outside of the cell which would allow for the extracelluar release of superoxide without phagocytosis and also before a phagosome is sealed. At the same time at which the distribution of flavocytochrome *b* changed following IFNγ stimulation, we also found IFNγ stimulated cells to produce superoxide in the absence of an exogenous stimulus. Taken together, our results suggest the IFNγ-induced redistribution of flavocytochrome *b* may be important for enhancing the production of superoxide at the cell surface and may be a potential new mechanism by which IFNγ enhances antimicrobial activity in macrophages.

In conclusion, we found the subcellular distribution of flavocytochrome *b* to be distinct in "resting" and IFNγ activated macrophages. These distinct locations provide new insight of how macrophages may localize superoxide production for microbial killing.

FUTURE STUDIES

Future goals of our studies include (I) to confirm Rab11-positive endosomes deliver flavocytochrome *b* to phagocytic cups during phagocytosis, (II) to define a mechanism(s) that regulates trafficking of flavocytochrome *b* to the cell surface following IFNγ stimulation, (III) to determine if the SPI-2 virulence factor SpiC alter trafficking of flavocytochrome *b*, and (IV) to determine the biological importance of the change in distribution of flavocytochrome *b* following prolonged exposure to IFNγ.

I. Confirmation that Rab11-positive endosomes deliver flavocytochrome *b* to the phagocytic cup using electron microscopy (EM) and video microscopy

Colocalization of flavocytochrome *b* with Rab11-positive endosomes in discrete patches near phagocytic cups was observed during phagocytosis of opsonized zymosan particles in macrophages using immunofluorescence light microscopy. While these observations suggest Rab11-positive endosomes may deliver flavocytochrome *b* to phagocytic cups, there are two experiments that would be required to prove this. First, time lapse video microscopy showing trafficking of flavocytochrome *b* in Rab11-positive endosomes (i.e., colocalization) directly to the phagocytic cup would be needed. Second, confirmation that flavocytochrome *b* and Rab11 colocalize in the same vesicles and that these vesicles actually fuse with the phagocytic cup would require immunogold labeling and electron microscopy. These sets of experiments would best be performed in CHO-91,22YFP cells stably expressing the Fcγ-receptor for two main reasons: 1) CHO cells transgenically expressing the Fcγ-receptor are a model system for evaluating protein

trafficking during Fcγ-mediated phagocytosis (Downey *et al.*, 1999) and 2) we have already shown colocalization of Rab11CFP and 22YFP by video microscopy in this cell line.

II. Changes in the recycling pathway may be the mechanism by which IFNγ changes trafficking of flavocytochrome *b* in macrophages

1. Rab4B

Prolonged exposure to IFNγ was found to change the trafficking of flavocytochrome *b* in macrophages and increase flavocytochrome b surface localization. MHCII expression is upregulated following IFNγ through transcription coactivator CIITA. Chromatin immunoprecipitation (CHIP) assays evaluating additional genes regulated by CIITA identified Rab4B (Krawczyk *et al.*, 2007). Rab4B regulates endosomal trafficking from early endosomes (Rab5) to the cell surface and is believed to be important for recycling of endosomes back to the cell surface via the "fast" track, in contrast to "stopping" at the Rab11 compartment. Increasing endosomal recycling back to the cell surface and preventing it from trafficking to the Rab11 compartment could lead to the increased localization of flavocytochrome *b* to the cell surface. The role of IFNγ-induced expression of Rab4B in changing trafficking of flavocytochrome *b* could be investigated by knocking down Rab4B via siRNA (Fernandez *et al.*, 2009) or by inhibiting IFNγ-induced transcription of CIITA (Tooze *et al.*, 2006). Increased protein expression and subsequently increased Rab4B activity could change the trafficking of flavocytochrome *b* and prevent it from trafficking to the Rab11 compartment and thus, would result in a net increase in flavocytochrome *b* cell surface localization.

Interestingly, maximum Rab4B expression was detected following 48 hr IFNγ treatment (Krawczyk *et al.*, 2007), which was the same time at which we observed the change in distribution of flavocytochrome *b*.

In addition to Rab4, changes in expression and/or activity of other Rab family members could regulate trafficking of flavocytochrome *b*. While preliminary studies utilizing a GFP-expressing Rab11 did not show a change in distribution of flavocytochrome *b* (not shown), many Rab members regulate trafficking to the plasma membrane. Recently, a less characterized Rab member, Rab10, was shown to regulate trafficking of GLUT4 from the ERC to the plasma membrane (Sano *et al.*, 2008) by knocking down Rab10 by shRNA.

2. Rab11 and/or VAMP3

In addition to Rab4B, Rab11 protein expression has also been shown to increase following IFNγ (0.5 ng/ml) treatment from 0 to 18 hr (Murray *et al.*, 2005), but was not examined at 48 or 72 hr. I performed preliminary experiments to compare (i) the protein expression of Rab11, by Western blot and (ii) and the localization of Rab11, by immunofluroescent staining, in unactivated to IFNγ (72 hr) activated RAW 264.7 cells, but these experiments were unsuccessful. Changes in protein expression of Rab11 could potentially lead to an increase in the cell surface expression of flavocytochrome *b* and thus, these experiments should be repeated.

Another attractive hypothesis is that VAMP3 may also regulate trafficking of flavocytochrome *b*. VAMP3, or cellubrevin, is a SNARE (soluble N-ethylmaleimide-sensitive factor attachment protein receptor) protein found on vesicles (v-SNARE) that

forms a complex with a target SNARE (t-SNARE) protein on the plasma membrane (Proux-Gillardeaux *et al.*, 2005). As described earlier in the discussion, IFNγ-induced upregulation of VAMP3 (Murray *et al.*, 2005) has been shown to increase secretion of TNFα to the phagocytic cup. Interestingly, theses studies also showed that both knockdown of VAMP3 via siRNA and transient expression of the inhibitory domain of VAMP3 (amino acids 1 to 81) decreased TNFα trafficking in Tfn-positive endosomes to the cell surface, showing VAMP3 can regulate trafficking of recycling endosomes to the cell surface. Since flavocytochrome *b* also localizes to recycling endosomes, we can speculate that VAMP3 may regulate flavocytochrome *b* trafficking to the cell surface, which may be upregulated in IFNγ activated macrophages.

III. Determine if SpiC alters trafficking of flavocytochrome *b*

It is not known how *Salmonella* interrupts the localization of flavocytochrome *b* to the *Salmonella*-containing phagosome. Investigations of individual virulence factors could provide answers. SpiC is a virulence factor that alters host protein trafficking and is necessary for inhibiting phagosome-lysosome fusion by *Salmonella* (Uchiya *et al.*, 1999). SpiC, encoded in the SpI-2 locus, inhibits vesicular trafficking of both the endocytic and degradative pathways (Holden, 2002) by hindering fusion events, internalization, and recycling (Uchiya *et al.*, 1999). Transient expression of SpiC from a plasmid into host cells also alters endocytic trafficking (Shotland *et al.*, 2003). Our studies showed flavocytochrome *b* localizes to recycling endosomes, providing a potential link between SpiC and *Salmonella*'s ability to alter trafficking of flavocytochrome *b*. Thus, evaluation of changes in trafficking of flavocytochrome *b*

using live imaging in macrophages following transgenic expression of SpiC or other *Salmonella* virulence factors would provide useful tools for determining if these individual virulence factors could disrupt trafficking of flavocytochorme *b* in the presence or absence of IFNγ. Notably, understanding how *Salmonella* excludes the flavocytochrome would not only explain the mechanism by which *Salmonella* evades destruction by superoxide, but would also provide a better understanding of the mechanism by which macrophages regulate the location of the flavocytochrome during "normal" phagocytosis.

IV. Determine the biological importance of the change in distribution of flavocytochrome *b* following sustained exposure to IFNγ

The increase in flavocytochrome *b* at the cell surface following IFNγ stimulation and the release of superoxide in the absence of an exogenous stimulus suggests these changes may facilitate the ability of macrophages to kill pathogens BEFORE they enter the cell through phagocytosis. To test this hypothesis, bacterial killing by IFNγ activated macrophages either in the presence or absence of SOD, and inhibitors of phagocytosis, such as Cytochalasin D, could be utilized. If killing was reduced in the presence of SOD and Cytochalasin D, this suggests that extracellular superoxide production was important for killing.

Alternatively, the change in distribution of flavocytochrome *b* may increase localization of flavocytochrome *b* into newly forming phagosomes. While we did not see a prominent increase in localization of flavocytochrome *b* to phagosomes by live imaging using our 22YFP-expressing $p22^{def}$ BMDMs during the phagocytosis of serum opsonized

yeast particles, we did observe a more uniform distribution in phagocytic cups. It is quite possible that additional stimulants from a live pathogen may yield a much different result. Thus, additional studies evaluating flavocytochrome *b* trafficking during phagocytosis of live pathogens are warranted.

REFERENCES

Adachi, Y., Kindzelskii, A.L., Petty, A.R., Huang, J.B., Maeda, N., Yotsumoto, S., Aratani, Y., Ohno, N., and Petty, H.R. (2006). IFN-gamma primes RAW264 macrophages and human monocytes for enhanced oxidant production in response to CpG DNA via metabolic signaling: roles of TLR9 and myeloperoxidase trafficking. J Immunol *176*, 5033-5040.

Aderem, A. (2003). Phagocytosis and the inflammatory response. J Infect Dis *187 Suppl 2*, S340-345.

Allen, L.A. (2008). Rate and extent of Helicobacter pylori phagocytosis. Methods Mol Biol *431*, 147-157.

Allen, L.A., and McCaffrey, R.L. (2007). To activate or not to activate: distinct strategies used by Helicobacter pylori and Francisella tularensis to modulate the NADPH oxidase and survive in human neutrophils. Immunol Rev *219*, 103-117.

Allen, L.A., Yang, C., and Pessin, J.E. (2002). Rate and extent of phagocytosis in macrophages lacking vamp3. J Leukoc Biol *72*, 217-221.

Ambasta, R.K., Kumar, P., Griendling, K.K., Schmidt, H.H., Busse, R., and Brandes, R.P. (2004). Direct interaction of the novel Nox proteins with p22phox is required for the formation of a functionally active NADPH oxidase. J Biol Chem *279*, 45935-45941.

Amezaga, M.A., Bazzoni, F., Sorio, C., Rossi, F., and Cassatella, M.A. (1992). Evidence for the involvement of distinct signal transduction pathways in the regulation of constitutive and interferon gamma-dependent gene expression of NADPH oxidase components (gp91-phox, p47-phox, and p22-phox) and high-affinity receptor for IgG (Fc gamma R-I) in human polymorphonuclear leukocytes. Blood *79*, 735-744.

Amigorena, S., Bonnerot, C., Drake, J.R., Choquet, D., Hunziker, W., Guillet, J.G., Webster, P., Sautes, C., Mellman, I., and Fridman, W.H. (1992). Cytoplasmic domain heterogeneity and functions of IgG Fc receptors in B lymphocytes. Science *256*, 1808-1812.

Babbey, C.M., Ahktar, N., Wang, E., Chen, C.C., Grant, B.D., and Dunn, K.W. (2006). Rab10 regulates membrane transport through early endosomes of polarized Madin-Darby canine kidney cells. Mol Biol Cell *17*, 3156-3175.

Babior, B.M., Lambeth, J.D., and Nauseef, W. (2002). The neutrophil NADPH oxidase. Arch Biochem Biophys *397*, 342-344.

Baehner, R.L., and Nathan, D.G. (1967). Leukocyte oxidase: defective activity in chronic granulomatous disease. Science *155*, 835-836.

Baehner, R.L., and Nathan, D.G. (1968). Quantitative nitroblue tetrazolium test in chronic granulomatous disease. N Engl J Med *278*, 971-976.

Bajno, L., Peng, X.R., Schreiber, A.D., Moore, H.P., Trimble, W.S., and Grinstein, S. (2000). Focal exocytosis of VAMP3-containing vesicles at sites of phagosome formation. J Cell Biol *149*, 697-706.

Baniulis, D., Nakano, Y., Nauseef, W.M., Banfi, B., Cheng, G., Lambeth, D.J., Burritt, J.B., Taylor, R.M., and Jesaitis, A.J. (2005). Evaluation of two anti-gp91phox antibodies as immunoprobes for Nox family proteins: mAb 54.1 recognizes recombinant full-length Nox2, Nox3 and the C-terminal domains of Nox1-4 and cross-reacts with GRP 58. Biochim Biophys Acta *1752*, 186-196.

Bastian, N.R., and Hibbs, J.B., Jr. (1994). Assembly and regulation of NADPH oxidase and nitric oxide synthase. Curr Opin Immunol *6*, 131-139.

Belosevic, M., Finbloom, D.S., Van Der Meide, P.H., Slayter, M.V., and Nacy, C.A. (1989). Administration of monoclonal anti-IFN-gamma antibodies in vivo abrogates natural resistance of C3H/HeN mice to infection with Leishmania major. J Immunol *143*, 266-274.

Benoit, M., Desnues, B., and Mege, J.L. (2008). Macrophage polarization in bacterial infections. J Immunol *181*, 3733-3739.

Biberstine-Kinkade, K.J., DeLeo, F.R., Epstein, R.I., LeRoy, B.A., Nauseef, W.M., and Dinauer, M.C. (2001). Heme-ligating histidines in flavocytochrome b(558): identification of specific histidines in gp91(phox). J Biol Chem *276*, 31105-31112.

Biberstine-Kinkade, K.J., Yu, L., Stull, N., LeRoy, B.A., Bennett, S., Cross, A.R., and Dinauer, M. (2002). Mutagenesis of p22phox Histidine 94. J Biol Chem *277*, 30368-30374.

Borregaard, N., and Cowland, J.B. (1997). Granules of the human neutrophilic polymorphonuclear leukocyte. Blood *89*, 3503-3521.

Borregaard, N., Heiple, J.M., Simons, E.R., and Clark, R.A. (1983). Subcellular localization of the b-cytochrome component of the human neutrophil microbicidal oxidase: translocation during activation. J Cell Biol *97*, 52-61.

Borregaard, N., Sorensen, O.E., and Theilgaard-Monch, K. (2007). Neutrophil granules: a library of innate immunity proteins. Trends Immunol *28*, 340-345.

Botelho, R.J., Teruel, M., Dierckman, R., Anderson, R., Wells, A., York, J.D., Meyer, T., and Grinstein, S. (2000). Localized biphasic changes in phosphatidylinositol-4,5-bisphosphate at sites of phagocytosis. J Cell Biol *151*, 1353-1368.

Bretscher, M.S. (1992). Circulating integrins: alpha 5 beta 1, alpha 6 beta 4 and Mac-1, but not alpha 3 beta 1, alpha 4 beta 1 or LFA-1. EMBO J *11*, 405-410.

Brumell, J.H., and Scidmore, M.A. (2007). Manipulation of rab GTPase function by intracellular bacterial pathogens. Microbiol Mol Biol Rev *71*, 636-652.

Burritt, J.B., Quinn, M.T., Jutila, M.A., Bond, C.W., and Jesaitis, A.J. (1995). Topological mapping of neutrophil cytochrome b epitopes with phage-display libraries. J Biol Chem *270*, 16974-16980.

Calafat, J., Kuijpers, T.W., Janssen, H., Borregaard, N., Verhoeven, A.J., and Roos, D. (1993). Evidence for small intracellular vesicles in human blood phagocytes containing cytochrome b558 and the adhesion molecule CD11b/CD18. Blood *81*, 3122-3129.

Carlyon, J.A., Abdel-Latif, D., Pypaert, M., Lacy, P., and Fikrig, E. (2004). Anaplasma phagocytophilum utilizes multiple host evasion mechanisms to thwart NADPH oxidase-mediated killing during neutrophil infection. Infect Immun *72*, 4772-4783.

Casanova, J.E., Wang, X., Kumar, R., Bhartur, S.G., Navarre, J., Woodrum, J.E., Altschuler, Y., Ray, G.S., and Goldenring, J.R. (1999). Association of Rab25 and Rab11a with the apical recycling system of polarized Madin-Darby canine kidney cells. Mol Biol Cell *10*, 47-61.

Cassatella, M.A., Bazzoni, F., Flynn, R.M., Dusi, S., Trinchieri, G., and Rossi, F. (1990). Molecular basis of interferon-gamma and lipopolysaccharide enhancement of phagocyte respiratory burst capability. Studies on the gene expression of several NADPH oxidase components. J Biol Chem *265*, 20241-20246.

Cohn, Z.A. (1978). Activation of mononuclear phagocytes: fact, fancy, and future. J Immunol *121*, 813-816.

Collart, M.A., Belin, D., Vassalli, J.D., de Kossodo, S., and Vassalli, P. (1986). Gamma interferon enhances macrophage transcription of the tumor necrosis factor/cachectin, interleukin 1, and urokinase genes, which are controlled by short-lived repressors. J Exp Med *164*, 2113-2118.

Cox, D., Lee, D.J., Dale, B.M., Calafat, J., and Greenberg, S. (2000). A Rab11-containing rapidly recycling compartment in macrophages that promotes phagocytosis. Proc Natl Acad Sci U S A *97*, 680-685.

Cox, D., Tseng, C.C., Bjekic, G., and Greenberg, S. (1999). A requirement for phosphatidylinositol 3-kinase in pseudopod extension. J Biol Chem *274*, 1240-1247.

Dahlgren, C., and Karlsson, A. (1999). Respiratory burst in human neutrophils. J Immunol Methods *232*, 3-14.

Damiani, M.T., Pavarotti, M., Leiva, N., Lindsay, A.J., McCaffrey, M.W., and Colombo, M.I. (2004). Rab coupling protein associates with phagosomes and regulates recycling from the phagosomal compartment. Traffic *5*, 785-797.

De Gassart, A., Camosseto, V., Thibodeau, J., Ceppi, M., Catalan, N., Pierre, P., and Gatti, E. (2008). MHC class II stabilization at the surface of human dendritic cells is the result of maturation-dependent MARCH I down-regulation. Proc Natl Acad Sci U S A *105*, 3491-3496.

DeLeo, F.R., Burritt, J.B., Yu, L., Jesaitis, A.J., Dinauer, M.C., and Nauseef, W.M. (2000). Processing and maturation of flavocytochrome b558 include incorporation of heme as a prerequisite for heterodimer assembly. J Biol Chem *275*, 13986-13993.
Desjardins, M. (1995). Biogenesis of phagolysosomes: the 'kiss and run' hypothesis. Trends Cell Biol *5*, 183-186.

Di, A., Nelson, D.J., Bindokas, V., Brown, M.E., Libunao, F., and Palfrey, H.C. (2003). Dynamin regulates focal exocytosis in phagocytosing macrophages. Mol Biol Cell *14*, 2016-2028.

Dinauer, M.C. (2003). Regulation of neutrophil function by Rac GTPases. Curr Opin Hematol *10*, 8-15.

Dinauer, M.C., Pierce, E.A., Erickson, R.W., Muhlebach, T.J., Messner, H., Orkin, S.H., Seger, R.A., and Curnutte, J.T. (1991). Point mutation in the cytoplasmic domain of the neutrophil p22-phox cytochrome b subunit is associated with a nonfunctional NADPH oxidase and chronic granulomatous disease. Proc Natl Acad Sci U S A *88*, 11231-11235.

Downey, G.P., Botelho, R.J., Butler, J.R., Moltyaner, Y., Chien, P., Schreiber, A.D., and Grinstein, S. (1999). Phagosomal maturation, acidification, and inhibition of bacterial growth in nonphagocytic cells transfected with FcgammaRIIA receptors. J Biol Chem *274*, 28436-28444.

Eklund, E.A., Jalava, A., and Kakar, R. (1998). PU.1, interferon regulatory factor 1, and interferon consensus sequence-binding protein cooperate to increase gp91(phox) expression. J Biol Chem *273*, 13957-13965.

Eng, E.W., Bettio, A., Ibrahim, J., and Harrison, R.E. (2007). MTOC reorientation occurs during FcgammaR-mediated phagocytosis in macrophages. Mol Biol Cell *18*, 2389-2399.

Fernandez, D.R., Telarico, T., Bonilla, E., Li, Q., Banerjee, S., Middleton, F.A., Phillips, P.E., Crow, M.K., Oess, S., Muller-Esterl, W., and Perl, A. (2009). Activation of mammalian target of rapamycin controls the loss of TCRzeta in lupus T cells through HRES-1/Rab4-regulated lysosomal degradation. J Immunol *182*, 2063-2073.

Gaborik, Z., and Hunyady, L. (2004). Intracellular trafficking of hormone receptors. Trends Endocrinol Metab *15*, 286-293.

Gallois, A., Klein, J.R., Allen, L.A., Jones, B.D., and Nauseef, W.M. (2001). Salmonella pathogenicity island 2-encoded type III secretion system mediates exclusion of NADPH oxidase assembly from the phagosomal membrane. J Immunol *166*, 5741-5748.

Gao, J., Morrison, D.C., Parmely, T.J., Russell, S.W., and Murphy, W.J. (1997). An interferon-gamma-activated site (GAS) is necessary for full expression of the mouse iNOS gene in response to interferon-gamma and lipopolysaccharide. J Biol Chem *272*, 1226-1230.

Garin, J., Diez, R., Kieffer, S., Dermine, J.F., Duclos, S., Gagnon, E., Sadoul, R., Rondeau, C., and Desjardins, M. (2001). The phagosome proteome: insight into phagosome functions. J Cell Biol *152*, 165-180.

Gauss, K.A., Nelson-Overton, L.K., Siemsen, D.W., Gao, Y., DeLeo, F.R., and Quinn, M.T. (2007). Role of NF-kappaB in transcriptional regulation of the phagocyte NADPH oxidase by tumor necrosis factor-alpha. J Leukoc Biol *82*, 729-741.

Ginsel, L.A., Onderwater, J.J., Fransen, J.A., Verhoeven, A.J., and Roos, D. (1990). Localization of the low-Mr subunit of cytochrome b558 in human blood phagocytes by immunoelectron microscopy. Blood *76*, 2105-2116.

Gonalons, E., Barrachina, M., Garcia-Sanz, J.A., and Celada, A. (1998). Translational control of MHC class II I-A molecules by IFN-gamma. J Immunol *161*, 1837-1843.

Gordon, M.A., Jack, D.L., Dockrell, D.H., Lee, M.E., and Read, R.C. (2005). Gamma interferon enhances internalization and early nonoxidative killing of Salmonella enterica serovar Typhimurium by human macrophages and modifies cytokine responses. Infect Immun *73*, 3445-3452.

Gordon, S., and Taylor, P.R. (2005). Monocyte and macrophage heterogeneity. Nat Rev Immunol *5*, 953-964.

Gough, D.J., Levy, D.E., Johnstone, R.W., and Clarke, C.J. (2008). IFNgamma signaling-does it mean JAK-STAT? Cytokine Growth Factor Rev *19*, 383-394.

Greenberg, S., and Grinstein, S. (2002). Phagocytosis and innate immunity. Curr Opin Immunol *14*, 136-145.

Griesbeck, O., Baird, G.S., Campbell, R.E., Zacharias, D.A., and Tsien, R.Y. (2001). Reducing the environmental sensitivity of yellow fluorescent protein. Mechanism and applications. J Biol Chem *276*, 29188-29194.

Griffiths, G. (2004). On phagosome individuality and membrane signalling networks. Trends Cell Biol *14*, 343-351.

Groemping, Y., and Rittinger, K. (2005). Activation and assembly of the NADPH oxidase: a structural perspective. Biochem J *386*, 401-416.

Groves, E., Dart, A.E., Covarelli, V., and Caron, E. (2008). Molecular mechanisms of phagocytic uptake in mammalian cells. Cell Mol Life Sci *65*, 1957-1976.

Guha, M., and Mackman, N. (2001). LPS induction of gene expression in human monocytes. Cell Signal *13*, 85-94.

Gupta, J.W., Kubin, M., Hartman, L., Cassatella, M., and Trinchieri, G. (1992). Induction of expression of genes encoding components of the respiratory burst oxidase during differentiation of human myeloid cell lines induced by tumor necrosis factor and gamma-interferon. Cancer Res *52*, 2530-2537.

Hackam, D.J., Rotstein, O.D., Sjolin, C., Schreiber, A.D., Trimble, W.S., and Grinstein, S. (1998). v-SNARE-dependent secretion is required for phagocytosis. Proc Natl Acad Sci U S A *95*, 11691-11696.

Hamilton, T.A., Weiel, J.E., and Adams, D.O. (1984). Expression of the transferrin receptor in murine peritoneal macrophages is modulated in the different stages of activation. J Immunol *132*, 2285-2290.

Haverkamp, M.H., van Dissel, J.T., and Holland, S.M. (2006). Human host genetic factors in nontuberculous mycobacterial infection: lessons from single gene disorders affecting innate and adaptive immunity and lessons from molecular defects in interferon-gamma-dependent signaling. Microbes Infect *8*, 1157-1166.

Hoebe, K., Janssen, E., and Beutler, B. (2004). The interface between innate and adaptive immunity. Nat Immunol *5*, 971-974.

Holden, D.W. (2002). Trafficking of the Salmonella vacuole in macrophages. Traffic *3*, 161-169.

Huang, S., Hendriks, W., Althage, A., Hemmi, S., Bluethmann, H., Kamijo, R., Vilcek, J., Zinkernagel, R.M., and Aguet, M. (1993). Immune response in mice that lack the interferon-gamma receptor. Science *259*, 1742-1745.

Jackson, S.H., Gallin, J.I., and Holland, S.M. (1995). The p47phox mouse knock-out model of chronic granulomatous disease. J Exp Med *182*, 751-758.

Janeway, C., and Travers, P. (1997). Immunobiology : the immune system in health and disease. Current Biology ; Garland Pub.: London ; San Francisco ; New York.

Jesaitis, A.J., Buescher, E.S., Harrison, D., Quinn, M.T., Parkos, C.A., Livesey, S., and Linner, J. (1990). Ultrastructural localization of cytochrome b in the membranes of resting and phagocytosing human granulocytes. J Clin Invest *85*, 821-835.

Johansson, A., Jesaitis, A.J., Lundqvist, H., Magnusson, K.E., Sjolin, C., Karlsson, A., and Dahlgren, C. (1995). Different subcellular localization of cytochrome b and the dormant NADPH-oxidase in neutrophils and macrophages: effect on the production of reactive oxygen species during phagocytosis. Cell Immunol *161*, 61-71.

Kakar, R., Kautz, B., and Eklund, E.A. (2005). JAK2 is necessary and sufficient for interferon-gamma-induced transcription of the gene encoding gp91PHOX. J Leukoc Biol *77*, 120-127.

Kamijo, R., Le, J., Shapiro, D., Havell, E.A., Huang, S., Aguet, M., Bosland, M., and Vilcek, J. (1993). Mice that lack the interferon-gamma receptor have profoundly altered responses to infection with Bacillus Calmette-Guerin and subsequent challenge with lipopolysaccharide. J Exp Med *178*, 1435-1440.

Kanaani, J., el-Husseini Ael, D., Aguilera-Moreno, A., Diacovo, J.M., Bredt, D.S., and Baekkeskov, S. (2002). A combination of three distinct trafficking signals mediates axonal targeting and presynaptic clustering of GAD65. J Cell Biol *158*, 1229-1238.

Kantari, C., Pederzoli-Ribeil, M., and Witko-Sarsat, V. (2008). The role of neutrophils and monocytes in innate immunity. Contrib Microbiol *15*, 118-146.

Katzmann, D.J., Odorizzi, G., and Emr, S.D. (2002). Receptor downregulation and multivesicular-body sorting. Nat Rev Mol Cell Biol *3*, 893-905.

Kinchen, J.M., Doukoumetzidis, K., Almendinger, J., Stergiou, L., Tosello-Trampont, A., Sifri, C.D., Hengartner, M.O., and Ravichandran, K.S. (2008). A pathway for phagosome maturation during engulfment of apoptotic cells. Nat Cell Biol *10*, 556-566.

Kollner, I., Sodeik, B., Schreek, S., Heyn, H., von Neuhoff, N., Germeshausen, M., Zeidler, C., Kruger, M., Schlegelberger, B., Welte, K., and Beger, C. (2006). Mutations in neutrophil elastase causing congenital neutropenia lead to cytoplasmic protein accumulation and induction of the unfolded protein response. Blood *108*, 493-500.

Kopydlowski, K.M., Salkowski, C.A., Cody, M.J., van Rooijen, N., Major, J., Hamilton, T.A., and Vogel, S.N. (1999). Regulation of macrophage chemokine expression by lipopolysaccharide in vitro and in vivo. J Immunol *163*, 1537-1544.

Krawczyk, M., Leimgruber, E., Seguin-Estevez, Q., Dunand-Sauthier, I., Barras, E., and Reith, W. (2007). Expression of RAB4B, a protein governing endocytic recycling, is co-regulated with MHC class II genes. Nucleic Acids Res *35*, 595-605.

Lacy, P. (2005). The role of Rho GTPases and SNAREs in mediator release from granulocytes. Pharmacol Ther *107*, 358-376.

Larsen, E.C., DiGennaro, J.A., Saito, N., Mehta, S., Loegering, D.J., Mazurkiewicz, J.E., and Lennartz, M.R. (2000). Differential requirement for classic and novel PKC isoforms in respiratory burst and phagocytosis in RAW 264.7 cells. J Immunol *165*, 2809-2817.

Leiva, N., Pavarotti, M., Colombo, M.I., and Damiani, M.T. (2006). Reconstitution of recycling from the phagosomal compartment in streptolysin O-permeabilized macrophages: role of Rab11. Exp Cell Res *312*, 1843-1855.

Levy, R., Rotrosen, D., Nagauker, O., Leto, T.L., and Malech, H.L. (1990). Induction of the respiratory burst in HL-60 cells. Correlation of function and protein expression. J Immunol *145*, 2595-2601.

Lin, C.F., Tsai, C.C., Huang, W.C., Wang, C.Y., Tseng, H.C., Wang, Y., Kai, J.I., Wang, S.W., and Cheng, Y.L. (2008). IFN-gamma synergizes with LPS to induce nitric oxide biosynthesis through glycogen synthase kinase-3-inhibited IL-10. J Cell Biochem *105*, 746-755.

Lodish, H., Berk, A., Kaiser, C., Krieger, M., Scott, M., Bretscher, A., Ploegh, H., and Matsudaira, P. (2008). Vesicular traffic, secretion and endocytosis. In: Molecular Cell Biology, vol. Sixth Edition, eds. Lodish, Berk, Kaiser, Krieger, Scott, Bretscher, Ploegh, and Matsudaira, New York: W.H. Freeman and Company, 279-620.

Ma, J., Chen, T., Mandelin, J., Ceponis, A., Miller, N.E., Hukkanen, M., Ma, G.F., and Konttinen, Y.T. (2003). Regulation of macrophage activation. Cell Mol Life Sci *60*, 2334-2346.

Maher, S.G., Romero-Weaver, A.L., Scarzello, A.J., and Gamero, A.M. (2007). Interferon: cellular executioner or white knight? Curr Med Chem *14*, 1279-1289.

Manderson, A.P., Kay, J.G., Hammond, L.A., Brown, D.L., and Stow, J.L. (2007). Subcompartments of the macrophage recycling endosome direct the differential secretion of IL-6 and TNFalpha. J Cell Biol *178*, 57-69.

Marecki, S., Riendeau, C.J., Liang, M.D., and Fenton, M.J. (2001). PU.1 and multiple IFN regulatory factor proteins synergize to mediate transcriptional activation of the human IL-1 beta gene. J Immunol *166*, 6829-6838.

Maxfield, F.R., and McGraw, T.E. (2004). Endocytic recycling. Nat Rev Mol Cell Biol *5*, 121-132.

May, R.C., and Machesky, L.M. (2001). Phagocytosis and the actin cytoskeleton. J Cell Sci *114*, 1061-1077.

Mayorga, L.S., Bertini, F., and Stahl, P.D. (1991). Fusion of newly formed phagosomes with endosomes in intact cells and in a cell-free system. J Biol Chem *266*, 6511-6517.

Mellman, I.S., Plutner, H., Steinman, R.M., Unkeless, J.C., and Cohn, Z.A. (1983). Internalization and degradation of macrophage Fc receptors during receptor-mediated phagocytosis. J Cell Biol *96*, 887-895.

Misaki, R., Nakagawa, T., Fukuda, M., Taniguchi, N., and Taguchi, T. (2007). Spatial segregation of degradation- and recycling-trafficking pathways in COS-1 cells. Biochem Biophys Res Commun *360*, 580-585.

Mosser, D.M. (2003). The many faces of macrophage activation. J Leukoc Biol *73*, 209-212.

Mosser, D.M., and Edwards, J.P. (2008). Exploring the full spectrum of macrophage activation. Nat Rev Immunol *8*, 958-969.

Mosser, D.M., and Zhang, X. (2008). Activation of murine macrophages. Curr Protoc Immunol *Chapter 14*, Unit 14 12.

Muller, I., Pedrazzini, T., Farrell, J.P., and Louis, J. (1989). T-cell responses and immunity to experimental infection with leishmania major. Annu Rev Immunol *7*, 561-578.

Murillo, I., and Henderson, L.M. (2005). Expression of gp91phox/Nox2 in COS-7 cells: cellular localization of the protein and the detection of outward proton currents. Biochem J *385*, 649-657.

Murray, R.Z., Kay, J.G., Sangermani, D.G., and Stow, J.L. (2005). A role for the phagosome in cytokine secretion. Science *310*, 1492-1495.

Nakano, Y., Longo-Guess, C.M., Bergstrom, D.E., Nauseef, W.M., Jones, S.M., and Banfi, B. (2008). Mutation of the Cyba gene encoding p22phox causes vestibular and immune defects in mice. J Clin Invest *118*, 1176-1185.

Nathan, C.F., Murray, H.W., Wiebe, M.E., and Rubin, B.Y. (1983). Identification of interferon-gamma as the lymphokine that activates human macrophage oxidative metabolism and antimicrobial activity. J Exp Med *158*, 670-689.

Nauseef, W.M. (2004). Assembly of the phagocyte NADPH oxidase. Histochem Cell Biol *122*, 277-291.

Nauseef, W.M. (2008). Biological roles for the NOX family NADPH oxidases. J Biol Chem *283*, 16961-16965.

Nester, E.W. (2007). Microbiology : a human perspective. McGraw-Hill: Boston.

Newburger, P.E., Dai, Q., and Whitney, C. (1991). In vitro regulation of human phagocyte cytochrome b heavy and light chain gene expression by bacterial lipopolysaccharide and recombinant human cytokines. J Biol Chem *266*, 16171-16177.

Newburger, P.E., Ezekowitz, R.A., Whitney, C., Wright, J., and Orkin, S.H. (1988). Induction of phagocyte cytochrome b heavy chain gene expression by interferon gamma. Proc Natl Acad Sci U S A *85*, 5215-5219.

Nisimoto, Y., Motalebi, S., Han, C.H., and Lambeth, J.D. (1999). The p67(phox) activation domain regulates electron flow from NADPH to flavin in flavocytochrome b(558). J Biol Chem *274*, 22999-23005.

Nomura, F., Akashi, S., Sakao, Y., Sato, S., Kawai, T., Matsumoto, M., Nakanishi, K., Kimoto, M., Miyake, K., Takeda, K., and Akira, S. (2000). Cutting edge: endotoxin tolerance in mouse peritoneal macrophages correlates with down-regulation of surface toll-like receptor 4 expression. J Immunol *164*, 3476-3479.

Ochs, H.D., and Igo, R.P. (1973). The NBT slide test: a simple screening method for detecting chronic granulomatous disease and female carriers. J Pediatr *83*, 77-82.
Paclet, M.H., Coleman, A.W., Vergnaud, S., and Morel, F. (2000). P67-phox-mediated NADPH oxidase assembly: imaging of cytochrome b558 liposomes by atomic force microscopy. Biochemistry *39*, 9302-9310.

Parkos, C.A., Allen, R.A., Cochrane, C.G., and Jesaitis, A.J. (1987). Purified cytochrome b from human granulocyte plasma membrane is comprised of two polypeptides with relative molecular weights of 91,000 and 22,000. J Clin Invest *80*, 732-742.

Phillips, W.A., Croatto, M., and Hamilton, J.A. (1990). Priming the macrophage respiratory burst with IL-4: enhancement with TNF-alpha but inhibition by IFN-gamma. Immunology *70*, 498-503.

Pitt, A., Mayorga, L.S., Stahl, P.D., and Schwartz, A.L. (1992). Alterations in the protein composition of maturing phagosomes. J Clin Invest *90*, 1978-1983.

Pollock, J.D., Williams, D.A., Gifford, M.A., Li, L.L., Du, X., Fisherman, J., Orkin, S.H., Doerschuk, C.M., and Dinauer, M.C. (1995). Mouse model of X-linked chronic granulomatous disease, an inherited defect in phagocyte superoxide production. Nat Genet *9*, 202-209.

Porter, C.D., Parkar, M.H., Verhoeven, A.J., Levinsky, R.J., Collins, M.K., and Kinnon, C. (1994). p22-phox-deficient chronic granulomatous disease: reconstitution by retrovirus-mediated expression and identification of a biosynthetic intermediate of gp91-phox. Blood *84*, 2767-2775.

Price, M.O., McPhail, L.C., Lambeth, J.D., Han, C.H., Knaus, U.G., and Dinauer, M.C. (2002). Creation of a genetic system for analysis of the phagocyte respiratory burst: high-level reconstitution of the NADPH oxidase in a nonhematopoietic system. Blood *99*, 2653-2661.

Proux-Gillardeaux, V., Rudge, R., and Galli, T. (2005). The tetanus neurotoxin-sensitive and insensitive routes to and from the plasma membrane: fast and slow pathways? Traffic *6*, 366-373.

Quinn, M.T., Deleo, F., and Bokoch, G.M. (2007). Neutrophil methods and protocols. Humana Press: Totowa, N.J.

Racoosin, E.L., and Swanson, J.A. (1989). Macrophage colony-stimulating factor (rM-CSF) stimulates pinocytosis in bone marrow-derived macrophages. J Exp Med *170*, 1635-1648.

Radi, R., Cosgrove, T.P., Beckman, J.S., and Freeman, B.A. (1993). Peroxynitrite-induced luminol chemiluminescence. Biochem J *290 (Pt 1)*, 51-57.

Rasband, W.S. (1997-2004). ImageJ, National Institutes of Health, Bethesda, Maryland, USA, http://rsb.info.nih.gov/ij/.

Rogers, L.D., and Foster, L.J. (2008). Contributions of proteomics to understanding phagosome maturation. Cell Microbiol *10*, 1405-1412.

Sano, H., Roach, W.G., Peck, G.R., Fukuda, M., and Lienhard, G.E. (2008). Rab10 in insulin-stimulated GLUT4 translocation. Biochem J *411*, 89-95.

Saraste, J., and Goud, B. (2007). Functional symmetry of endomembranes. Mol Biol Cell *18*, 1430-1436.

Savina, A., Peres, A., Cebrian, I., Carmo, N., Moita, C., Hacohen, N., Moita, L.F., and Amigorena, S. (2009). The Small GTPase Rac2 Controls Phagosomal Alkalinization and Antigen Crosspresentation Selectively in CD8(+) Dendritic Cells. Immunity.

Schroder, K., Hertzog, P.J., Ravasi, T., and Hume, D.A. (2004). Interferon-gamma: an overview of signals, mechanisms and functions. J Leukoc Biol *75*, 163-189.

Scott, C.C., Botelho, R.J., and Grinstein, S. (2003). Phagosome maturation: a few bugs in the system. J Membr Biol *193*, 137-152.

Seachrist, J.L., and Ferguson, S.S. (2003). Regulation of G protein-coupled receptor endocytosis and trafficking by Rab GTPases. Life Sci *74*, 225-235.

Shin, J.S., Ebersold, M., Pypaert, M., Delamarre, L., Hartley, A., and Mellman, I. (2006). Surface expression of MHC class II in dendritic cells is controlled by regulated ubiquitination. Nature *444*, 115-118.

Shotland, Y., Kramer, H., and Groisman, E.A. (2003). The Salmonella SpiC protein targets the mammalian Hook3 protein function to alter cellular trafficking. Mol Microbiol *49*, 1565-1576.

Smith, A.C., Cirulis, J.T., Casanova, J.E., Scidmore, M.A., and Brumell, J.H. (2005). Interaction of the Salmonella-containing vacuole with the endocytic recycling system. J Biol Chem *280*, 24634-24641.

Sonnichsen, B., De Renzis, S., Nielsen, E., Rietdorf, J., and Zerial, M. (2000). Distinct membrane domains on endosomes in the recycling pathway visualized by multicolor imaging of Rab4, Rab5, and Rab11. J Cell Biol *149*, 901-914.

Sorkin, A., and Goh, L.K. (2008). Endocytosis and intracellular trafficking of ErbBs. Exp Cell Res *314*, 3093-3106.

Sorkin, A., and Von Zastrow, M. (2002). Signal transduction and endocytosis: close encounters of many kinds. Nat Rev Mol Cell Biol *3*, 600-614.

Subramaniam, P.S., Torres, B.A., and Johnson, H.M. (2001). So many ligands, so few transcription factors: a new paradigm for signaling through the STAT transcription factors. Cytokine *15*, 175-187.

Swanson, J.A., and Hoppe, A.D. (2004). The coordination of signaling during Fc receptor-mediated phagocytosis. J Leukoc Biol *76*, 1093-1103.

Takemura, R., Stenberg, P.E., Bainton, D.F., and Werb, Z. (1986). Rapid redistribution of clathrin onto macrophage plasma membranes in response to Fc receptor-ligand interaction during frustrated phagocytosis. J Cell Biol *102*, 55-69.

Taylor, R.M., Burritt, J.B., Baniulis, D., Foubert, T.R., Lord, C.I., Dinauer, M.C., Parkos, C.A., and Jesaitis, A.J. (2004). Site-specific inhibitors of NADPH oxidase activity and structural probes of flavocytochrome b: characterization of six monoclonal antibodies to the p22phox subunit. J Immunol *173*, 7349-7357.

Thomas, V., Samanta, S., Wu, C., Berliner, N., and Fikrig, E. (2005). Anaplasma phagocytophilum modulates gp91phox gene expression through altered interferon regulatory factor 1 and PU.1 levels and binding of CCAAT displacement protein. Infect Immun *73*, 208-218.

Tooze, R.M., Stephenson, S., and Doody, G.M. (2006). Repression of IFN-gamma induction of class II transactivator: a role for PRDM1/Blimp-1 in regulation of cytokine signaling. J Immunol *177*, 4584-4593.

Tsang, A.W., Oestergaard, K., Myers, J.T., and Swanson, J.A. (2000). Altered membrane trafficking in activated bone marrow-derived macrophages. J Leukoc Biol *68*, 487-494.

Turvy, D.N., and Blum, J.S. (2001). Biotin labeling and quantitation of cell-surface proteins. Curr Protoc Immunol *Chapter 18*, Unit 18 17.

Uchiya, K., Barbieri, M.A., Funato, K., Shah, A.H., Stahl, P.D., and Groisman, E.A. (1999). A Salmonella virulence protein that inhibits cellular trafficking. Embo J *18*, 3924-3933.

Ullrich, O., Reinsch, S., Urbe, S., Zerial, M., and Parton, R.G. (1996). Rab11 regulates recycling through the pericentriolar recycling endosome. J Cell Biol *135*, 913-924.

Underhill, D.M., and Ozinsky, A. (2002). Phagocytosis of microbes: complexity in action. Annu Rev Immunol *20*, 825-852.

Underhill, D.M., Rossnagle, E., Lowell, C.A., and Simmons, R.M. (2005). Dectin-1 activates Syk tyrosine kinase in a dynamic subset of macrophages for reactive oxygen production. Blood *106*, 2543-2550.

Urbe, S., Huber, L.A., Zerial, M., Tooze, S.A., and Parton, R.G. (1993). Rab11, a small GTPase associated with both constitutive and regulated secretory pathways in PC12 cells. FEBS Lett *334*, 175-182.

van den Berg, T.K., and Kraal, G. (2005). A function for the macrophage F4/80 molecule in tolerance induction. Trends Immunol *26*, 506-509.

van Niel, G., Wubbolts, R., and Stoorvogel, W. (2008). Endosomal sorting of MHC class II determines antigen presentation by dendritic cells. Curr Opin Cell Biol *20*, 437-444.

van Niel, G., Wubbolts, R., Ten Broeke, T., Buschow, S.I., Ossendorp, F.A., Melief, C.J., Raposo, G., van Balkom, B.W., and Stoorvogel, W. (2006). Dendritic cells regulate exposure of MHC class II at their plasma membrane by oligoubiquitination. Immunity *25*, 885-894.

Vazquez-Torres, A., Fantuzzi, G., Edwards, C.K., 3rd, Dinarello, C.A., and Fang, F.C. (2001). Defective localization of the NADPH phagocyte oxidase to Salmonella-containing phagosomes in tumor necrosis factor p55 receptor-deficient macrophages. Proc Natl Acad Sci U S A *98*, 2561-2565.

Vazquez-Torres, A., Xu, Y., Jones-Carson, J., Holden, D.W., Lucia, S.M., Dinauer, M.C., Mastroeni, P., and Fang, F.C. (2000). Salmonella pathogenicity island 2-dependent evasion of the phagocyte NADPH oxidase. Science *287*, 1655-1658.

Vieira, O.V., Botelho, R.J., and Grinstein, S. (2002). Phagosome maturation: aging gracefully. Biochem J *366*, 689-704.

Vila-del Sol, V., Diaz-Munoz, M.D., and Fresno, M. (2007). Requirement of tumor necrosis factor alpha and nuclear factor-kappaB in the induction by IFN-gamma of inducible nitric oxide synthase in macrophages. J Leukoc Biol *81*, 272-283.

Wang, E., Pennington, J.G., Goldenring, J.R., Hunziker, W., and Dunn, K.W. (2001). Brefeldin A rapidly disrupts plasma membrane polarity by blocking polar sorting in common endosomes of MDCK cells. J Cell Sci *114*, 3309-3321.

Wang, I.M., Contursi, C., Masumi, A., Ma, X., Trinchieri, G., and Ozato, K. (2000). An IFN-gamma-inducible transcription factor, IFN consensus sequence binding protein (ICSBP), stimulates IL-12 p40 expression in macrophages. J Immunol *165*, 271-279.

Ward, A.C., and Dale, D.C. (2009). Genetic and molecular diagnosis of severe congenital neutropenia. Curr Opin Hematol *16*, 9-13.

Welte, K., Zeidler, C., and Dale, D.C. (2006). Severe congenital neutropenia. Semin Hematol *43*, 189-195.

Winkelstein, J.A., Marino, M.C., Johnston, R.B., Jr., Boyle, J., Curnutte, J., Gallin, J.I., Malech, H.L., Holland, S.M., Ochs, H., Quie, P., Buckley, R.H., Foster, C.B., Chanock, S.J., and Dickler, H. (2000). Chronic granulomatous disease. Report on a national registry of 368 patients. Medicine (Baltimore) *79*, 155-169.

Yagisawa, M., Yuo, A., Yonemaru, M., Imajoh-Ohmi, S., Kanegasaki, S., Yazaki, Y., and Takaku, F. (1996). Superoxide release and NADPH oxidase components in mature human phagocytes: correlation between functional capacity and amount of functional proteins. Biochem Biophys Res Commun *228*, 510-516.

Yamashiro, D.J., Tycko, B., Fluss, S.R., and Maxfield, F.R. (1984). Segregation of transferrin to a mildly acidic (pH 6.5) para-Golgi compartment in the recycling pathway. Cell *37*, 789-800.

Yamauchi, A., Marchal, C.C., Molitoris, J., Pech, N., Knaus, U., Towe, J., Atkinson, S.J., and Dinauer, M.C. (2005). Rac GTPase isoform-specific regulation of NADPH oxidase and chemotaxis in murine neutrophils in vivo. Role of the C-terminal polybasic domain. J Biol Chem *280*, 953-964.

Yamauchi, A., Yu, L., Potgens, A.J., Kuribayashi, F., Nunoi, H., Kanegasaki, S., Roos, D., Malech, H.L., Dinauer, M.C., and Nakamura, M. (2001). Location of the epitope for 7D5, a monoclonal antibody raised against human flavocytochrome b558, to the extracellular peptide portion of primate gp91phox. Microbiol Immunol *45*, 249-257.

Yoon, S.O., Shin, S., and Mercurio, A.M. (2005). Hypoxia stimulates carcinoma invasion by stabilizing microtubules and promoting the Rab11 trafficking of the alpha6beta4 integrin. Cancer Res *65*, 2761-2769.

Yu, L., DeLeo, F.R., Biberstine-Kinkade, K.J., Renee, J., Nauseef, W.M., and Dinauer, M.C. (1999). Biosynthesis of flavocytochrome b558 . gp91(phox) is synthesized as a 65-kDa precursor (p65) in the endoplasmic reticulum. J Biol Chem *274*, 4364-4369.

Yu, L., Zhen, L., and Dinauer, M.C. (1997). Biosynthesis of the phagocyte NADPH oxidase cytochrome b558. Role of heme incorporation and heterodimer formation in maturation and stability of gp91phox and p22phox subunits. J Biol Chem *272*, 27288-27294.

Zhen, L., King, A.A., Xiao, Y., Chanock, S.J., Orkin, S.H., and Dinauer, M.C. (1993). Gene targeting of X chromosome-linked chronic granulomatous disease locus in a human myeloid leukemia cell line and rescue by expression of recombinant gp91phox. Proc Natl Acad Sci U S A *90*, 9832-9836.

Zhen, L., Yu, L., and Dinauer, M.C. (1998). Probing the role of the carboxyl terminus of the gp91phox subunit of neutrophil flavocytochrome b558 using site-directed mutagenesis. J Biol Chem *273*, 6575-6581.

Zhu, Y., Marchal, C.C., Casbon, A.J., Stull, N., von Lohneysen, K., Knaus, U.G., Jesaitis, A.J., McCormick, S., Nauseef, W.M., and Dinauer, M.C. (2006). Deletion mutagenesis of p22phox subunit of flavocytochrome b558: identification of regions critical for gp91phox maturation and NADPH oxidase activity. J Biol Chem *281*, 30336-30346.